Geological Society of America Bulletin

Geologic correlation of the Himalayan orogen and Indian craton: Part 2. Structural geology, geochronology, and tectonic evolution of the Eastern Himalaya

An Yin, C.S. Dubey, T.K. Kelty, A.A.G. Webb, T.M. Harrison, C.Y. Chou and Julien Célérier

Geological Society of America Bulletin 2010;122;360-395
doi: 10.1130/B26461.1

Notes

Geologic correlation of the Himalayan orogen and Indian craton: Part 2. Structural geology, geochronology, and tectonic evolution of the Eastern Himalaya

An Yin[1,2,†], C.S. Dubey[3], T.K. Kelty[4], A.A.G. Webb[1], T.M. Harrison[1], C.Y. Chou[1], and Julien Célérier[5]

[1]*Department of Earth and Space Sciences and Institute of Geophysics and Planetary Physics, University of California, Los Angeles, California 90095-1567, USA*

[2]*Structural Geology Group, School of Earth Sciences and Resources, China University of Geosciences (Beijing), Beijing 10083, China*

[3]*Department of Geology, Delhi University, Delhi-110007, India*

[4]*Department of Geological Sciences, California State University, Long Beach, California 90840-3902, USA*

[5]*Research School of Earth Sciences, Building 61, Mills Road, Australian National University, Canberra, ACT 0200, Australia*

ABSTRACT

Despite being the largest active collisional orogen on Earth, the growth mechanism of the Himalaya remains uncertain. Current debate has focused on the role of dynamic interaction between tectonics and climate and mass exchanges between the Himalayan and Tibetan crust during Cenozoic India-Asia collision. A major uncertainty in the debate comes from the lack of geologic information on the eastern segment of the Himalayas from 91°E to 97°E, which makes up about one-quarter of the mountain belt. To address this issue, we conducted detailed field mapping, U-Pb zircon age dating, and $^{40}Ar/^{39}Ar$ thermochronology along two geologic traverses at longitudes of 92°E and 94°E across the eastern Himalaya. Our dating indicates the region experienced magmatic events at 1745–1760 Ma, 825–878 Ma, 480–520 Ma, and 28–20 Ma. The first three events also occurred in the northeastern Indian craton, while the last is unique to the Himalaya. Correlation of magmatic events and age-equivalent lithologic units suggests that the eastern segment of the Himalaya was constructed in situ by basement-involved thrusting, which is inconsistent with the hypothesis of high-grade Himalaya rocks derived from Tibet via channel flow. The Main Central thrust in the eastern Himalaya forms the roof of a major thrust duplex; its northern part was initiated at ca. 13 Ma, while the southern part was initiated at ca. 10 Ma, as indicated by $^{40}Ar/^{39}Ar$ thermochronometry. Crustal thickening of the Main Central thrust hanging wall was expressed by discrete ductile thrusting between 12 Ma and 7 Ma, overlapping in time with motion on the Main Central thrust below. Restoration of two possible geologic cross sections from one of our geologic traverses, where one assumes the existence of pre-Cenozoic deformation below the Himalaya and the other assumes flat-lying strata prior to the India-Asia collision, leads to estimated shortening of 775 km (~76% strain) and 515 km (~70% strain), respectively. We favor the presence of significant basement topography below the eastern Himalaya based on projections of early Paleozoic structures from the Shillong Plateau (i.e., the Central Shillong thrust) located ~50 km south of our study area. Since northeastern India and possibly the eastern Himalaya both experienced early Paleozoic contraction, the estimated shortening from this study may have resulted from a combined effect of early Paleozoic and Cenozoic deformation.

INTRODUCTION

The Himalayan orogen was created by the Cenozoic India-Asia collision starting at ca. 65–60 Ma (Yin and Harrison, 2000; Ding et al., 2005) or earlier (e.g., Zhu et al., 2005; Aitchison et al., 2007). Although its plate-tectonic setting is well understood, the growth mechanism of the orogen remains debated. Competing models emphasizing different controlling factors include: (1) vertical stacking of basement-involved thrust sheets (Heim and Gansser, 1939; Gansser, 1964; LeFort, 1975; Lyon-Caen and Molnar, 1985), (2) southward propagation of a thin-skinned thrust belt (e.g., Schelling and Arita, 1991; Srivastava and Mitra, 1994; DeCelles et al., 1998, 2001, 2002; Avouac, 2003; Robinson et al., 2003, 2006; Robinson and Pearson, 2006; Kohn, 2008), and (3) southward transport of high-grade metamorphic rocks via lower-crustal channel flow or wedge extrusion (Burchfiel and Royden, 1985; Chemenda et al., 1995, 2000; Grujic et al., 1996; Nelson et al., 1996; Grasemann et al., 1999; Beaumont et al., 2001, 2004, 2006; Hodges et al., 2001; Grujic et al., 2002; Searle et al., 2003; Klemperer, 2006; Godin et al., 2006). The central issue with the aforementioned models is that they were all established from the geology of the central Himalaya in Nepal and south-central Tibet (77°E–88°E), where the classic Himalayan relationships as originally defined by Heim and Gansser (1939) are exposed (Fig. 1). That is, the Main Boundary thrust places the Lesser Himalayan Sequence over Tertiary strata, the Main Central thrust places the Greater Himalayan Crystalline Complex over the Lesser Himalayan Sequence, and the later discovered South Tibet detachment places the Tethyan Himalayan Sequence over the Greater Himalayan Crystalline Complex (e.g., LeFort, 1996; Yin and Harrison, 2000). These studies generally neglect significant differences in geological relationships along the Himalayan strike and have treated Himalayan evolution as a two-dimensional problem in cross-section view. As pointed out by DiPietro and Pogue (2004), Yin (2006), and Webb et al. (2007), such an approach may disguise critical information on the mechanism of the Himalayan development when the regional map relationship across the whole orogen is not fully considered. For

†E-mail: yin@ess.ucla.edu

GSA Bulletin; March/April 2010; v. 122; no. 3/4; p. 360–395; doi: 10.1130/B26461.1; 15 figures; 2 tables.

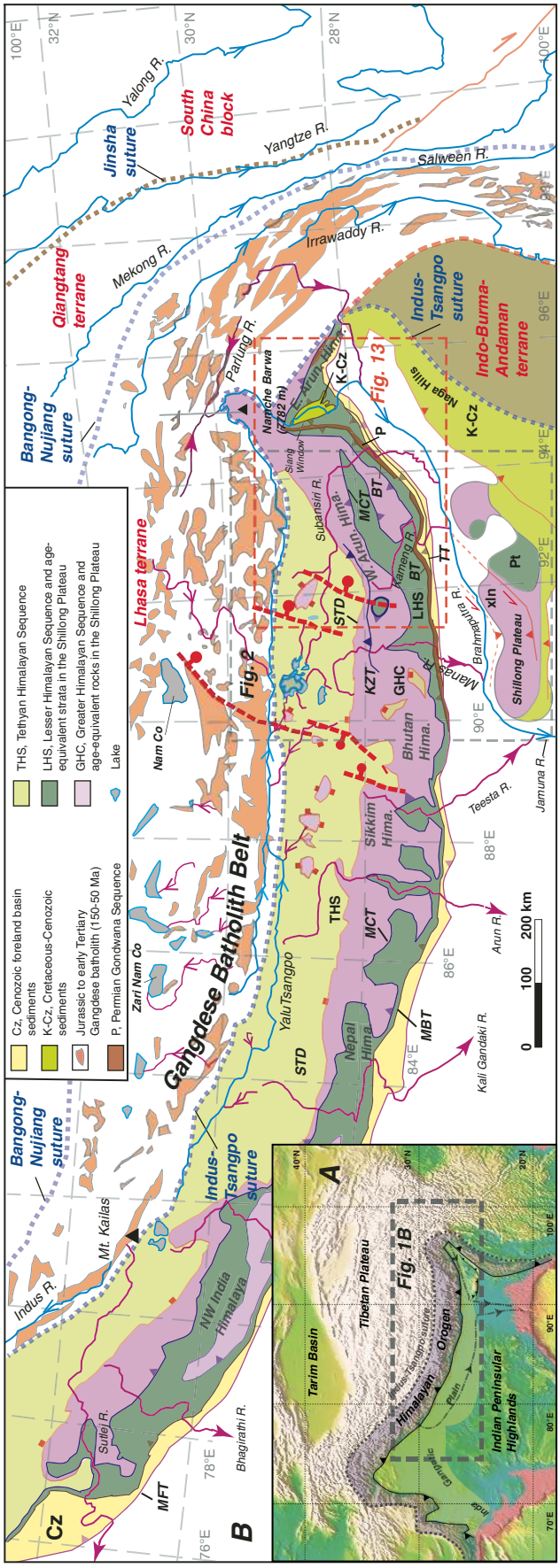

Figure 1. (A) A sketch map of the Himalayan-Tibetan orogen. (B) Regional geologic map of the Himalayan orogen simplified from Yin and Harrison (2000) and Yin (2006). Locations of Figures 2 and 13 are also shown. Abbreviations for major faults: MFT—Main Frontal thrust; MBT—Main Boundary thrust; MCT—Main Central thrust; STD—South Tibet detachment; BT—Bome thrust; TT—Tipi thrust. Abbreviations for lithologic units: xln—crystalline basement of the northeastern Indian craton; Pt—Proterozoic strata of the Shillong Group in northeastern India; LHS—Lesser Himalayan Sequence; GHC—Greater Himalayan Crystalline Complex; THS—Tethyan Himalayan Sequence.

example, the western Himalaya (70°E–77°E) does not preserve the classic Greater Himalayan Crystalline Complex-over-Lesser Himalayan Sequence relationship across the Main Central thrust (e.g., Yeats and Lawrence, 1984; Fuchs and Linner, 1995; Frank et al., 1995; Thakur, 1992, 1998; Pogue et al., 1999; Yin, 2006; Webb et al., 2007) (Fig. 1). The eastern part of the Himalaya (88°E–98°E) also displays dramatically different geology from that in the central Himalaya: its foreland exhibits a 400-km-long basement-involved uplift: the Shillong Plateau (Fig. 1) (Bilham and England, 2001; Jade et al., 2007; Biswas et al., 2007; Clark and Bilham, 2008) and the foreland basin is locally absent (Gansser, 1983). Our work presented here shows that (1) the development of major contractional structures in the eastern Himalaya started at 5–10 Ma after the onset of the equivalent structures in the central Himalaya, (2) crustal thickening was accomplished by basement-involved thick-skinned thrusting rather than thin-skinned thrusting as observed in the western and central Himalaya, and (3) the eastern segment of the Himalaya has accommodated at least 315 km of Cenozoic shortening derived purely from the map relationships without invoking any assumptions in constructing balanced cross sections.

REGIONAL GEOLOGY

Bhutan Himalaya

The eastern Himalaya consists of the Bhutan and Arunachal segments (Fig. 1). In Bhutan, the work of Jangpangi (1974) and Gansser (1983) laid a foundation for the general geology that led to prolific studies across the country in the past three decades (Ray et al., 1989; Swapp and Hollister, 1991; Ray, 1995; Bhargava, 1995; Edwards et al., 1996; Grujic et al., 1996, 2002, 2006; Davidson et al., 1997; Stüwe and Foster, 2001; Wiesmayr et al., 2002; Daniel et al., 2003; Tangri et al., 2003; Baillie and Norbu, 2004; Carosi et al., 2006; Meyer et al., 2006; Richards et al., 2006; Drukpa et al., 2006; Hollister and Grujic, 2006; McQuarrie et al., 2008). Following the traditional definition of major Himalayan structures and lithologic units by Heim and Gansser (1939), the Bhutan Himalaya is divided into the Lesser Himalayan Sequence, Greater Himalayan Crystalline Complex, and Tethyan Himalayan Sequence units bounded by the Main Boundary thrust below, the Main Central thrust in the middle, and the later discovered South Tibet detachment at the top (Fig. 2) (Gansser, 1983; Grujic et al., 2002).

The Lesser Himalayan Sequence in Bhutan consists of the Proterozoic Daling-Shumar Group and Proterozoic-Cambrian Baxa Group

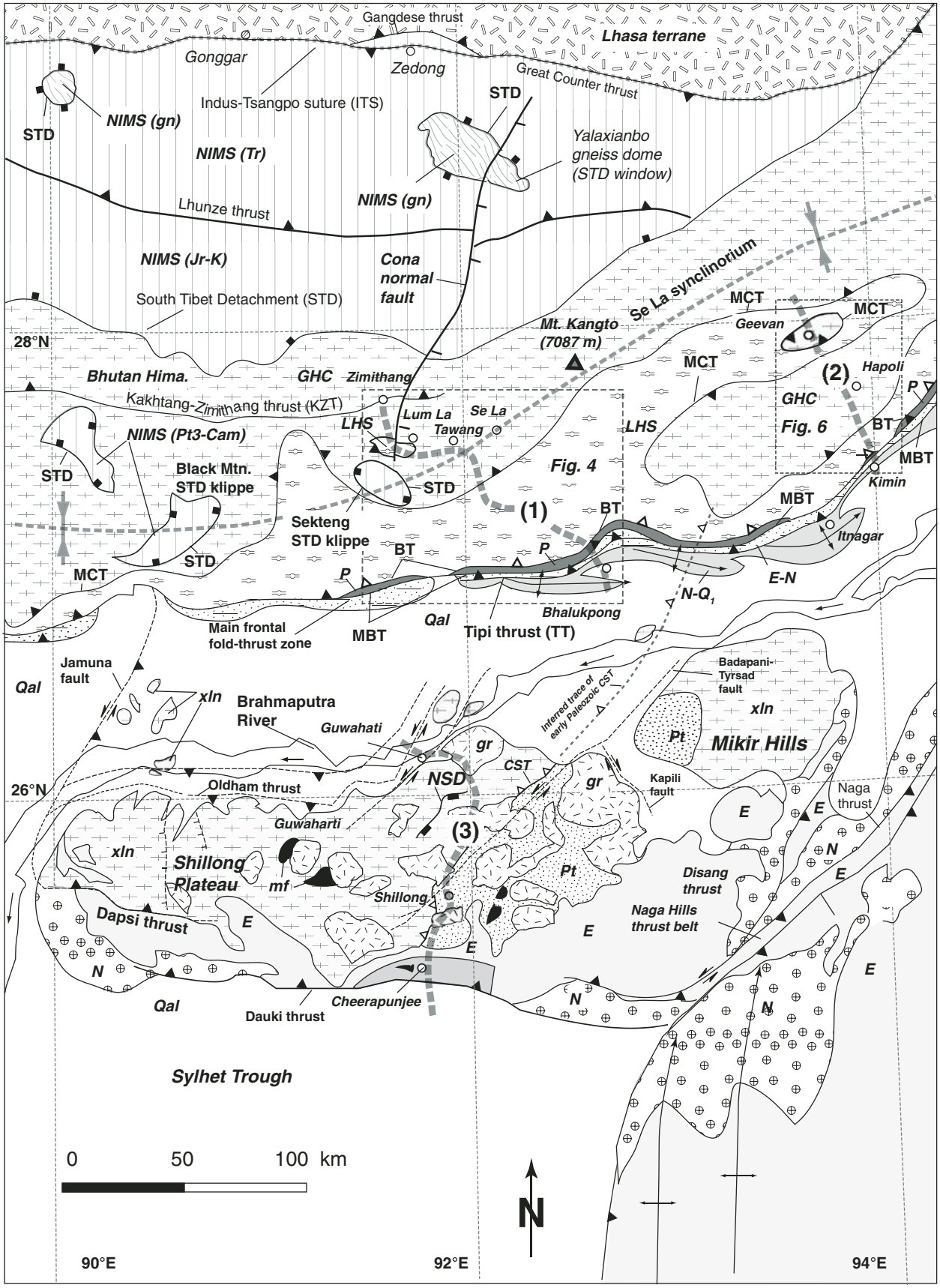

Figure 2 (*legend on following page*).

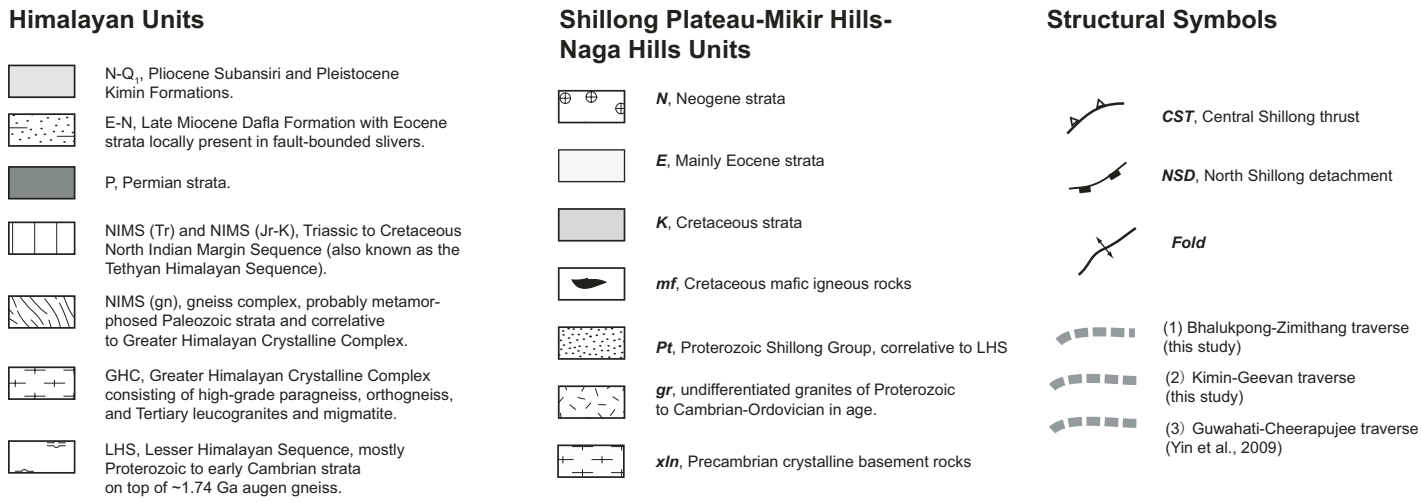

Figure 2 (*legend*).

Figure 2. Tectonic map of the eastern Himalayan orogen and the Shillong Plateau between longitude 90°E and 94°E based on Yin et al. (1994, 1999), Harrison et al. (2000), Kumar (1997), Pan et al. (2004), and this study. Numbers in parentheses represent the following geologic traverses: (1) Bhalukpong-Zimithang traverse, (2) Kimin-Geevan traverse, and (3) Guwahati-Cheerapunjee traverse. The geology of traverses 1 and 2 are presented in this study, while traverse 3 across the Shillong Plateau is discussed in Yin et al. (2009). Locations of Figures 4 and 6 are also shown. MBT—Main Boundary thrust; MCT—Main Central thrust; STD—South Tibet detachment; BT—Bome thrust; CST—Central Shillong thrust; TT—Tipi thrust.

(Fig. 3). The Daling-Shumar Group is composed of garnet-bearing schist (Jaishidanda Formation), quartzite (Shumar Formation), phyllite (Daling Formation), and tectonically (?) interlayered mylonitized granitic gneisses; the Baxa Group above consists of quartzite, phyllite, and carbonate (Gansser, 1983; Bhargava, 1995; McQuarrie et al., 2008) (Fig. 3). The garnet schist of the Jaishidanda Formation below the Main Central thrust experienced peak metamorphism at 650–675 °C and 9–13 kbar during 18–22 Ma (Daniel et al., 2003), while the granitic gneiss units (Jhumo Ri gneiss of Jangpangi, 1974; Gachhang gneiss of Ray et al., 1989) have yielded a Rb-Sr age of ca. 1.1 Ga (Bhargava, 1995) and a U-Pb zircon age of ca. 1.76 Ga (Daniel et al., 2003). The Daling-Shumar Group contains a 1.8–1.9 Ga metarhyolite layer and an arenite unit with U-Pb detrital zircon ages between 1.8 and 2.5 Ga (Richards et al., 2006). Although the 1.8–1.9 Ga metarhyolite was inferred to be in depositional contact within the lower Lesser Himalayan Sequence (Richards et al., 2006), given the intense deformation within the Lesser Himalayan Sequence strata that have generally obliterated the original contact relationships, it is possible the metarhyolite is part of the mylonitic augen lying as a basement to the Lesser Himalayan Sequence.

McQuarrie et al. (2008) showed two types of detrital zircon age distributions for samples from the Baxa Group. One sample from its lower part has a youngest zircon age of ca. 950 Ma, while another sample from its upper part has a youngest age of ca. 490 Ma. McQuarrie et al. (2008) also showed that samples from the younger Shumar Formation yield an age of ca. 1.7 Ga for the youngest zircon. As noted in this study, the age distributions of detrital zircon from the lower Baxa Group and Shumar Formation in Bhutan are similar to those from the middle and lower Rupa Group in Arunachal (Fig. 3). Carboniferous-Permian strata (also known as the Gondwana Sequence) are present in the Main Boundary thrust zone in the Bhutan Himalaya, and they are commonly thrust over Tertiary foreland sediments and in some places Quaternary deposits (Gansser, 1983; Bhargava, 1995).

The Greater Himalayan Crystalline Complex in Bhutan lies above the Main Central thrust and consists of paragneiss, orthogneiss, migmatite, and leucogranite (Gansser, 1983). Kyanite-bearing migmatites experienced peak pressure-temperature (*P-T*) conditions of ~750–800 °C and 10–14 kbar at ca. 18 Ma, followed by retrograde metamorphism under conditions of 500–600 °C and 5 kbar (Swapp and Hollister, 1991; Davidson et al., 1997; Daniel et al., 2003). Retrograde metamorphism was accompanied by emplacement of leucogranite at ca. 13 Ma and cooling below ~350–400 °C at 14–11 Ma in the Main Central thrust zone (Stüwe and Foster, 2001; Daniel et al., 2003). Continued cooling below ~100–60 °C occurred from late Miocene to Pliocene time (Grujic et al., 2006). An 825 Ma orthogneiss intrudes a quartzite unit in the Greater Himalayan Crystalline Complex, and it yields U-Pb detrital zircon ages between 980 and 1820 Ma (Richards et al., 2006). These observations suggest that part of the Greater Himalayan Crystalline Complex must have been deposited between 980 Ma and 825 Ma.

The Tethyan Himalayan Sequence in Bhutan is exposed mostly in the South Tibetan detachment klippen (Fig. 2), which make up the Proterozoic garnet-bearing Chekha Formation, rhyolite-dacite flows of the Singhi Formation, and quartz arenite of the Deshichiling Formation (Bhargava, 1995; Grujic et al., 2002) (Fig. 3). The latter is overlain by Cambrian to Jurassic strata that are parts of the North Indian passive-margin sequence (Yin, 2006) (Fig. 3). The Chekha Formation overlying the South Tibetan detachment yielded a detrital zircon age distribution similar to that obtained from the lower Baxa Group, with the youngest zircon having an age of ca. 950 Ma (McQuarrie et al., 2008). This relationship suggests that the Main Central thrust and South Tibetan detachment together may have duplicated the original Himalayan crustal section that was part of the cover sequence above the Precambrian Indian craton.

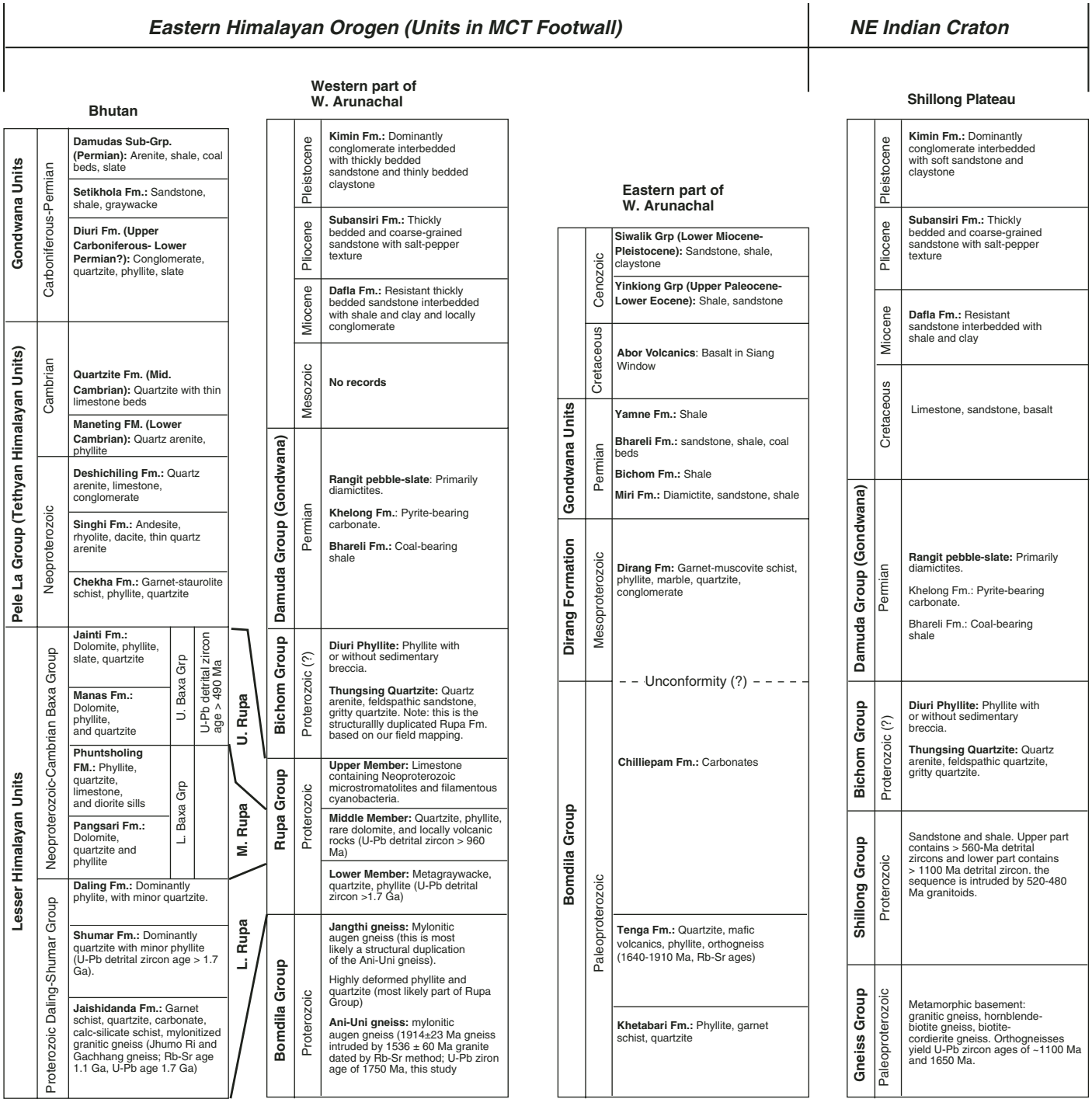

Compiled from Jangpangi (1974), Gansser (1983), Bhargava (1995), Edwards et al. (1996), Grujic et al. (2002), Tangri et al. (2003), Daniel et al. (2003), and McQuarrie et al. (2008).

Modified from Acharyya et al. (1975), Acharyya (1994), Dikshitulu et al. (1995), Tewari (2001), Yin et al. (2006), and this study.

Kumar (1997)

Ghosh et al. (1994), Das Gupta and Biswas (2000), and Yin et al. (2009).

Figure 3. Lithostratigraphy and nomenclature of the eastern Himalayan orogen and northeastern Indian craton. References are listed at the bottom of each lithologic column.

The South Tibetan detachment exhibits two important relationships across Bhutan and southeastern Tibet. First, it cuts up-section northward by placing Jurassic-Cretaceous strata over the Greater Himalayan Crystalline Complex in southeast Tibet to the north (Pan et al., 2004) and by juxtaposing Proterozoic-Cambrian strata over the Greater Himalayan Crystalline Complex in southern Bhutan to the south (Fig. 2) (Grujic et al., 2002). This relationship can be explained by northward thrusting or out-of-sequence top-to-the-north normal faulting along the South Tibetan detachment. Second, the traces of the South Tibetan detachment and Main Central thrust are located within 1.5 km to 3 km in southern Bhutan (Gansser, 1983; Grujic et al., 2002) (Fig. 2). As the Chekha Formation above the South Tibetan detachment is a garnet-grade schist (Bhargava, 1995), which must have been exhumed from a depth of 10–15 km, restoring this crustal section above the South Tibetan detachment would require the South Tibetan detachment trace to extend 15–20 km southward, assuming the fault dips at 20°–30° to the north. This would require the Main Central thrust and South Tibetan detachment to approach each other and eventually merge to the south in cross-section view (in other words, the Greater Himalayan Crystalline Complex must thin to the south in order to place the South Tibetan detachment klippen so close to the Main Central thrust in southern Bhutan; see Fig. 2). The inferred up-dip branch line between the Main Central thrust and South Tibetan detachment is not unique in the Himalaya: it was established in the western and central Himalaya by Webb et al. (2007) and Webb (2008), indicating that this is a regional feature along the Himalayan orogen.

Arunachal Himalaya

Although Godwin-Austin (1875), La Touche (1885), MaClaren (1904), and Brown (1912) explored the Arunachal Himalaya more than 90 years ago, its general stratigraphy, structural framework, and metamorphic conditions were not established until the 1970s, when Indian geologists first started a systematic survey of the region (Thakur and Jain, 1974; Jain et al., 1974; Jangpangi, 1974; Acharyya et al., 1975; Verma and Tandon, 1976). Subsequent work of Tripathi et al. (1982), Thakur (1986), Kumar (1997), Acharyya (1998), and Verma (2002) has correlated the Arunachal geology with that in the central Himalaya using Heim and Gansser's (1939) stratigraphic (Greater Himalayan Crystalline Complex, Lesser Himalayan Sequence, and Tethyan Himalayan Sequence) and structural divisions (Main Central thrust and Main Boundary thrust).

The Arunachal Himalaya may be divided into the western and eastern domains separated by the Siang window directly south of the eastern Himalayan syntaxis (Fig. 1) (Singh and Chowdhary, 1990; Singh, 1993; Acharyya, 1998; Burg et al., 1998; Ding et al., 2001; Zeitler et al., 2001). The Siang window is defined by a closed trace of the Main Boundary thrust that places Lesser Himalayan Sequence strata over Cretaceous-Paleogene strata (Kumar, 1997). Regional structural features such as the Main Central thrust, Bome thrust, and the Indus-Tsangpo suture all make sharp U-turns around the window (Fig. 1).

The western Arunachal Himalaya exposes six regionally extensive and laterally continuous north-dipping thrusts. From north to south, they are the Zimithang thrust (KZT; correlative to the Kakthang thrust in Bhutan), the Dirang thrust (correlative with the Main Central thrust in the central Himalaya), the Bome thrust (BT; also known as the upper Main Boundary thrust in our field description), the Main Boundary thrust (also known as the lower Main Boundary thrust in our field description), the Tipi thrust (TT), and the Main Frontal thrust zone (Fig. 2) (Kumar, 1997; Yin et al., 2006; this study). The Dirang thrust places the Greater Himalayan Crystalline Complex over the Lesser Himalayan Sequence, the Bome thrust places the Lesser Himalayan Sequence over the Permian Gondwana Sequence, the Main Boundary thrust places the Permian Gondwana Sequence over Tertiary strata, and the Tipi thrust places the Miocene Dafla Formation over the Pliocene Subansiri and Pleistocene Kimin Formations (Kumar, 1997). The Main Frontal thrust zone consists of a series of en echelon folds that branch off obliquely from the main Himalayan Range front toward the Indian craton (Fig. 2). The fold arrangement implies broad left-slip shear parallel to and across the Himalayan front.

Traditionally, the Arunachal Lesser Himalayan Sequence is divided into the Paleoproterozoic Bomdila Group (augen gneiss interlayered with phyllite) and the overlying Mesoproterozoic-Neoproterozoic Rupa Group (quartzite and phyllite below and carbonate above) (Kumar, 1997) (Fig. 3). The augen gneisses yield Rb-Sr ages of ca. 1.9 Ga and 1.5 Ga (Dikshitulu et al., 1995). The Bomdila and Rupa Groups were correlated with the Daling-Shumar Group in the Bhutan Himalaya (Kumar, 1997); specifically, the carbonate horizon in the upper Rupa Group of Tewari (2001) may be equivalent to the Baxa limestone in Bhutan, and the 1.5–1.9 Ga Bomdila augen gneiss may be equivalent to the 1.76 Ga granitic gneiss in the Bhutan Lesser Himalayan Sequence (Daniel et al., 2003; Richards et al., 2006). As shown in this and our earlier study (Yin et al., 2006), the mylonitic augen gneiss and interlayered phyllite are in tectonic contact. The abundance of augen gneiss and low metamorphic grades of the Arunachal Lesser Himalayan Sequence contrast sharply to the equivalent rocks in Nepal of the central Himalaya, which have much higher metamorphic grade up to the amphibolite facies (e.g., LeFort, 1996; Kohn et al., 2004).

The Greater Himalayan Crystalline Complex in Arunachal consists of kyanite-sillimanite-staurolite schist, paragneiss, augen gneiss, and Tertiary leucogranites (Kumar, 1997; Yin et al., 2006). Although the Tethyan Himalayan Sequence is not exposed in the region, the sequence is documented directly to the north in southeast Tibet as highly folded Triassic to Cretaceous strata (Pan et al., 2004; Aikman et al., 2008); there, bedding of the folded Tethyan Himalayan Sequence strata is mostly transposed by axial cleavage (Yin et al., 1999).

In the eastern Arunachal Himalaya, east of the Siang window, the Cretaceous-Tertiary Gangdese Batholith thrusts over the Greater Himalayan Crystalline Complex, omitting the entire section of the Tethyan Himalayan Sequence (Fig. 1) (Gururajan and Choudhuri, 2003). This relationship is in sharp contrast to that in southeast Tibet, where the Gangdese Batholith thrusts over the Tethyan Himalayan Sequence or mélange complexes in the Indus-Tsangpo suture zone (e.g., Yin et al., 1994, 1999; Harrison et al., 2000). In places, the Greater Himalayan Crystalline Complex also thrusts over Quaternary sediments, omitting the Lesser Himalayan Sequence that we commonly see in the rest of the Himalaya (Gururajan and Choudhuri, 2003; Yin, 2006).

Shillong Plateau and NE Indian Craton

The eastern Himalaya is unique in that its foreland exposes scattered outcrops of Indian basement rocks where the modern foreland basin is mostly absent (Fig. 2) (Gansser, 1983; Yin et al., 2009). The geology of the NE Indian craton is best exposed in the Shillong Plateau directly south of the eastern Himalaya. There, four phases of magmatism at ca. 1600 Ma, ca. 1100 Ma, ca. 500 Ma, and ca. 105–95 Ma and four episodes of deformation at 1100 Ma, 500 Ma, 100 Ma, and 20–0 Ma have been documented (see Yin et al., 2009, and references therein). The first two events of deformation were contractional, induced by assembly of Rodinia and Eastern Gondwana, while the 100 Ma event was extensional, possibly related to breakup of Gondwana (Yin et al., 2009). Because of its proximity to the Himalaya and the north-northeast strike, the 500 Ma contractional structures may extend

into the eastern Himalaya. The most prominent early Paleozoic structure in the Shillong Plateau is the Central Shillong thrust, which places Precambrian crystalline basement rocks over the Proterozoic Shillong Group (Fig. 2), and which created basement relief of >15 km (see Figure 3b of Yin et al., 2009). This fault can be projected along strike into the eastern Himalaya between the two structural traverses mapped in this study (Fig. 2). Motion on this early Paleozoic fault may have created significant structural and stratigraphic complexities that affected our estimates of overall Cenozoic crustal shortening across the eastern Himalaya (see Discussion).

STRUCTURAL GEOLOGY

We conducted geologic mapping and sample collections in two areas in the western Arunachal Himalaya: (1) the Bhalukpong-Zimithang traverse in 2003 and 2006, and (2) the Kimin-Geevan traverse in 2004. Yin et al. (2006) reported the initial mapping result from the 2003 field work along the Bhalukpong-Zimithang traverse. We update that work in this paper by presenting additional field data collected in 2006 along the same traverse.

To separate observations from interpretations, particularly with respect to regional structural and stratigraphic correlations along Himalayan strike, we group lithologic units with respect to their underlying structures as the Main Boundary thrust hanging wall, Main Central thrust hanging wall, and South Tibetan detachment hanging wall, respectively. We avoid using Greater Himalayan Crystalline Complex, Lesser Himalayan Sequence, and Tethyan Himalayan Sequence in our field description because they are defined strictly by age range, metamorphic grade, and lithology (Heim and Gansser, 1939; LeFort, 1996) and thus preclude the possibility that major Himalayan faults may cut up and down sections laterally if the definitions were enforced strictly (see discussion by Yin, 2006). As shown in the western Himalaya, the Main Central thrust juxtaposes lithologic units that depart significantly from the traditional definitions by Heim and Gansser (1939) as a result of the fault cutting up-section westward and the merging of the Main Central thrust and South Tibetan detachment in their updip directions (DiPietro and Pogue, 2004; Yin, 2006; Webb et al., 2007). Our description here also strictly separates the use of the Main Central thrust and Main Central thrust zone. The former refers to the fault contact that separates different lithologic units, while the latter refers to the extent of deformation related to motion of the Main Central thrust, which may involve rocks from both the hanging wall and footwall of the Main Central thrust fault.

Bhalukpong-Zimithang Traverse

The Bhalukpong-Zimithang traverse exposes the following major structures from south to north: the active Main Frontal thrust zone, the Main Boundary thrust, the Main Central thrust, the Se La synclinorium, and the Zimithang ductile thrust zone (KZT) (Figs. 4A and 4B). We describe these structures in detail next.

Main Frontal Thrust Zone

The Main Frontal thrust zone is ~30 km wide and consists of an east-plunging anticline and the north-dipping Bhalukpong and Tipi thrusts (Figs. 4A and 4B). The east-plunging anticline is active and folds Quaternary alluvial and fluvial sediments. The Bhalukpong thrust is also active in the Quaternary, placing the Pliocene Subansiri Formation over Pleistocene Kimin Formation and Quaternary alluvial deposits (Fig. 4A; see Fig. 3 for stratigraphic nomenclature). The Tipi thrust juxtaposes the Miocene Dafla Formation over the Pliocene Subansiri Formation. The Tipi thrust zone locally contains Eocene marine strata that are not shown in Figure 4 (Acharyya et al., 1975; Acharyya, 1998). The Tipi thrust appears to be inactive in the Quaternary. Directly above the Bhalukpong thrust, there is a south-verging overturned recumbent fold in the Subansiri Formation; the overturned forelimb parallels the thrust below. The hanging wall of the Tipi thrust is a homoclinally north-dipping sequence, within which the Dafla Formation is repeated by a north-dipping thrust with a S20°E transport direction (Fig. 4A).

Main Boundary Thrust and its Hanging-Wall Structures

The Main Boundary thrust is a deformation zone consisting of upper and lower faults. The upper fault places Proterozoic Rupa Group over Permian sandstone and conglomerates (see Acharyya et al., 1975), while the lower fault places the Permian strata over the Miocene Dafla Formation (Fig. 4A). The upper Main Boundary thrust is laterally continuous and may correlate with the Bome thrust along the western limb of the Siang window (Fig. 2). Its hanging wall consists of phyllite, quartzite, metavolcanic rocks, carbonate, and augen gneiss (Fig. 4A).

We divide the upper Main Boundary thrust hanging wall in the Bhalukpong area into three units: the Bomdila augen gneiss (gn-1) below, the middle Rupa Group (Pt_{R2}), and the upper Rupa Group (Pt_{R3}). We divide the upper and middle Rupa units by a prominent medium-bedded (20–30 cm) quartz arenite sequence (Fig. 5A; MB in Fig. 4A), which shares a similar detrital-zircon age distribution over a large area (Yin et al., 2006). The unit preserves cross-bedding that indicates northward sediment transport. The upper Rupa Group is characterized by the presence of a gray limestone sequence with an assigned early Cambrian age, which is possibly correlative to the upper Baxa Group in Bhutan (Tewari, 2001) (Fig. 3).

At one location (27°08.991′N, 92°33.419′E), we observed the contact between augen gneiss (gn-1) below and a coarse-grained pebble quartzite unit above that lies at the base of the Rupa Group (Fig. 4A). The augen gneiss below is strongly deformed, as expressed by penetrative mylonitic foliation with a downdip stretching lineation and a top-to-the-south sense of shear (Fig. 5B). The overlying quartzite layers are not deformed and have well-preserved primary bedding, fining-upward sedimentary structures, and small channels (7–10 cm across), all indicating a right-way-up depositional contact. These observations suggest that shear deformation in augen gneiss predates deposition of the Rupa Group.

The upper Main Boundary thrust hanging wall consists of four major north-dipping thrusts that repeat the augen gneiss and Rupa units (Fig. 4A). Phyllite and slate units inside each thrust sheets experienced extensive isoclinal folding, and their bedding in many places is replaced by axial cleavage (Fig. 5C). The transposed bedding in these units in turn is refolded by asymmetric kink folds (Fig. 5D), indicating a temporal change in folding style, and thus deformation mechanism, as thrust sheets were progressively cooled as they moved upward.

Figure 4 (*on following five pages*). (A) Geological map of the Bhalukpong-Zimithang traverse based on our mapping and a compilation of the existing mapping. See map symbols to differentiate our field measurements from those made by the early workers. Major structures are defined as following: BLT—Bhalukpong thrust; TPT—Tipi thrust; MBT-low—lower Main Boundary thrust; MBT-up—upper Main Boundary thrust; BDT—Bomdila thrust; MCT—Main Central thrust; ZT—Zimithang thrust; STD—South Tibet detachment. Also see Yin et al. (2006) for detailed credits of early mapping in the area. Lines A-B, C-D, and E-F represent the locations of the cross section shown in B. See Figure 2 for location of the map area. Sample and field photograph locations discussed in the text are also shown. MB—quartz arenite marker bed mapped in the study area.

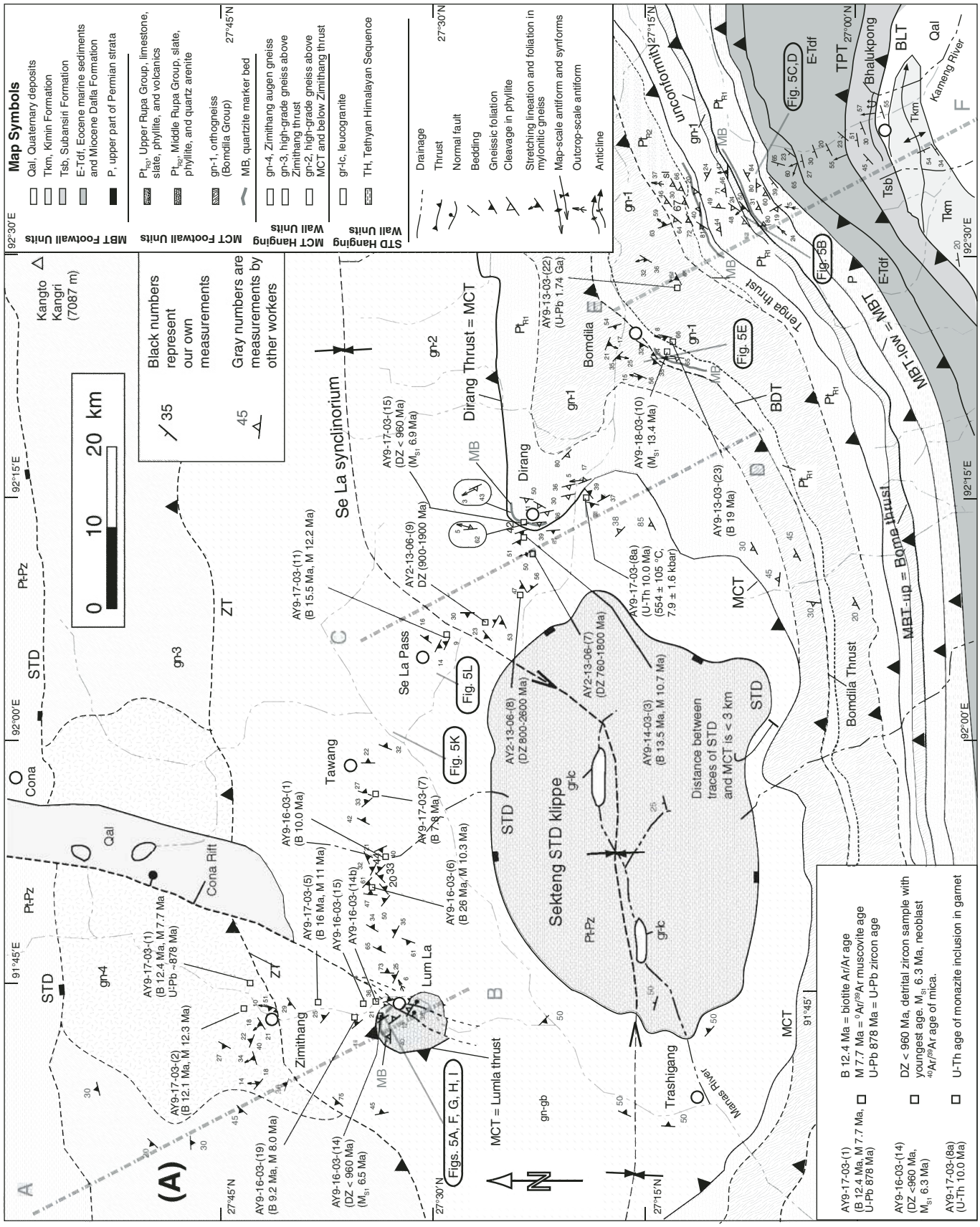

Figure 4.

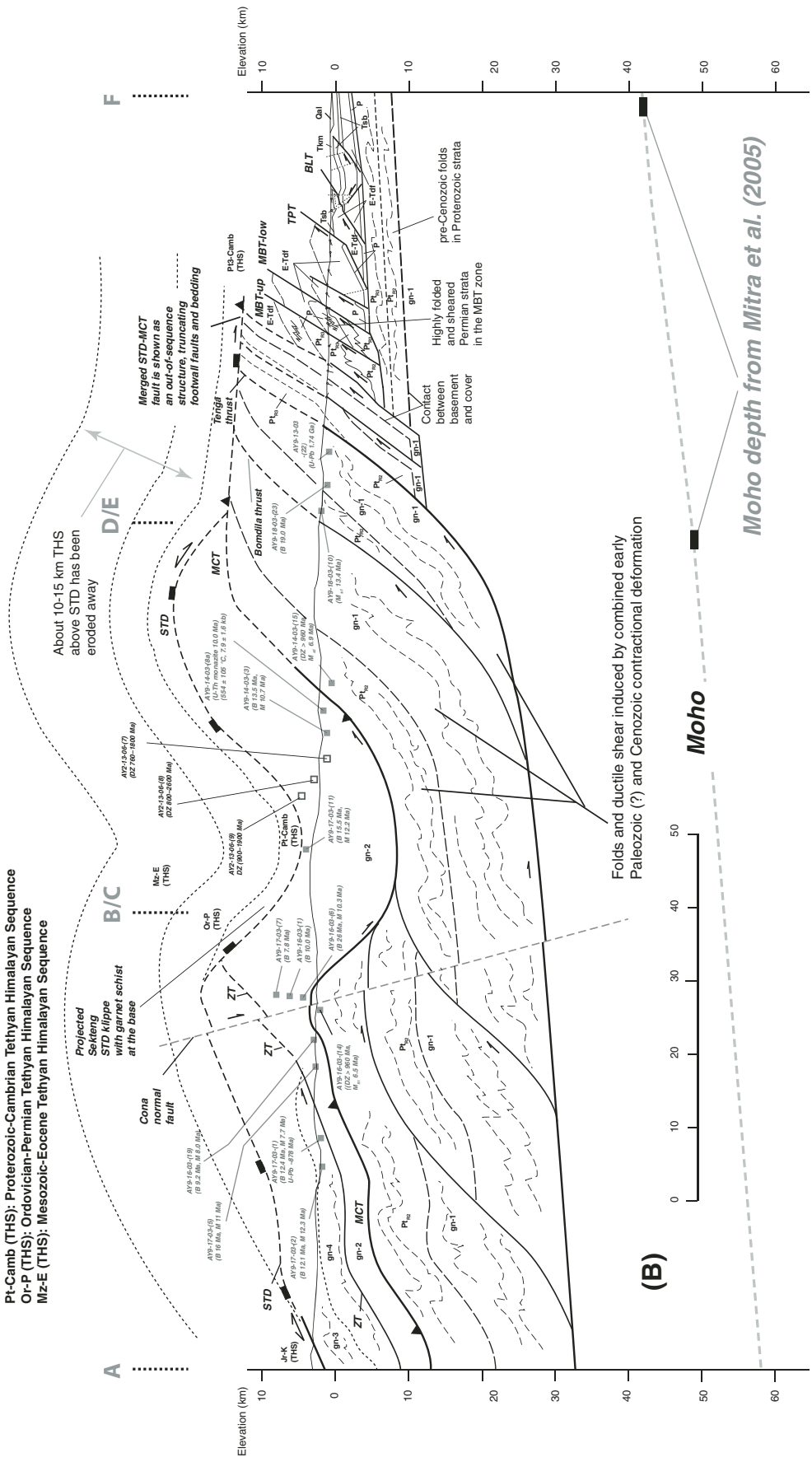

Figure 4 (*continued*). (B) Geologic cross section across the Bhalukpong-Zimithang traverse. The depth to the Moho follows that of Mitra et al. (2005), and in the cross section, we assume that the regional thrust detachment below the study area parallels the Moho. For simplicity, strong internal deformation as expressed by folding and foliation development within individual thrust sheets is not shown in the cross section. The ductile deformation could have resulted from combined early Paleozoic and Cenozoic deformation. All unit symbols are same as in A. The U-Pb zircon ages of orthogneiss, $^{40}Ar/^{39}Ar$ cooling ages of mica and biotite, U-Th age of monazite inclusions in garnet, and U-Pb detrital zircon ages are from Yin et al. (2006). South Tibetan detachment klippe in the cross section is projected along strike from the geology west of the cross-section line in A based on mapping by Bhargava (1995) and Grujic (2002).

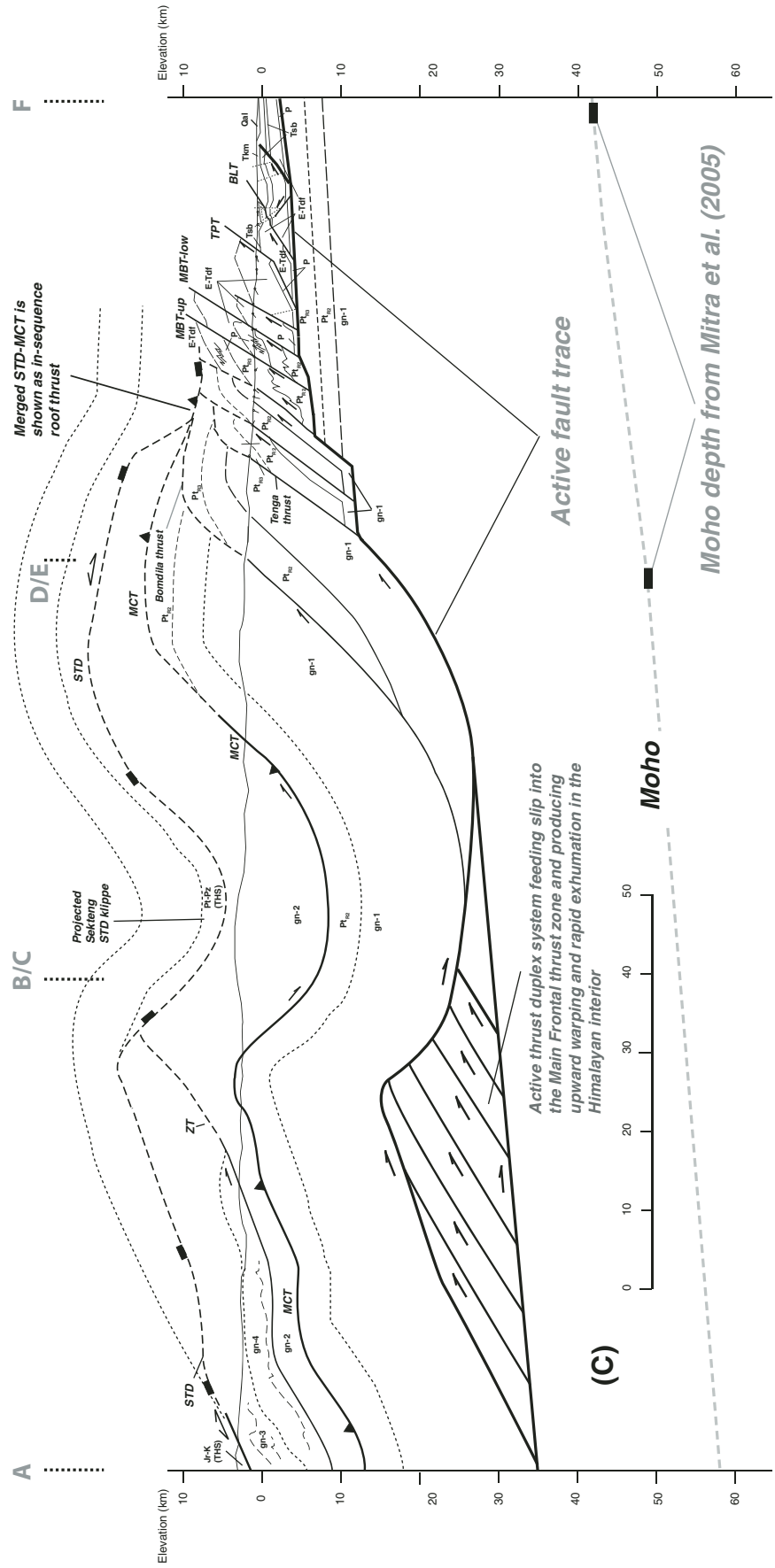

Figure 4 (*continued*). (C) An alterative geologic cross section of the Bhalukpong-Zimithang traverse, with emphasis on the role of active duplex development below the interior of the Himalaya to explain young cooling ages around the Main Central thrust window at Lum La.

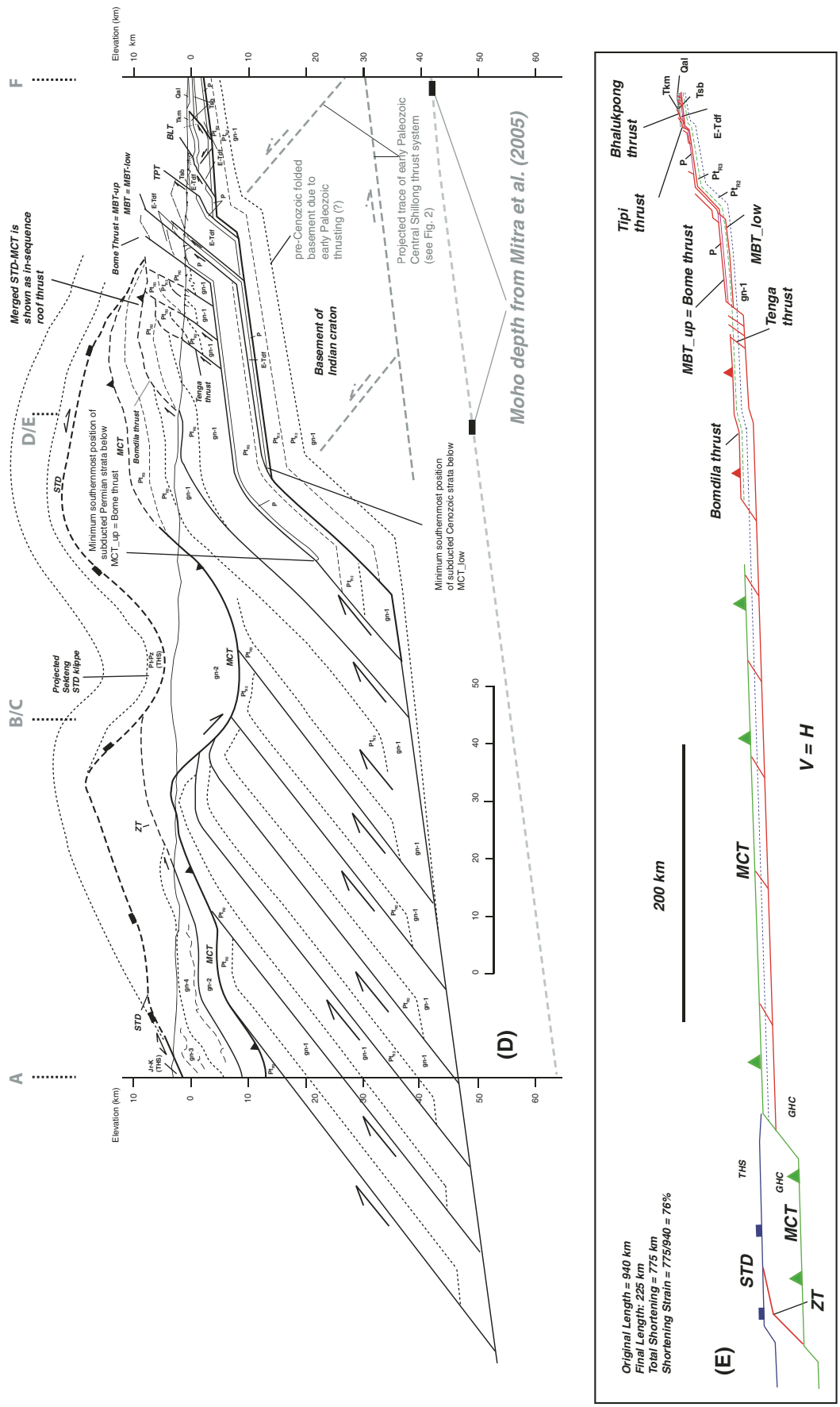

Figure 4 (*continued*). (D) Geologic cross section with emphasis on long-distance underthrusting of Permian and Tertiary strata below the Bome and Main Boundary thrusts and the existence of pre-Cenozoic basement contractional structures below the Himalaya. The unit symbols are the same as in A. (E) Restored geologic cross section in D, which yields a total shortening of 775 km equivalent to ~76% of shortening strain.

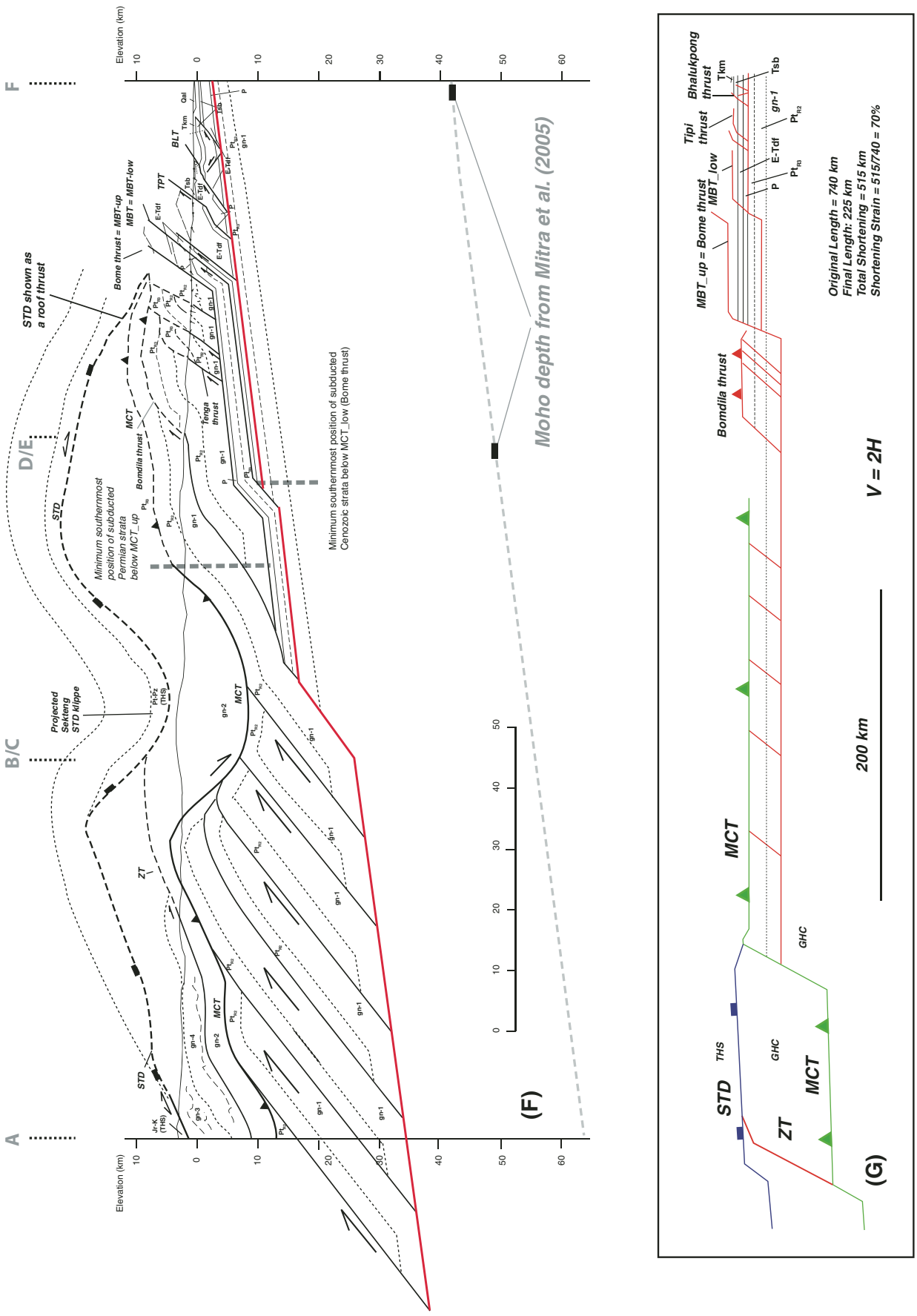

Figure 4 (*continued*). (F) Balanced cross section assuming all pre-Cenozoic strata were flat-lying and the structural relationship around the Siang window can be projected below the Bhalukpong section. (G) Restored geologic cross section shown in F, which yields a total shortening of ~515 km equivalent to ~70% shortening strain.

All the augen gneiss units we mapped are mylonitized, and kinematic indicators (S-C fabrics and asymmetric porphyroblasts) consistently indicate a top-to-the-south sense of shear (Fig. 5E). However, at one location, we observed top-to-the-north shear fabrics in an augen gneiss unit. The dominantly top-to-the-south kinematics in the augen gneiss are consistent with the regional top-to-the-south Cenozoic thrust transport direction along the Main Central and Main Boundary thrusts. As shown by our newly obtained $^{40}Ar/^{39}Ar$ cooling-age data, some of the shear fabrics in augen gneiss may have formed in the Miocene.

The trend of stretching mineral lineation in the augen gneisses varies from place to place. Directly above the upper Main Boundary thrust, the lineation trends northwest, nearly perpendicular to the local north-northeast strike of the nearby thrusts (Fig. 4A). However, higher up in the section, the stretching lineation mostly trends to the north and north-northeast directions, subparallel to the nearby northeast-striking thrusts (Fig. 4A). It is not clear whether this discrepancy in lineation trend and sense of shear was induced by local rotation of thrust sheets about vertical axes, variable fault kinematics from structure to structure (i.e., lower thrust moved southeastward while the upper thrust moved southward), or superposition of Precambrian and Cenozoic tectonism.

Main Central Thrust and its Hanging-Wall Structures

The Main Central thrust exposed in Arunachal is remarkably sharp, placing garnet schist over quartz arenite or phyllite. The classic site of Main Central thrust exposure is near Dirang along the Bhalukpong-Zimithang traverse, where a major thrust juxtaposes garnet- and kyanite-bearing gneiss and schist over phyllite, quartzite, and metavolcanic rocks of the Rupa Group (Fig. 4A) (Verma and Tandon, 1976; Kumar, 1997). There, the Main Central thrust shear zone above the Main Central thrust fault is ~100–300 m thick and characterized by isoclinally folded calc-schist and garnet-bearing quartzo-feldspathic gneiss. The folds in the hanging-wall shear zone have amplitudes of 3–5 m with fold hinges trending between N5°W and N45°W. As the fold hinges are nearly perpendicular to the northeasterly trending eastern Himalaya and subparallel to the fault striations in the N10–20°W direction in the Main Central thrust zone, the observed fold hinges may have been rotated about vertical axes nearly 90° from their original orientation perpendicular to the thrust transport direction. Shear deformation in the

Figure 5 (*on this and following page*). (A) Quartz arenite at Lum La, immediately below the Main Central thrust window. See Figure 4A for location. (B) Depositional contact between mylonitic augen gneiss below and pebble quartz arenite above. See Figure 4A for location. (C) Isoclinal folds transposing original bedding in the lower Rupa Group. See Figure 4A for location. (D) Refolded kink folds of phyllite in the Rupa Group. (E) Mylonitic augen gneiss near Bomdila with a top-to-the-south sense of shear. See Figure 4A for location. (F) Exposure of Main Central thrust fault near Lum La. See Figure 4A for location. (G) The Main Central thrust at Lum La placing garnet-kyanite gneiss over phyllite and quartzite of upper Rupa Group. See Figure 4A for location. (H) Gouge zone of the Main Central thrust near Lum La. See Figure 4A for location. (I) Cross-bedding in quartz arenite directly below the Main Central thrust. See Figure 4A for location. (J) East-dipping normal faults of the Cona rift zone cutting garnet-kyanite gneiss in the Main Central thrust hanging wall near Lum La. These faults also offset the Main Central thrust. See Figure 4A for location. (K) Greater Himalayan Crystalline Complex garnet gneiss interlayered with boudinaged leucogranites and amphibolite ~5 km east of Tawang. See Figure 4A for location. (L) Leucogranite sills interlayered with sillimanite schist at Se La Pass. See Figure 4A for location. (M) Main Central thrust fault gouge zone near Geevan on the Kimin-Geevan traverse. Asymmetric folds indicate top-to-the-south sense of motion. See Figure 6A for location. (N) Mylonitic augen gneiss (1.74 Ga) immediately above the Main Central thrust zone at the northern end of the Kimin-Geevan traverse. See Figure 6A for location.

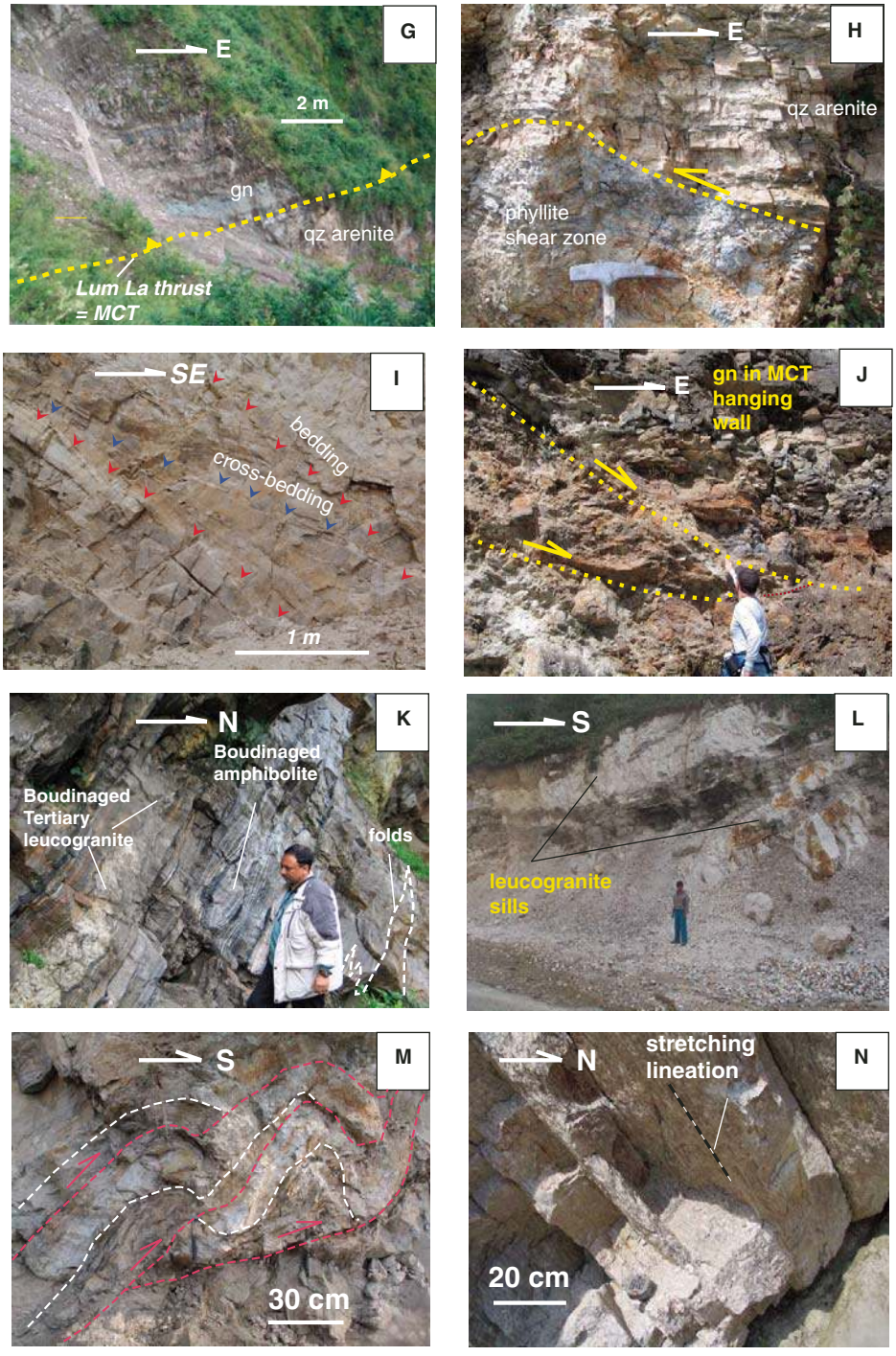

Figure 5 (*continued*).

Main Central thrust footwall near Dirang is heterogeneous. A 40–50-m-thick sequence of quartz arenite lying directly below the fault is little deformed, while the weaker phyllite structurally farther below the arenite displays numerous discrete 5–10-m-thick shear zones with faint downdip stretching lineation over a distance of 200–250 m below the arenite.

The Main Central thrust is also exposed as a thrust window near Lum La (Fig. 4A) (Yin et al., 2006). There, the fault is knife sharp (Fig. 5E) and places garnet schist and quartzofeldspathic gneiss over a 40-m-thick quartz arenite unit (i.e., the marker bed dividing the upper and middle Rupa Group) (Fig. 4A). The Main Central thrust lies parallel to the foliation and bedding above and below (Fig. 5G), and the fault is expressed by a 0.3–0.5-m-thick black gouge zone (Fig. 5E). The quartz arenite is only mildly deformed by small-scale kink folds induced by a minor south-directed ramp-flat thrust (Fig. 5A). The quartz arenite beds also exhibit well-preserved cross-bedding sedimentary structures (Fig. 5I). In contrast to the little deformed quartz arenite, a shear zone, ~5 m thick, in phyllite was developed immediately below. It contains a well-developed stretching lineation trending N30–50°W (Fig. 5H) and numerous small southeast-verging folds trending N30–75°E, perpendicular to the stretching lineation. These observations suggest that strain distribution across the Main Central thrust shear zone is uneven, depending on the mechanical properties of the lithologic units. Thus, using the maximum strain alone as a criterion to define the location of the Main Central thrust can be misleading (cf. Searle et al., 2008).

Several north-striking and east-dipping normal faults offset the Main Central thrust between 5 m and 200 m (Fig. 5J). We interpret these faults to be parts of the north-trending Cona rift zone extending from southeastern Tibet to the Himalaya (Armijo et al., 1986; Yin, 2000; Taylor et al., 2003) (Figs. 2 and 4A). Although the initiation age of the Cona rift zone is unconstrained, the aforementioned relationships suggest that the Main Central thrust is no longer active, and east-west extension postdated motion on the Main Central thrust.

The east-trending Se La synclinorium folds the South Tibet detachment and its hanging-wall strata above and the Main Central thrust and its footwall rocks below (Fig. 4B). The presence of the Se La synclinorium allows us to examine a change in metamorphic petrology and the prevalence of Tertiary leucogranites across a tilted section in the Main Central thrust hanging wall. At the base of the Main Central thrust hanging wall near Dirang and Lum La, phyllitic schist immediately above the Main Central thrust contains kyanite and minor Tertiary leucogranites ranging in size from tens of centimeters to a few meters, with total volume less than 1% (Fig. 5K). At higher structural levels, the size of the leucogranites increases to 20–40 m thick and >100 m long (Fig. 5L), and this increase is associated with the appearance of sillimanite. The total volume of the leucogranite is ~3%–5%. An increase in the size of the Tertiary leucogranites in the Main Central thrust hanging wall may be a function of strain, since the size of the leucogranites increases as the bedding-parallel stretching strain decreases upward. The upward decrease in strain is expressed by the highly boudinaged leucogranites at lower structural levels (Fig. 5K) and undeformed leucogranites

crosscutting gneissic foliation at higher structural levels (Fig. 5L). Alternatively, the lack of deformation of leucogranites at higher structural levels could be related to their younger ages as observed in the Bhutan Himalaya (e.g., Swapp and Hollister, 1991; Daniel et al., 2003; Hollister and Grujic, 2006). This interpretation applied to the Arunachal Himalaya requires the early deformed Tertiary leucogranites to be cut by the later undeformed leucogranites at higher structural levels, a relationship we did not see along our traverse. The presence of the boudinaged Tertiary leucogranites in the Main Central thrust hanging-wall gneisses suggests that the rock experienced significant foliation-parallel stretching in the Cenozoic. As the foliation is parallel to the Main Central thrust at both the Dirang and Lum La locations, it suggests that the Main Central thrust sheet experienced, at least at a local scale, a significant fault-perpendicular flattening strain. We relate this strain to mesoscopic folding widespread in the Main Central thrust hanging wall.

The Zimithang ductile thrust zone is exposed at the highest structural level in the northern end of our traverse, where it places a mylonitic augen gneiss (U-Pb zircon age of 878 Ma, see following) over garnet-biotite and quartzo-feldspathic gneisses. This shear zone at the Arunachal-Bhutan border lies along the strike of the Kakthang thrust mapped by Gansser (1983) and Grujic et al. (2002) immediately to the west in Bhutan (Fig. 4A), suggesting that the shear zones are parts of the same structure. Like the Kakthang shear zone, S-C fabric and asymmetric porphyroblasts in the Zimithang zone indicate a top-to-the-south sense of shear. Stretching lineation in the shear zone trends between N10°E and N45°W perpendicular to the strike of the fault (Fig. 4A). The 878 Ma augen gneiss intrudes into garnet schist and quartzo-feldspathic gneiss in the Greater Himalayan Crystalline Complex. This relationship is expressed by: (1) irregular geometry of the contact between the augen gneiss and its surrounding paragneisses, and (2) the augen gneiss unit, which contains numerous xenoliths of the intruded garnet schist that is identical to the country rocks. The intrusive relationship suggests that some of the Greater Himalayan Crystalline Complex metasedimentary rocks were deposited and metamorphosed(?) prior to 870 Ma.

Kimin-Geevan Traverse

The Kimin-Geevan traverse exposes from south to north the Main Frontal thrust zone, the Tipi thrust, the Main Boundary thrust zone, and the Main Central thrust (Fig. 6A). We describe the faults and their hanging-wall structures next.

Main Frontal Thrust Zone and the Hanging-Wall Structures

The Main Frontal thrust zone consists of an eastward-growing and eastward-plunging anticlinorium that folds coarse-grained sandstone and conglomerate beds of the Pleistocene Kimin Formation along its south limb and the Pliocene Subansiri Formation along its north limb (Figs. 2 and 6A). The eastward fold growth in the Main Frontal thrust zone is expressed in the eastern Himalaya by eastward deflection of south-flowing rivers, a subject that will be discussed in detail elsewhere.

The Tipi thrust is the most dominant structure in the Main Frontal thrust hanging wall, which lies structurally above the active fold belt (Fig. 6A). It places the Miocene Dafla Formation over the Pliocene Subansiri Formation. The latter forms a tight and south-verging syncline directly below the thrust. Two top-to-the-northwest back thrusts are present in the hanging wall of the Tipi thrust and bound a pair of synclines and anticlines (Fig. 6A). The lateral extent and the magnitude of slip on the two back thrusts are unknown.

Main Boundary Thrust

The Main Boundary thrust zone places an augen gneiss unit over the Miocene Dafla Formation. A thrust sliver, ~200 m thick and consisting of sandstone and siltstone, is present in the fault zone (Fig. 6A). Beds in the sliver are deformed by isoclinal folds and outcrop-scale thrust duplexes. The thrust sliver may be the lower part of the Dafla Formation that thrusts over the upper part of the same unit or part of the Permian sequence. We correlate the upper bounding fault with the upper fault of the Main Boundary thrust zone in the Bhalukpong area and the Bome fault in the western Siang window area.

The Main Boundary thrust hanging wall is composed of isoclinally folded low-grade metagraywacke strata (Fig. 6A). Quartz arenite and phyllite are present locally in the northern part of the traverse, which is similar in lithology and sedimentary structures to the marker bed dividing the upper and middle Rupa Group along the Bhalukpong-Zimithang traverse. Despite this correlation, the graywacke unit differs from the middle Rupa Group in that it is coarse-grained and rich in detrital feldspars and lithic fragments. Since the metagraywacke unit lies below the middle Rupa Group observed across the Bhalukpong-Zimithang traverse, we assign this unit to be the lower member of the Rupa Group (Pt_{R1}) (Fig. 6A). This part of the Rupa Group is missing in the Bhalukpong-Zimithang traverse (Fig. 4).

Main Central Thrust

The position of the Main Central thrust along the Kimin-Geevan Road has been debated. Kumar (1997) placed the fault in the interior of the Himalaya, north of latitude 28°20′N, directly south of the Himalayan crest line, while Singh and Chowdhary (1990) interpreted the thrust to lie significantly to the south near Hapoli (~27.20°N) (Fig. 6A). Specifically, Singh and Chowdhary (1990) envisioned the Main Central thrust to be a folded low-angle fault with a large half window opening to the west. We attribute the confusion of locating the Main Central thrust to the difficulties of assigning the structural positions of the orthogneiss with similar lithology and structural fabrics in the Main Central thrust hanging wall and footwall (Kumar, 1997). This problem is compounded by the lack of age constraints and detailed mapping in the area. We took three approaches to overcome these problems. First, we used the appearance of Tertiary leucogranites as a proxy for the presence of the high-grade Main Central thrust hanging-wall rocks; this correlation was well established along the well-exposed Bhalukpong-Zimithang traverse (Yin et al., 2006; this study). Second, we used the occurrence of an abrupt change in metamorphic grade to indicate the position of the Main Central thrust. In these cases, the Main Central thrust places garnet-bearing schist or quartzo-feldspathic gneiss over low-grade metagraywacke. Third, we examined shear-zone deformation and variation of strain to support the inferred position of the Main Central thrust in the field. Using these criteria, we found that the Main Central thrust displays a small full klippe and a small half klippe in the north and a large west-facing half window in the south (Fig. 6A). This pattern is quite similar to the geometry of the Main Central thrust in Nepal (e.g., Brunel, 1986; DeCelles et al., 2001) and NW Indian Himalaya (Thakur, 1998; Yin, 2006; Webb et al., 2007), suggesting that the fault is a folded structure along the entire Himalaya. The north-south width of the exposed Main Central thrust requires a minimum of 60 km slip on the Main Central thrust along this traverse (Fig. 6B).

Near Geevan, the Main Central thrust is a sharp contact placing garnet-biotite schist over the metagraywacke unit. The fault zone is composed of a fine-grained gouge zone associated with southeast-verging folds (Fig. 5M). Directly above the thrust, there is a mylonitic shear zone involving garnet-biotite schist and an orthogneiss unit (Fig. 5N) (U-Pb zircon age of 1752 Ma; see Geochronology section) (Fig. 6A). Stretching lineation trends north-northwest in the Main Central thrust zone (Fig. 6A). The footwall metagraywacke unit near Geevan is folded, and hinges trend northeast and are locally sheared with a northwest-trending stretching lineation (Fig. 6A).

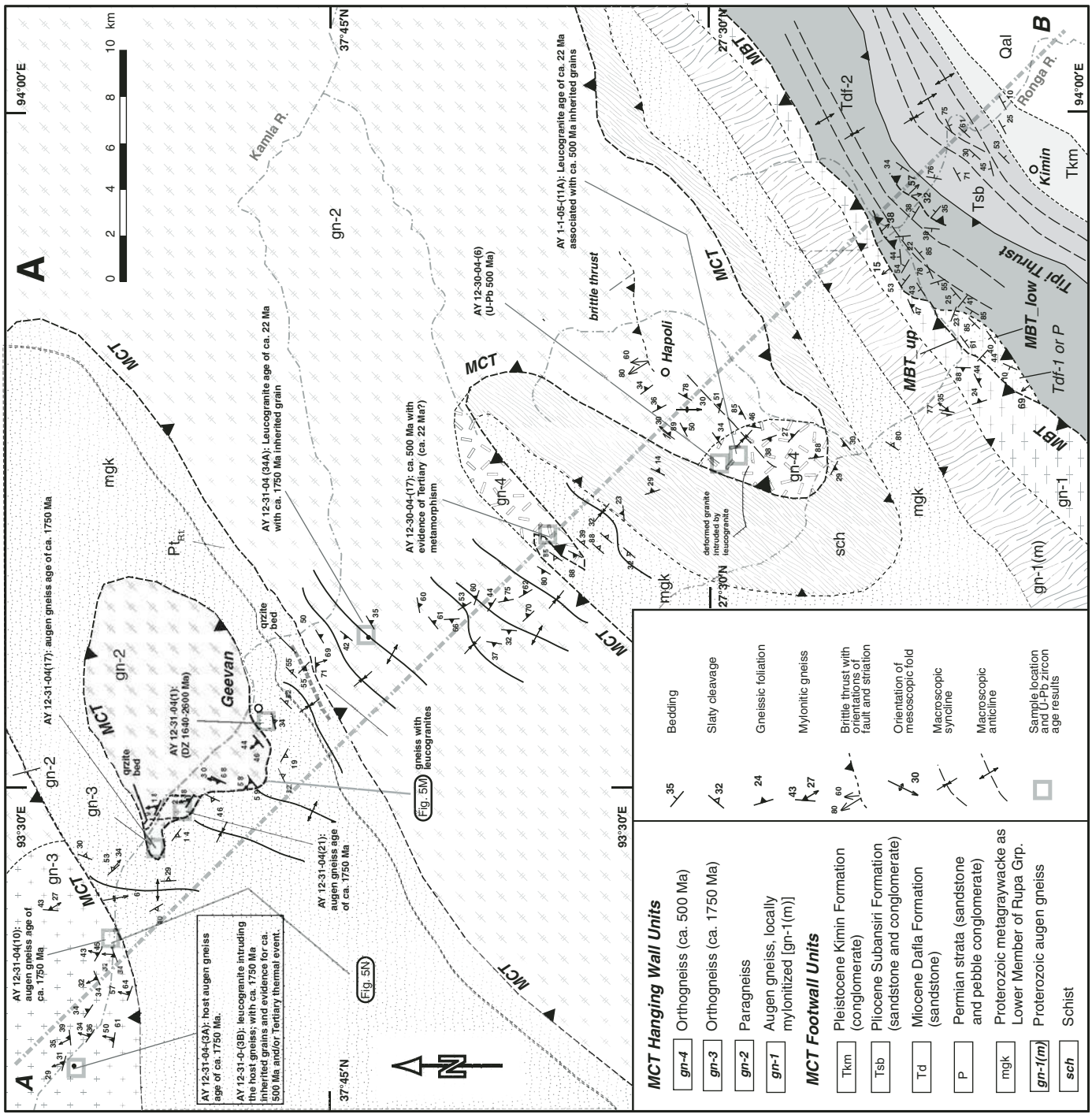

Figure 6 (*on this and following page*). (A) Geological map of the Kimin-Geevan traverse. Line A-B represents the location of cross section shown in B. See Figure 2 for location of the map area. Sample and field photograph locations discussed in the text are also shown. (B) A possible cross section along the Kimin-Geevan traverse. Unit Pt_{Rp1} represents the Lower Member of the Rupa Group, equivalent to unit *mgk*. Unit $Pt_{Rp2/3}$ represents the Middle and Upper Members of the Rupa Group that are not exposed in the Kimin-Geevan traverse.

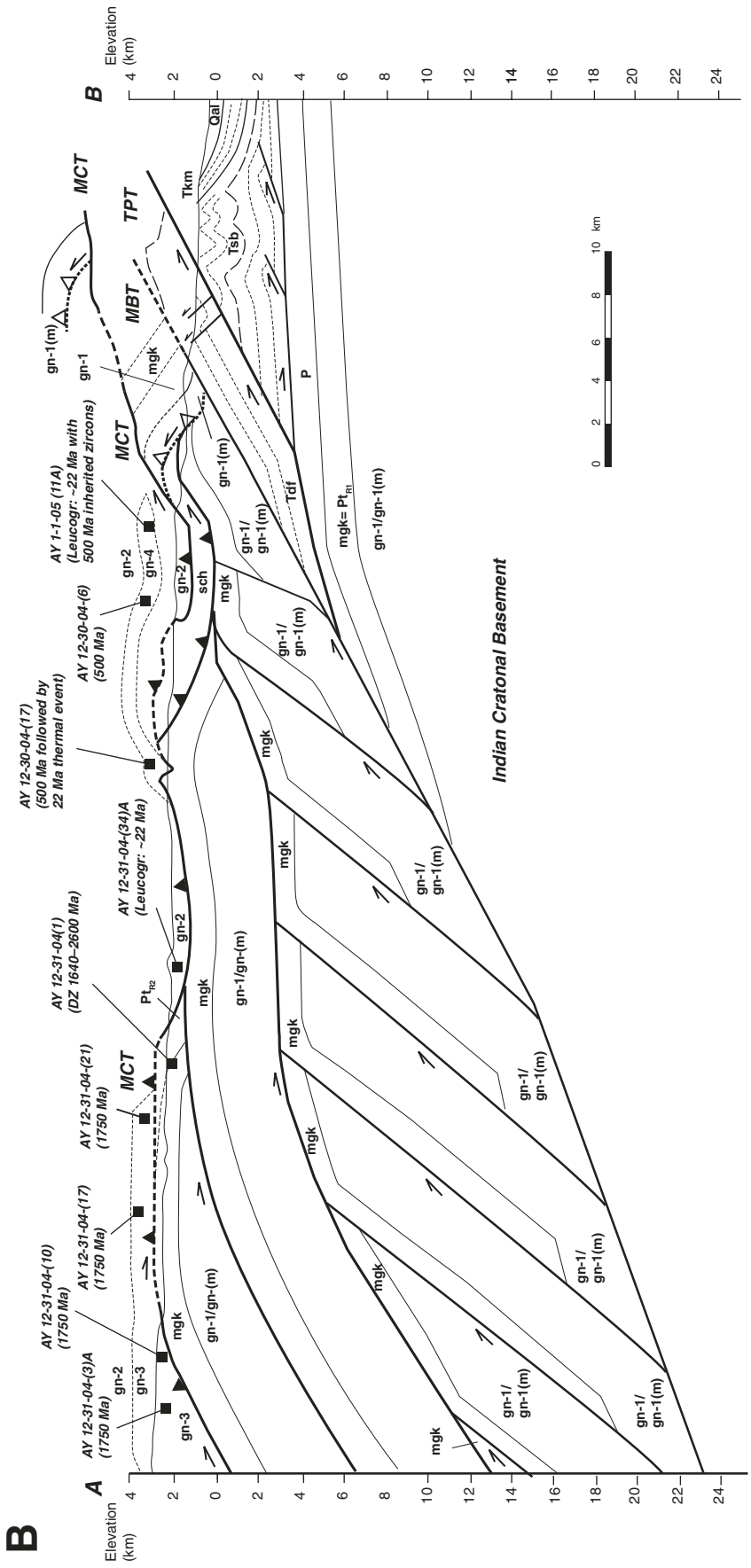

Figure 6 (*continued*). (B) A possible cross section along the Kimin-Geevan traverse. Unit Pt$_{Rp1}$ represents the Lower Member of the Rupa Group, equivalent to unit *mgk*. Unit Pt$_{Rp2/3}$ represents the Middle and Upper Members of the Rupa Group that are not exposed in the Kimin-Geevan traverse.

U-Pb ZIRCON DATING

Methods

We conducted U-Pb spot dating of zircons from orthogneiss and leucogranite samples collected from the Bhalukpong-Zimithang and Kimin-Geevan traverses using the Cameca 1270 ion microprobe at the University of California–Los Angeles (UCLA). The analytical procedure follows that of Quidelleur et al. (1997). All of the analyses were conducted using an 8–15 nA O^- primary beam and an ~25-µm-diameter spot size. U-Pb ratios were determined using a calibration curve based on UO/U versus Pb/U from zircon standard AS3 (age 1099.1 Ma; Paces and Miller, 1993). We collected our age data during four analytical sessions, each of which has a different calibration curve over distinct ranges in UO/U values (see notes in Table 1 for the range of UO/U values). We also adjusted isotopic ratios for common Pb corrections following Stacey and Kramers (1975). We calculated concentrations of U by comparison with zircon standard 91500, which has a U concentration of 81.2 ppm (Wiedenbeck et al., 2004). Data reduction was accomplished via the in-house program ZIPS 3.0.3 written by Dr. Chris Coath.

Results

We analyzed 11 samples, among which two are augen gneiss from the Bhalukpong-Zimithang traverse, six are orthogneiss from the Kimin-Geevan traverse, and three are leucogranites from the Kimin-Geevan traverse. We described the results in detail next.

Orthogneiss from the Bhalukpong-Zimithang Traverse

Sample AY 09–13–03-(22) was collected from mylonitic augen gneiss of the Paleoproterozoic Bomdila Group of Kumar (1997) (Fig. 3) in the Main Central thrust footwall (Fig. 4A). We analyzed 13 different zircons and obtained a weighted mean $^{207}Pb/^{206}Pb$ age of 1743 ± 4 Ma (2σ) by excluding one inherited grain and two very discordant analyses (Fig. 7A; Table 1). Sample AY 9–17–03-(1) was collected from mylonitic augen gneiss in the Zimithang shear zone above the Main Central thrust (Fig. 4A). Fourteen zircons were analyzed, 10 of which lie on or just above the concordia and form a cluster with a weighted mean $^{206}Pb/^{238}U$ age of 878 ± 12.6 Ma (Fig. 7B; Table 1). Two zircons yielded younger ages that lie along the concordia at ca. 627.6 Ma (mean square of weighted deviates [MSWD] = 0.8) (Fig. 7B). The younger ages correspond to low Th/U ratios (Table 1) typical for metamorphic zircons (e.g., Ding et al., 2001; Mojzsis and Harrison, 2002). We interpret the 878 Ma age to represent the time of crystallization for the pluton and the younger age of 627 Ma to represent a later metamorphic event.

Orthogneiss from the Kimin-Geevan Traverse

Sample AY 12–30–04-(6) was from an orthogneiss unit in the Main Central thrust hanging wall near Hapoli (Fig. 6A). We obtained 17 spot analyses on 15 zircons (Fig. 8A). Fifteen of the analyses yielded $^{207}Pb/^{206}Pb$ ages ranging from 460.5 Ma to 546.1 Ma, and a weighted mean age of 504.9 ± 8.3 Ma (2σ). These 15 analyses are concordant or reversely discordant on the U-Pb concordia plot; the increased reverse discordance is associated with higher U concentrations (Table 1). The other two analyses yielded $^{207}Pb/^{206}Pb$ ages of 836.9 ± 13.2 Ma and 730.2 ± 13.1 Ma (1σ) and plot along the concordia. Th/U ratios of all of the above analyses are >0.01, with more than half of them over 0.1 (Table 1). The grain that yielded the 826 Ma age is subhedral, and its cathodoluminescence image shows distinct domains without clear definition of the core from the rim. A spot yielding the 836.9 ± 13.2 Ma $^{207}Pb/^{206}Pb$ age corresponds to a high Th/U ratio of 0.419 and is typical of igneous origin (e.g., Ding et al., 2001; Mojzsis and Harrison, 2002). Another spot analysis from the same grain yielded a reversely discordant result with a 505.8 ± 8.3 Ma $^{207}Pb/^{206}Pb$ age; it corresponds to a low Th/U ratio of 0.034 and a UO/U ratio below the range of the calibration (Table 1). The dominant age population of 15 out of 17 analyses and moderate-to-high Th/U ratios all indicate that the crystallization age of the augen gneiss is ca. ~505 Ma, with one inherited grain at 836 Ma. Because an 825 Ma pluton exists in the Bhutan Himalaya, and an 878 Ma augen gneiss is present in the Bhalukpong-Zimithang traverse, the 836 Ma zircon may have come from a pluton emplaced during the same igneous event and was later intruded by the 505 Ma pluton.

Sample AY 12–31–04-(3A) was collected from a mylonitic augen gneiss unit in the Main Central thrust hanging wall (Fig. 6A). Of the 15 total analyses from 15 zircons, 13 yielded $^{207}Pb/^{206}Pb$ ages ranging from 1703 Ma to 1780 Ma, with a weighted mean age of 1752 ± 12 Ma (2σ) (Fig. 8B). Of these 13 analyses, the one with the lowest Th/U ratio (0.038) is strongly discordant, plotting along a discordia line with a projected intersection of a Phanerozoic age along the concordia curve. The remaining two analyses have $^{207}Pb/^{206}Pb$ ages of 1921 ± 13 Ma and 2515 ± 12 Ma (2σ); while the younger analysis is nearly concordant, the older one is strongly discordant. We consider these analyses to represent older wall-rock zircons assimilated during emplacement of the granitoid at ca. 1752 Ma. The discordant, low Th/U analysis hints at a Phanerozoic metamorphic event.

We analyzed six spots of different zircons from sample AY 12–30–04-(17) collected from an augen gneiss unit directly above the Main Central thrust (Fig. 6A). The results form a discordia line with intercepts on the concordia at 28 ± 13 Ma (2σ) and 512 ± 14 Ma (MSWD = 1.3). Four spot ages cluster near the upper intercept, one plots near the lower intercept with a low Th/U value, and one plots between the two age groups (Figs. 8C). We interpret these results to indicate crystallization of the augen gneiss at ca. 512 Ma, which was succeeded by a thermal event at ca. 28 Ma.

Sample AY 12–31–04-(17) was from mylonitic augen gneiss in the Main Central thrust footwall (Fig. 6A). We acquired five spot analyses from different zircons. Three analyses cluster together along the concordia, yielding a weighted mean $^{207}Pb/^{206}Pb$ age of 1747 ± 7 Ma (2σ) (Fig. 8D). The other two ages are discordant, potentially drawn down from ca. 1750 Ma toward the Phanerozoic portion of the concordia. We interpret these results to indicate crystallization of the granitic protolith at ca. 1747 Ma and a later Late Proterozoic or Phanerozoic Pb-loss event that may correlate with metamorphism.

We analyzed five spots of different zircons from sample AY 12–31–04-(21) collected from a biotite-quartz mylonitic granitoid that lies directly above the Main Central thrust in the Geevan klippe (Fig. 6A). Four analyses clustering on the concordia yielded a weighted mean $^{207}Pb/^{206}Pb$ age of 1743 ± 7 Ma (2σ) (Fig. 8E). One spot age was slightly older, showing a $^{207}Pb/^{206}Pb$ age of 1939 ± 9 Ma (2σ). We interpret these results to indicate crystallization of the granitic protolith at ca. 1743 Ma, with the single older age representing an inherited component.

Sample AY 12–31–04-(10) was from an augen gneiss directly above the Main Central thrust and north of sample AY 12–31–04-(21) (Fig. 6A). We acquired four spot analyses from different zircons. Three analyses cluster on the concordia and indicate a weighted mean $^{207}Pb/^{206}Pb$ age of 1772 ± 6 Ma (2σ) (Fig. 8F). We interpret these results to indicate crystallization of the granitic protolith at ca. 1772 Ma. Based on the similar ages and proximity of samples AY 12–31–04-(10) and AY 12–31–04-(21), we interpret the mylonitic orthogneiss represented by the two samples to have been parts of the same unit defining the Main Central thrust shear zone (Fig. 6A).

TABLE 1. ION MICROPROBE U-(Th)-Pb ZIRCON DATA

Spot ID[#]	Isotopic ratios										Ages (Ma ±1 s.e.)[§]		
	$^{206}Pb^*/^{238}U$	±1 s.e.[§]	$^{207}Pb^*/^{235}U$	±1 s.e.[§]	$^{207}Pb^*/^{206}Pb^*$	±1 s.e.[§]	$^{206}Pb^*$ (%)	U (ppm)	U O / U	Th/ U	$^{206}Pb^*/^{238}U$	$^{207}Pb^*/^{235}U$	$^{207}Pb^*/^{206}Pb^*$
								U-Pb calibration established for U O / U values of:	8.5–9.4[†]				
(1) AY 09-13-03 22													
1, a	2.60E–01	1.07E–02	3.78E+00	1.55E–01	1.05E–01	5.22E–04	99.59	1.23E+03	8.67	0.014	1489.0 ± 54.8	1587.0 ± 33.0	1721.0 ± 9.1
2, a	3.94E–01	1.61E–02	8.94E+00	3.68E–01	1.65E–01	1.05E–03	99.41	2.95E+02	8.80	0.207	2141.0 ± 74.6	2332.0 ± 37.6	2503.0 ± 10.8
3, a	3.04E–01	1.21E–02	4.46E+00	1.75E–01	1.06E–01	9.48E–04	99.38	3.62E+02	8.86	0.467	1713.0 ± 59.8	1723.0 ± 32.5	1736.0 ± 16.4
4, a	2.08E–01	8.27E–03	2.94E+00	1.17E–01	1.02E–01	3.16E–04	99.75	1.59E+03	8.66	0.153	1219.0 ± 44.1	1392.0 ± 30.2	1668.0 ± 5.7
6, a	2.76E–01	1.01E–02	4.08E+00	1.51E–01	1.07E–01	6.47E–04	99.57	8.90E+02	8.93	0.112	1572.0 ± 51.0	1650.0 ± 30.3	1751.0 ± 11.1
7, a	2.49E–01	9.06E–03	3.65E+00	1.35E–01	1.06E–01	7.39E–04	99.67	1.00E+03	8.98	0.137	1433.0 ± 46.8	1560.0 ± 29.4	1736.0 ± 12.8
8, a	1.89E–01	6.42E–03	2.69E+00	1.00E–01	1.03E–01	1.33E–03	98.79	4.27E+02	9.37	0.422	1115.0 ± 34.8	1327.0 ± 27.6	1687.0 ± 23.7
9, a	2.54E–01	8.86E–03	3.76E+00	1.33E–01	1.07E–01	7.52E–04	99.44	6.68E+02	9.10	0.169	1458.0 ± 45.5	1584.0 ± 28.3	1756.0 ± 12.8
10, a	2.82E–01	1.06E–02	4.09E+00	1.59E–01	1.05E–01	9.48E–04	99.27	7.58E+02	9.06	0.145	1602.0 ± 53.1	1652.0 ± 31.7	1717.0 ± 16.6
11, a	3.10E–01	1.12E–02	4.55E+00	1.69E–01	1.07E–01	8.15E–04	99.47	7.24E+02	9.04	0.174	1739.0 ± 55.2	1741.0 ± 30.9	1743.0 ± 14.0
12, a	2.73E–01	9.75E–03	3.97E+00	1.43E–01	1.06E–01	6.32E–04	99.49	8.51E+02	9.06	0.138	1554.0 ± 49.4	1628.0 ± 29.3	1724.0 ± 11.0
13, a	2.75E–01	9.36E–03	4.15E+00	1.44E–01	1.10E–01	6.52E–04	99.54	4.14E+02	9.28	0.166	1565.0 ± 47.3	1665.0 ± 28.5	1792.0 ± 10.8
								U-Pb calibration established for U O / U values of:	9–9.9[†]				
(3) AY 12-30-04-(6)													
1, a	8.60E–02	3.04E–03	6.84E–01	2.49E–02	5.77E–02	8.17E–04	99.9	5.33E+02	9.06	0.483	532.1 ± 18.0	529.4 ± 15.0	517.8 ± 31.1
2, a	1.06E–01	3.80E–03	8.38E–01	2.99E–02	5.72E–02	1.98E–04	100.0	9.18E+03	9.00	0.027	650.5 ± 22.1	617.8 ± 16.5	499.8 ± 7.6
3, a	8.28E–02	2.85E–03	6.57E–01	2.28E–02	5.76E–02	4.32E–04	99.9	1.20E+03	9.19	0.429	512.5 ± 17.0	512.9 ± 13.9	514.5 ± 16.5
4, a	8.04E–02	2.53E–03	6.23E–01	2.08E–02	5.62E–02	8.76E–04	99.9	5.10E+02	9.92	0.206	498.4 ± 15.1	491.7 ± 13.0	460.5 ± 34.5
5, a	9.00E–02	2.87E–03	7.15E–01	2.30E–02	5.76E–02	2.12E–04	100.0	5.87E+03	9.30	0.073	555.7 ± 17.0	547.9 ± 13.6	515.7 ± 8.1
6, a	1.00E–01	3.08E–03	8.06E–01	2.49E–02	5.84E–02	2.99E–04	100.0	2.62E+03	9.48	0.137	614.8 ± 18.1	600.4 ± 14.0	546.1 ± 11.2
7, a	8.46E–02	2.89E–03	6.61E–01	2.40E–02	5.66E–02	6.76E–04	99.9	9.95E+02	9.19	0.400	523.7 ± 17.2	515.2 ± 14.7	477.3 ± 26.4
8, a	1.37E–01	4.72E–03	1.27E+00	4.47E–02	6.70E–02	4.26E–04	99.9	1.00E+03	9.22	0.419	829.2 ± 26.7	831.3 ± 20.0	836.9 ± 13.2
8, b	1.17E–01	4.64E–03	9.24E–01	3.73E–02	5.74E–02	2.17E–04	100.0	8.40E+03	8.69	0.034	712.4 ± 26.8	664.6 ± 19.7	505.8 ± 8.3
9, a	7.90E–02	2.48E–03	6.17E–01	1.94E–02	5.66E–02	2.36E–04	100.0	5.93E+03	9.40	0.083	490.0 ± 14.8	487.7 ± 12.2	476.8 ± 9.2
10, a	9.13E–02	2.61E–03	7.22E–01	2.08E–02	5.74E–02	2.68E–04	100.0	8.24E+03	9.73	0.021	562.9 ± 15.4	551.9 ± 12.2	506.8 ± 10.3

(*Continued*)

TABLE 1. ION MICROPROBE U-(Th)-Pb ZIRCON DATA (*Continued*)

Spot ID[#]	Isotopic ratios										Ages (±1 s.e.)[§]		
	$^{206}Pb^*/^{238}U$	±1 s.e.[§]	$^{207}Pb^*/^{235}U$	±1 s.e.[§]	$^{207}Pb^*/^{206}Pb^*$	±1 s.e.[§]	$^{206}Pb^*$ (%)	U (ppm)	U O / U	Th/U	$^{206}Pb^*/^{238}U$	$^{207}Pb^*/^{235}U$	$^{207}Pb^*/^{206}Pb^*$
11, a	1.18E–01	3.60E–03	1.04E+00	3.20E–02	6.37E–02	3.95E–04	99.9	1.68E+03	9.55	0.100	719.8 ± 20.7	722.3 ± 16.0	730.2 ± 13.1
12, a	9.24E–02	3.36E–03	7.34E–01	2.81E–02	5.77E–02	5.08E–04	100.0	6.23E+03	9.76	0.220	569.6 ± 19.8	559.1 ± 16.4	516.7 ± 19.3
13, a	9.21E–02	2.45E–03	7.26E–01	1.93E–02	5.72E–02	1.21E–04	100.0	1.01E+04	9.99	0.058	567.7 ± 14.4	554.2 ± 11.3	499.1 ± 4.7
14, a	8.59E–02	2.67E–03	6.77E–01	2.32E–02	5.71E–02	5.96E–04	100.0	9.30E+02	9.54	0.376	531.4 ± 15.9	524.9 ± 14.0	497.0 ± 23.0
3, b	8.94E–02	2.66E–03	7.11E–01	2.15E–02	5.77E–02	3.04E–04	100.0	3.75E+03	9.60	0.350	551.8 ± 15.8	545.1 ± 12.8	517.2 ± 11.6
15, a	9.01E–02	2.70E–03	7.14E–01	2.15E–02	5.75E–02	2.48E–04	100.0	4.60E+03	9.55	0.031	555.8 ± 16.0	547.3 ± 12.7	512.1 ± 9.5
(4) AY 12-31-04 3A								*U-Pb calibration established for U O / U values of:*	9–9.9[†]				
1, a	3.63E–01	1.36E–02	5.89E+00	2.31E–01	1.18E–01	8.37E–04	99.6	3.03E+02	9.23	0.675	1998.0 ± 64.3	1960.0 ± 34.0	1921.0 ± 12.8
2, a	2.88E–01	9.45E–03	4.33E+00	1.42E–01	1.09E–01	5.18E–04	99.7	1.24E+03	9.34	0.051	1633.0 ± 47.3	1698.0 ± 27.1	1780.0 ± 8.7
3, a	3.10E–01	1.02E–02	4.60E+00	1.51E–01	1.08E–01	4.14E–04	99.9	1.72E+03	9.24	0.078	1743.0 ± 50.4	1749.0 ± 27.4	1757.0 ± 7.0
4, a	3.17E–01	1.06E–02	4.68E+00	1.56E–01	1.07E–01	7.45E–04	99.7	4.45E+02	9.31	0.242	1777.0 ± 51.9	1764.0 ± 27.9	1750.0 ± 12.7
5, a	3.27E–01	1.20E–02	4.79E+00	1.80E–01	1.06E–01	6.57E–04	99.7	3.88E+02	9.27	0.717	1825.0 ± 58.4	1783.0 ± 31.6	1734.0 ± 11.4
6, a	2.24E–01	7.21E–03	3.27E+00	1.06E–01	1.06E–01	3.71E–04	99.9	3.33E+03	9.30	0.038	1301.0 ± 38.0	1474.0 ± 25.1	1732.0 ± 6.4
7, a	3.90E–01	1.39E–02	8.92E+00	3.16E–01	1.66E–01	1.21E–03	99.7	3.46E+02	9.53	0.370	2125.0 ± 64.2	2330.0 ± 32.3	2515.0 ± 12.2
8, a	3.36E–01	1.26E–02	5.02E+00	2.11E–01	1.08E–01	1.67E–03	99.4	1.82E+02	9.28	0.420	1868.0 ± 60.5	1823.0 ± 35.5	1772.0 ± 28.1
9, a	2.97E–01	8.65E–03	4.39E+00	1.31E–01	1.07E–01	5.98E–04	99.8	8.85E+02	9.77	0.173	1676.0 ± 43.0	1711.0 ± 24.6	1753.0 ± 10.2
10, a	3.24E–01	9.11E–03	4.83E+00	1.37E–01	1.08E–01	3.06E–04	99.9	1.62E+03	9.81	0.067	1808.0 ± 44.4	1790.0 ± 23.8	1769.0 ± 5.2
11, a	3.07E–01	9.87E–03	4.42E+00	1.44E–01	1.04E–01	9.86E–04	99.5	5.70E+02	9.71	0.195	1726.0 ± 48.7	1716.0 ± 27.0	1703.0 ± 17.4
12, a	3.23E–01	1.05E–02	4.73E+00	1.67E–01	1.06E–01	1.12E–03	99.5	6.32E+02	9.67	0.222	1806.0 ± 51.1	1773.0 ± 29.6	1734.0 ± 19.4
13, a	3.02E–01	9.41E–03	4.39E+00	1.41E–01	1.05E–01	7.13E–04	99.7	8.91E+02	9.49	0.130	1703.0 ± 46.6	1711.0 ± 26.5	1720.0 ± 12.4
14, a	3.28E–01	1.24E–02	4.80E+00	1.84E–01	1.06E–01	7.00E–04	99.6	4.06E+02	9.40	0.570	1830.0 ± 60.0	1785.0 ± 32.1	1733.0 ± 12.1
15, a	2.99E–01	1.08E–02	4.32E+00	1.94E–01	1.05E–01	2.40E–03	98.6	2.87E+02	9.64	0.563	1686.0 ± 53.8	1698.0 ± 37.0	1713.0 ± 42.0
(5) AY 12-30-04-(17)								*U-Pb calibration established for U O / U values of:*	7.8–9.9[†]				
1, a	8.38E–02	7.98E–04	6.60E–01	6.72E–03	5.71E–02	3.83E–04	100.0	2.38E+03	8.385	0.080	518.5 ± 4.7	514.3 ± 4.1	495.7 ± 14.8

(*Continued*)

TABLE 1. ION MICROPROBE U-(Th)-Pb ZIRCON DATA (*Continued*)

Spot ID[#]	Isotopic ratios										Ages (±1 s.e.)[§]		
	$^{206}Pb^*/^{238}U$	±1 s.e.[§]	$^{207}Pb^*/^{235}U$	±1 s.e.[§]	$^{207}Pb^*/^{206}Pb^*$	±1 s.e.[§]	$^{206}Pb^*$ (%)	U (ppm)	U O / U	Th/U	$^{206}Pb^*/^{238}U$	$^{207}Pb^*/^{235}U$	$^{207}Pb^*/^{206}Pb^*$
2, a	7.75E–02	9.58E–04	6.18E–01	7.80E–03	5.79E–02	2.67E–04	100.0	1.30E+03	8.586	0.2 82	481.2 ± 5.7	488.9 ± 4.9	525.0 ± 10.1
3, a	5.79E–02	1.00E–03	4.56E–01	7.18E–03	5.71E–02	5.15E–04	100.0	3.01E+03	8.721	0.3 81	362.8 ± 6.1	381.2 ± 5.0	494.2 ± 19.9
4, a	8.30E–02	1.44E–03	6.62E–01	1.29E–02	5.79E–02	5.07E–04	100.0	5.41E+02	8.829	0.4 50	513.8 ± 8.6	515.9 ± 7.9	525.3 ± 19.2
5, a	1.17E–02	2.54E–04	8.69E–02	2.24E–03	5.39E–02	8.32E–04	100.0	2.70E+03	8.723	0.0 27	74.9 ± 1.6	84.6 ± 2.1	366.3 ± 34.8
6, a	7.72E–02	1.64E–03	6.08E–01	1.37E–02	5.71E–02	3.90E–04	100.0	2.22E+03	9.312	0.7 53	479.6 ± 9.8	482.1 ± 8.6	494.3 ± 15.1
(6) AY 12-31-04-(17)								*U-Pb calibration established for U O / U values of:*	7.8–9.9[†]				
1, a	1.24E–01	1.93E–03	1.41E+00	2.48E–02	8.28E–02	8.49E–04	99.4	2.27E+03	8.802	0.1 72	752.9 ± 11.1	894.8 ± 10.4	1264.0 ± 20.1
2, a	3.14E–01	3.81E–03	4.61E+00	6.51E–02	1.07E–01	7.78E–04	99.8	3.35E+02	8.657	0.4 24	1759.0 ± 18.7	1751.0 ± 11.8	1742.0 ± 13.4
3, a	3.12E–01	4.60E–03	4.58E+00	8.02E–02	1.07E–01	8.83E–04	99.8	2.58E+02	8.692	0.2 50	1748.0 ± 22.6	1746.0 ± 14.6	1743.0 ± 15.2
4, a	2.65E–01	3.20E–03	4.05E+00	4.87E–02	1.11E–01	7.89E–04	99.5	1.05E+03	8.579	0.3 63	1516.0 ± 16.3	1645.0 ± 9.8	1813.0 ± 12.9
5, a	3.24E–01	4.98E–03	4.78E+00	6.86E–02	1.07E–01	5.63E–04	99.9	5.26E+02	8.735	0.3 78	1807.0 ± 24.3	1781.0 ± 12.1	1751.0 ± 9.6
(7) AY 12-31-04-(21)								*U-Pb calibration established for U O / U values of:*	7.8–9.9[†]				
1, a	3.05E–01	4.75E–03	4.48E+00	6.80E–02	1.07E–01	8.22E–04	99.7	2.65E+02	8.374	0.3 23	1717.0 ± 23.5	1727.0 ± 12.6	1740.0 ± 14.2
2, a	3.14E–01	4.34E–03	4.60E+00	7.06E–02	1.06E–01	8.50E–04	99.7	2.86E+02	8.477	0.2 93	1761.0 ± 21.3	1749.0 ± 12.8	1734.0 ± 14.7
3, a	3.24E–01	7.97E–03	4.77E+00	1.22E–01	1.07E–01	7.65E–04	99.8	4.25E+02	8.506	0.4 88	1807.0 ± 38.8	1780.0 ± 21.4	1748.0 ± 13.1
4, a	3.15E–01	5.57E–03	4.65E+00	9.67E–02	1.07E–01	1.02E–03	98.6	2.99E+02	8.535	0.2 58	1764.0 ± 27.3	1758.0 ± 17.4	1752.0 ± 17.4
5, a	3.58E–01	5.33E–03	5.87E+00	1.02E–01	1.19E–01	5.78E–04	99.8	4.51E+02	8.814	0.4 71	1973.0 ± 25.3	1956.0 ± 15.1	1939.0 ± 8.7
(8) AY 12-31-04-(10)								*U-Pb calibration established for U O / U values of:*	7.8–9.9[†]				
1, a	3.40E–01	5.27E–03	5.05E+00	8.79E–02	1.08E–01	8.14E–04	99.8	2.99E+02	8.804	0.4 92	1888.0 ± 25.4	1827.0 ± 14.8	1759.0 ± 13.8
2, a	3.36E–01	4.68E–03	4.97E+00	7.43E–02	1.07E–01	7.31E–04	99.8	5.32E+02	8.691	0.3 25	1866.0 ± 22.6	1815.0 ± 12.6	1756.0 ± 12.5
3, a	3.14E–01	5.03E–03	4.77E+00	8.00E–02	1.10E–01	6.29E–04	99.8	4.65E+02	8.869	0.2 24	1760.0 ± 24.7	1780.0 ± 14.1	1804.0 ± 10.4
4, a	3.27E–01	6.17E–03	4.82E+00	9.99E–02	1.07E–01	8.71E–04	99.7	1.72E+02	8.739	0.4 90	1826.0 ± 30.0	1789.0 ± 17.4	1746.0 ± 14.9
(9) AY 12-31-04-(3B)								*U-Pb calibration established for U O / U values of:*	7.8–9.9[†]				
1, a	1.92E–01	3.01E–03	2.65E+00	4.15E–02	1.00E–01	9.37E–04	99.7	3.29E+03	8.752	0.0 22	1130.0 ± 16.3	1314.0 ± 11.6	1630.0 ± 17.4
2, a	2.12E–01	2.31E–03	2.97E+00	4.78E–02	1.02E–01	9.21E–04	99.6	3.26E+03	8.569	0.0 38	1241.0 ± 12.3	1400.0 ± 12.2	1651.0 ± 16.8
3, a	1.71E–01	6.39E–03	2.34E+00	9.74E–02	9.92E–02	1.62E–03	99.8	1.68E+03	9.443	0.1 14	1017.0 ± 35.2	1224.0 ± 29.6	1609.0 ± 30.4

(*Continued*)

TABLE 1. ION MICROPROBE U-(Th)-Pb ZIRCON DATA (*Continued*)

Spot ID[#]	Isotopic ratios										Ages (±1 s.e.)[§]		
	$^{206}Pb^*/^{238}U$	±1 s.e.[§]	$^{207}Pb^*/^{235}U$	±1 s.e.[§]	$^{207}Pb^*/^{206}Pb^*$	±1 s.e.[§]	$^{206}Pb^*$ (%)	U (ppm)	U O / U	Th/U	$^{206}Pb^*/^{238}U$	$^{207}Pb^*/^{235}U$	$^{207}Pb^*/^{206}Pb^*$
4, a	2.75E–01	7.09E–03	4.00E+00	1.15E–01	1.06E–01	9.94E–04	99.4	2.72E+02	9.172	0.677	1566.0 ± 35.9	1634.0 ± 23.4	1723.0 ± 17.3
5, a	1.27E–01	2.59E–03	1.60E+00	5.10E–02	9.14E–02	2.18E–03	94.7	4.21E+03	9.317	0.046	769.8 ± 14.8	969.2 ± 19.9	1454.0 ± 45.4
6, a	1.52E–01	4.13E–03	1.93E+00	5.04E–02	9.24E–02	6.84E–04	99.7	2.64E+03	9.269	0.052	910.3 ± 23.1	1092.0 ± 17.4	1475.0 ± 14.1
(10) AY 01-01-05-(11A)								*U-Pb calibration established for U O / U values of:*		7.8–9.9[†]			
1, a	3.83E–03	8.18E–05	2.48E–02	1.88E–03	4.70E–02	3.08E–03	99.6	1.39E+03	8.969	0.007	24.6 ± 0.5	24.9 ± 1.9	47.2 ± 156.7
2, a	3.80E–03	5.04E–05	2.62E–02	8.51E–04	5.00E–02	1.34E–03	99.8	3.31E+03	8.674	0.010	24.4 ± 0.3	26.2 ± 0.8	194.8 ± 62.3
3, a	8.34E–02	1.09E–03	6.52E–01	8.83E–03	5.68E–02	5.02E–04	100.0	7.91E+02	8.752	0.350	516.1 ± 6.5	510.0 ± 5.4	482.6 ± 19.5
4, a	7.92E–02	1.11E–03	6.25E–01	9.86E–03	5.72E–02	3.98E–04	100.0	1.02E+03	8.895	0.800	491.5 ± 6.6	492.6 ± 6.2	497.7 ± 15.4
5, a	1.03E–02	1.57E–04	7.36E–02	3.14E–03	5.17E–02	2.12E–03	98.1	2.39E+03	8.575	0.065	66.2 ± 1.0	72.1 ± 3.0	272.4 ± 94.1
6, a	7.19E–02	1.66E–03	5.62E–01	1.38E–02	5.67E–02	4.09E–04	100.0	1.19E+03	9.142	0.661	447.7 ± 10.0	452.9 ± 9.0	479.2 ± 16.0
7, a	8.15E–02	1.13E–03	6.39E–01	1.26E–02	5.68E–02	6.95E–04	99.9	7.00E+02	8.631	0.379	505.3 ± 6.7	501.4 ± 7.8	483.9 ± 27.0
(11) AY 12-31-04-(34A)								*U-Pb calibration established for U O / U values of:*		7.8–9.9[†]			
1, a	3.41E–03	5.08E–05	2.08E–02	7.69E–04	4.43E–02	1.55E–03	99.7	3.58E+03	8.79	0.026	21.9 ± 0.3	20.9 ± 0.8	negative
2, a	3.44E–03	3.44E–05	2.22E–02	6.27E–04	4.70E–02	1.28E–03	99.8	3.88E+03	8.629	0.022	22.1 ± 0.2	22.3 ± 0.6	46.7 ± 65.1
3, a	3.11E–03	3.62E–05	1.96E–02	9.42E–04	4.56E–02	2.19E–03	99.5	2.72E+03	8.609	0.020	20.0 ± 0.2	19.7 ± 0.9	negative
4, a	3.29E–01	5.82E–03	4.85E+00	8.83E–02	1.07E–01	7.90E–04	99.8	2.75E+02	8.737	0.778	1834.0 ± 28.3	1793.0 ± 15.3	1746.0 ± 13.5
5, a	6.97E–03	2.60E–04	4.19E–02	9.14E–03	4.36E–02	9.00E–03	95.8	4.37E+02	8.674	0.020	44.7 ± 1.7	41.7 ± 8.9	negative
6, a	3.55E–03	5.40E–05	2.26E–02	1.50E–03	4.61E–02	3.01E–03	99.5	1.57E+03	8.648	0.033	22.8 ± 0.3	22.7 ± 1.5	2.8 ± 157.2
7, a	3.67E–03	3.93E–05	2.36E–02	1.12E–03	4.66E–02	2.17E–03	99.5	2.99E+03	8.507	0.029	23.6 ± 0.3	23.6 ± 1.1	29.7 ± 111.6
8, a	4.42E–03	6.91E–05	2.79E–02	1.64E–03	4.59E–02	2.39E–03	99.2	2.54E+03	8.774	0.092	28.4 ± 0.4	28.0 ± 1.6	negative
10, a	3.13E–03	4.46E–05	2.02E–02	9.57E–04	4.67E–02	2.02E–03	99.7	2.78E+03	8.523	0.021	20.1 ± 0.3	20.3 ± 1.0	34.2 ± 103.6

*Radiogenic Pb corrected for common Pb with composition $^{206}Pb/^{204}Pb$ = 18.86, $^{207}Pb/^{204}Pb$ = 15.62, $^{208}Pb/^{204}Pb$ = 38.34 for samples AY12/30/04-6, AY12/31/04-3A, AY1/3/05-1A, AY1/3/05-1B, AY1/3/05-1C, AY02/05/06-6B, AY02/04/06-9, AY9/13/03-22, AY02/04/06-3, AY02/05/06-4, AY02/05/06-5, AY02/07/06-2, AY06/29/06-10B, and AY07/02/06-1, and with composition $^{206}Pb/^{204}Pb$ = 16.2, $^{207}Pb/^{204}Pb$ = 15.35, $^{208}Pb/^{204}Pb$ = 36.7 for samples AY12/31/04-3B, AY12/30/04-17, AY12/31/04-17, AY1/1/05-11A, AY12/31/04-34A, AY12/31/04-21, and AY12/31/04-10, estimated from model of Stacey and Kramers (1975).

[†]These data were collected in four sessions, each with distinct analytical conditions. Calibration curves for the four sessions are well determined for U O / U values ranging from 9.0–9.9 [AY 12-30-04 6, AY 12-31-04 3A, AY 01-03-05 1A, AY 01-03-05 1B, AY 01-03-05 1C], 7.8–8.9 [AY 12-31-04 3B, AY 12-30-04 17, AY 12-31-04 17, AY 01-01-05 11A, AY 12-31-04 34A, AY 12-31-04 21, AY 12-31-04 10], 8.5–9.4 [AY 02-05-06 6B, AY 02-04-06 9, AY 09-13-03 22], and 9.2–10 [AY 02-04-06 3, AY 02-05-06 4, AY 02-05-06 5, AY 02-07-06 2, AY 06-29-06 10B, AY 07-02-06 1]. Negative apparent ages are due to reverse discordance.

[§]s.e.—standard error.

[#]Spot ID: #, #—zircon number, spot name.

E–01—× 0.1; E–02—× 0.01; E–03—× 0.001; E+01—× 10; E+02—× 100; E+03—× 1000.

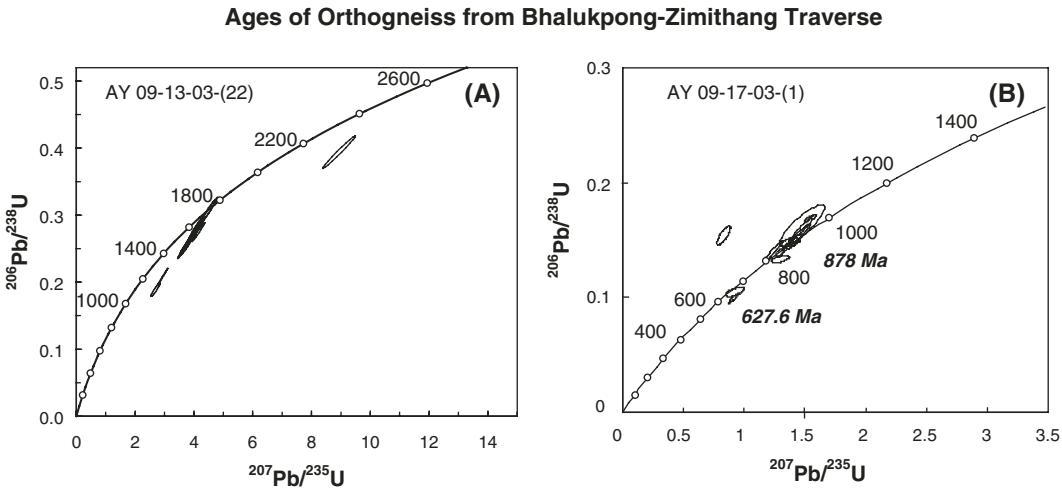

Figure 7. Concordia diagrams for augen gneiss samples collected from the Bhalukpong-Zimithang traverse. (A) Concordia plot for sample AY 09-13-03-(22). (B) Concordia plot for sample AY 09-17-03-(1).

Leucogranites from the Kimin-Geevan Traverse

Sample AY 12–31–04-(3B) was from a leucogranite that intrudes 1752 Ma augen gneiss as represented by sample AY 12–31–04-(3A) (Fig. 6A). Of the 15 analyses we obtained, six spot analyses of different zircons were discordant, four had UO/U values exceeding the range of calibration, and another four analyses had Th/U values below 0.1 (Fig. 9A; Table 1). The data plot along a discordia line that intercepts the concordia curve at 373 ± 59 Ma below and 1759 ± 36 Ma above (MSWD = 1.4). The upper-intercept age overlaps with the crystallization age of the host rock at 1752 ± 12 Ma and likely reflects inheritance of wall-rock zircons. The wall-rock zircons may have experienced Phanerozoic metamorphism during zircon growth, as indicated by moderate to low Th/U values (Table 1). Considering the large uncertainty for this age, it is likely that the metamorphic event was related to the widespread Cambrian-Ordovician plutonism and metamorphism across the Himalaya (450–520 Ma; see Gehrels et al., 2006a, 2006b; Martin et al., 2007). This interpretation suggests that some Himalayan leucogranite may have been emplaced in the early Paleozoic, as suggested by Gehrels et al. (2006a, 2006b).

Sample AY 01–01–05-(11A) is from a leucogranite that intrudes a 500 Ma granitoid as represented by sample AY 12–30–04-(6) (Fig. 6A). Five analyses plot in two concordant clusters, three of which yield a $^{207}Pb/^{206}Pb$ weighted mean age of 491 ± 11 Ma (2σ) and the other two of which feature very low Th/U ratios, yielding $^{238}U/^{206}Pb$ weighted mean ages of 24.6 ± 0.5 Ma and 24.4 ± 0.3 Ma (Fig. 9B; Table 1). Additional two spot analyses plotted along a discordia line between the two age clusters. The ca. 491 Ma zircons may represent inherited zircons from the wall rocks, and the younger zircons may result from crystallization of the leucogranite at ca. 24 Ma.

Sample AY 12–31–04-(34A) is from a leucogranite intruding high-grade gneiss in the Main Central thrust hanging wall (Fig. 6A). We analyzed nine spots on different zircons (Fig. 9C). One analysis with a high Th/U ratio yielded a $^{207}Pb/^{206}Pb$ weighted mean age of 1746 ± 14 Ma (2σ); the rest yielded moderate to low Th/U ratios and Cenozoic $^{238}U/^{206}Pb$ ages, with a dominant age cluster from ca. 23.5 Ma to ca. 20 Ma. We interpret the ca. 1746 Ma age as reflecting inheritance from the wall rocks and the younger ages as indicating crystallization of the leucogranite at 23–20 Ma.

$^{40}Ar/^{39}Ar$ THERMOCHRONOLOGY

Determining Cooling History by $^{40}Ar/^{39}Ar$ Thermochronology

We analyzed biotite and muscovite for $^{40}Ar/^{39}Ar$ thermochronometry. All mineral separates, packed in copper foil in quartz tubes or aluminum-holding containers, were irradiated within a nuclear reactor. The Fish Canyon Tuff standard (FCT) was used to monitor the amount of ^{39}Ar produced in the reactor from ^{39}K within each sample and was packed at regular intervals of 1 cm within the tube of unknowns. Correction factors were determined for Ca- and K-derived argon by irradiating and measuring salts (CaF_2, K_2SO_4) included within the tube of unknowns. Each sample was step-heated at UCLA's noble gas laboratory. Different mineral phases had specialized step-heating schedules from a minimum of 400 °C to a maximum of 1550 °C. Total gas ages are reported here for biotite and muscovite (Table 2).

Because the closure temperature of biotite for retention of ^{40}Ar is 350 ± 50 °C, which is lower than 400 ± 50 °C for muscovite (McDougall and Harrison, 1999), biotite ages from the same samples should be older than the muscovite ages. However, for all but one of our samples from which mica and biotite ages were both determined, the biotite ages are consistently older than the mica ages (Table 2). This implies the existence of excess argon in biotite that has caused overestimates of its cooling ages. For this reason, we consider all the biotite ages as maximum age bounds for the time of the sample cooled below ~350 °C. For example, the 19 Ma biotite cooling age of sample AY9–18–03-(23) indicates that the Tenga thrust sheet where the sample was collected was exhumed to a depth of <14 km after 19 Ma (assuming a geothermal gradient of 25 °C/km). This inference is consistent with the initiation age of contraction fabrics at 13 Ma in the Tenga thrust sheet obtained from mica in sample AY9–18–03-(10) (Fig. 4B), located nearby (see Discussion).

The most robust result of our thermochronological study is that the muscovite ages increase with an increase in structural level from the nearby thrusts (Fig. 4B). For the Zimithang thrust, the mica age increases from ca. 7 Ma directly above the fault to about ca. 12 Ma a few kilometers higher in its hanging wall (Fig. 4B). For the Main Central thrust near Lum La, the muscovite age increases from ca. 8 Ma directly

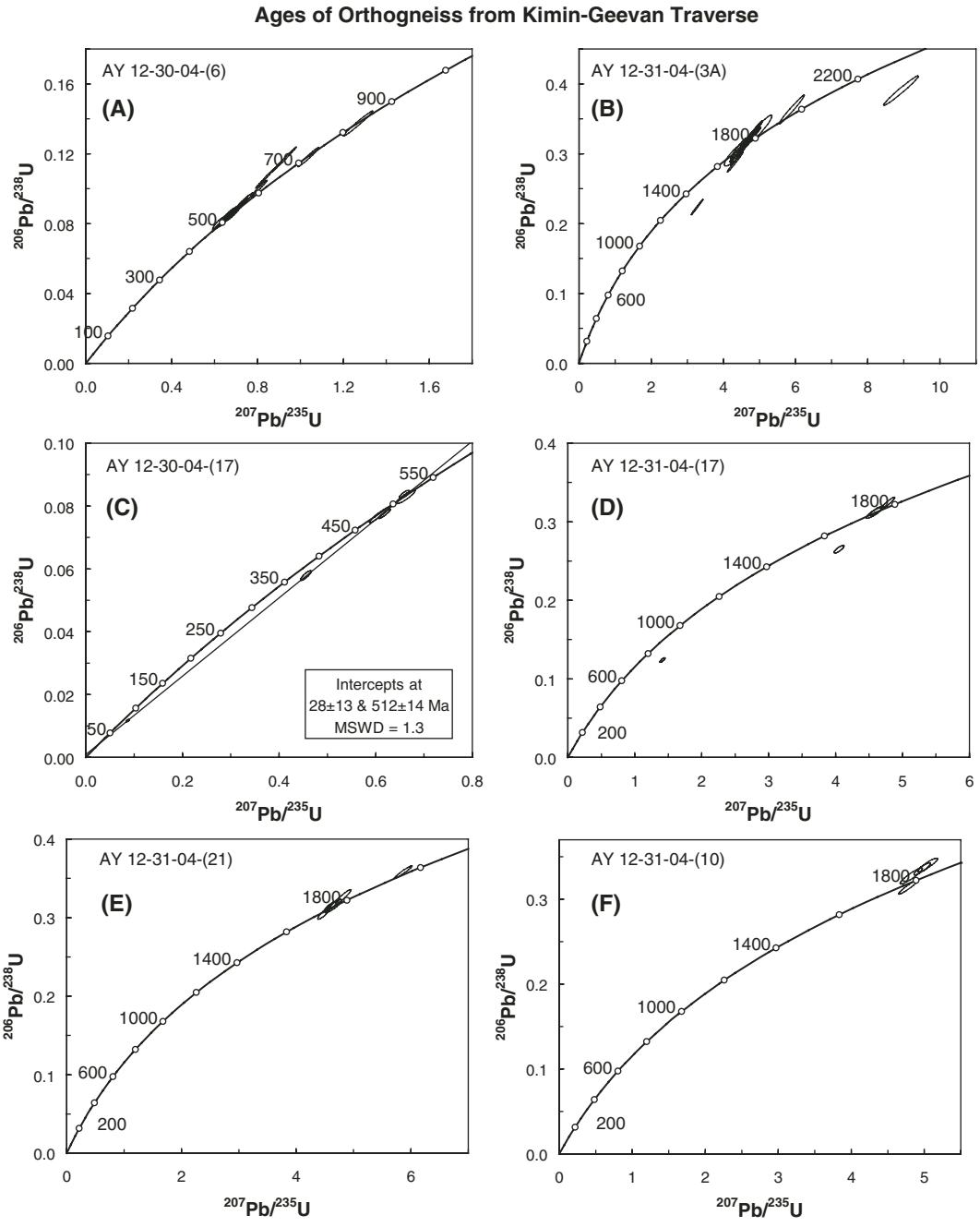

Figure 8. Concordia diagrams for augen gneiss samples from the Kimin-Geevan traverse. (A) Concordia plot for sample AY 12-30-04-(6). (B) Concordia plot for sample AY 12-31-04-(3A). (C) Concordia plot for sample AY 12-30-04-(17). (D) Concordia plot for sample AY 12-31-04-(17). (E) Concordia plot for sample AY 12-31-04-(21). (F) Concordia plot for sample AY 12-31-04-(10). MSWD—mean square of weighted deviates.

above the Main Central thrust to 10–11 Ma ~3–4 km higher and to ca. 12 Ma ~8–10 km above the Main Central thrust (Fig. 4B). For the Main Central thrust near Dirang, the muscovite age near the Main Central thrust is ca. 10 Ma and ca. 12 Ma 8–10 km higher up in the Main Central thrust hanging wall (Fig. 4B).

$^{40}Ar/^{39}Ar$ Thermochronology of White Micas from Main Central Thrust Footwall Quartzite

In order to determine the age of contractional fabrics in the Main Central thrust footwall, we separated mineral-stretching and lineation-defining white micas from quartz arenite directly below the Main Central thrust near Lum La and Dirang and in the hanging wall of the Tenga thrust below the Main Central thrust (Figs. 4A and 10). The $^{40}Ar/^{39}Ar$ thermochronologic analyses of white mica were conducted in the noble gas laboratory of the Australian National

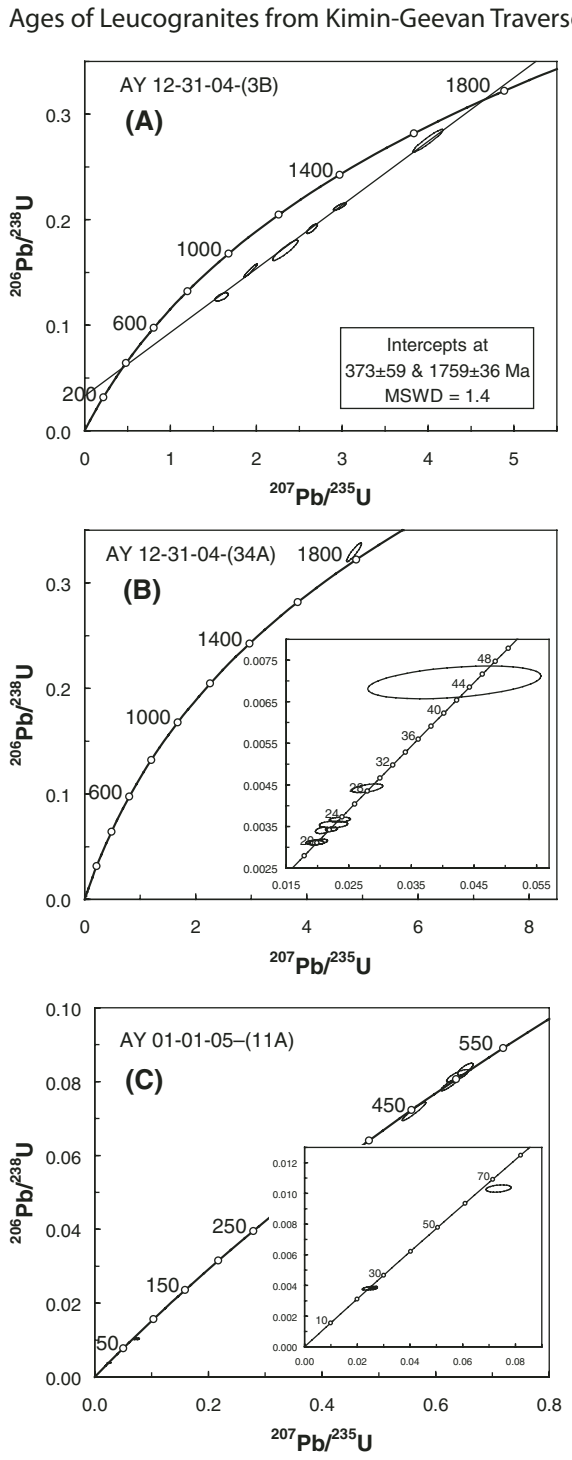

Figure 9. Concordia diagrams for leucogranite samples from the Kimin-Geevan traverse. (A) Concordia plot for sample AY 12-31-04-(3B). (B) Concordia plot for sample AY 12-31-04-(34A). (C) Concordia plot for sample AY 01-01-05-(11A).

University. The $^{40}Ar/^{39}Ar$ white mica ages in low-grade metasedimentary rocks associated with cleavage development may represent crystallization of new mica crystals along contractional fabrics or cooling of preexisting mica (Dunlap et al., 1997). Our results reveal an interesting pattern: the mica ages in the Main Central thrust footwall become younger toward the Main Central thrust. This age pattern is opposite to those obtained from the Main Central thrust hanging wall (Fig. 4B). Specifically, the $^{40}Ar/^{39}Ar$ weighted mean plateau age of mica directly below the Main Central thrust is 6.5 ± 0.1 Ma at the Lum La window and 6.9 ± 0.1 Ma near Dirang (Fig. 10). In contrast, the $^{40}Ar/^{39}Ar$ weighted mean plateau age of mica is 13.4 ± 0.1 Ma near Bomdila, directly above the Tenga thrust in the Main Central thrust footwall (Figs. 4A and 4B). This age pattern of mica may be explained by out-of-sequence thrusting, where the Tenga thrust was active at ca. 13 Ma, followed by motion on the Bomdila thrust at a higher structural level initiated at 6–7 Ma.

DISCUSSION

Our mapping suggests that the Main Central thrust is a folded low-angle fault bounding a thrust duplex below (Figs. 4B and 6B). Our U-Pb zircon dating reveals six igneous/metamorphic events in the eastern Himalaya: (1) emplacement of orthogneiss at ca. 1750 Ma in both the hanging wall and footwall of the Main Central thrust, (2) emplacement of orthogneiss during 825–878 Ma in the Main Central thrust hanging wall, (3) a thermal event causing metamorphic zircon growth at ca. 630 Ma in the Main Central thrust hanging wall, (4) emplacement of orthogneiss at ca. 500 Ma in the Main Central thrust hanging wall, (5) emplacement of early Paleozoic leucogranite (or a metamorphic event) at 373 ± 59 Ma, and (6) emplacement of Tertiary leucogranite at 28–20 Ma. The $^{40}Ar/^{39}Ar$ thermochronology in this study suggests that the Main Central thrust hanging wall was cooled below ~350–400 °C at ~12 Ma in its upper part and at ~8 Ma in its lower part; this was probably related to unroofing of the Main Central thrust sheet. The depositional relationship between the middle Rupa Group and a mylonitic augen unit below suggests Precambrian shear-zone development. Inclusion of garnet schist in the 870-Ma pluton may also imply a possible Precambian metamorphic event in the region. Next, we discuss the implications of our new findings.

Estimates of Cenozoic Crustal Shortening

A first-order issue related to the India-Asia collision is the way in which the convergence of the two continents was absorbed by intracontinental deformation (England and Houseman, 1986; Avouac and Tapponnier, 1993). Resolving this question requires knowledge of Cenozoic strain across the India-Asia collision zone, including the Himalayan-Tibetan orogen. The large magnitude of Cenozoic shortening across the central Himalaya as determined by reconstructing balanced cross sections has been used to infer underplating of Indian lower crust beneath the Tibetan Plateau (e.g., DeCelles et al., 2002). In addition, the magnitude of shortening estimated from different parts of the 2000-km-long Himalayan orogen has been used to infer possible along-strike variation of strain in response to the India-Asia convergence boundary

TABLE 2. SUMMARY OF $^{40}Ar/^{39}Ar$ DATA

Sample number	Mineral	Total gas age (Ma, 1σ)	Weighted mean age (Ma, 1σ)	K_2O (wt%)	$^{40}Ar^*$ (%)	Geology
AY9-17-03-(2)	Bio	12.1 ± 0.2	11.5 ± 0.6	7.6	75.2	GHC
	Mus	12.3 ± 0.3	9.7 ± 1.4	5.0	64.3	
AY9-17-03-(5)	Bio	16.7 ± 0.2	16.2 ± 0.8	7.8	81.4	GHC
	Mus	11.0 ± 0.2	9.4 ± 1.5	7.7	70.2	
AY9-16-03-(19)	Bio	9.2 ± 0.2	8.9 ± 0.3	7.2	68.8	GHC
	Mus	8.0 ± 0.3	7.6 ± 0.7	6.4	38.3	
AY9-17-03-(1)	Bio	12.4 ± 0.3	11.6 ± 0.8	7.1	73.2	GHC
	Mus	7.7 ± 0.2	7.5 ± 0.4	19.6	44.0	
AY9-16-03-(1)	Bio	10.0 ± 0.2	8.7 ± 2.3	5.0	85.7	GHC
AY9-17-03-(7A)	Bio	7.8 ± 0.2	7.6 ± 0.2	8.5	75.2	GHC
AY9-16-03-(6)	Bio	26.8 ± 0.2	26.0 ± 1.0	8.6	81.7	GHC
	Mus	10.3 ± 0.2	9.9 ± 0.7	9.2	46.0	
AY9-14-03-(3)	Bio	13.5 ± 0.2	13.5 ± 0.09	7.6	83.6	GHC
	Mus	10.7 ± 0.2	10.4 ± 0.2	9.7	52.1	
AY9-17-03-(11)	Bio	15.5 ± 0.2	15.2 ± 0.4	7.8	74.2	GHC
	Mus	12.2 ± 0.2	12.1 ± 0.1	10.0	56.5	
AY9-17-03-(11)	Bio	19.2 ± 0.6	19.2 ± 0.07	0.5	75.2	LHS

Note: Bio.—biotite; Mus—muscovite; GHC—Greater Himalayan Crystalline Complex; LHS—Lesser Himalayan Sequence.

conditions (Yin et al., 2006; cf. McQuarrie et al., 2008). Before presenting our estimates of Cenozoic crustal shortening in the Arunachal Himalaya, we discuss some of the major uncertainties in our calculations.

Pre-Cenozoic Deformation

Argles et al. (1999), Catlos et al. (2002), Gehrels et al. (2003, 2006a, 2006b), Kohn et al. (2004, 2005), and Martin et al. (2007) have presented evidence for the occurrence of Cambrian-Ordovician contractional deformation, pluton emplacement, and high-grade metamorphism across the western and central Himalaya. Our companion study across the Shillong Plateau and Mikir Hills of northeastern India also indicates the occurrence of early Paleozoic contractional deformation (Yin et al., 2009). Although we do not have direct structural evidence in this study for early Paleozoic deformation in the eastern Himalaya, the 630 Ma zircon growth, 375 Ma thermal disturbance, and widespread occurrence of 500 Ma plutonic rocks correlate well with a broadly coeval event in the northeastern Indian craton (Yin et al., 2009). This suggests that early Paleozoic deformation may have affected the eastern Himalayan region. The correlation raises the possibility that the Proterozoic sedimentary strata in the eastern Himalaya may have been already deformed prior to the Cenozoic India-Asia collision. Ideally, we may use the strata deposited after the early Paleozoic contractional event (i.e., post-Ordovician strata) to reconstruct Cenozoic deformation. In reality, the Lesser Himalayan Sequence units across our study areas and the rest of the Himalaya are dominantly Precambrian strata; they have been used extensively in the Himalaya for estimating the total crustal shortening across the orogen (e.g., Murphy and Yin, 2003). Such an approach may overestimate the Cenozoic strain because the effect of early Paleozoic deformation is not removed.

Deformation Mechanism

The existing balanced cross sections across the Himalaya all assume that folding was accommodated by flexural slip, so that bed length and bed thickness can be preserved before and after deformation. This may not be the case for most rocks in the Arunachal Himalaya. In the Main Central thrust hanging wall, deformation is mostly expressed by foliation-parallel stretching and widespread mesocopic folding, which thickens the folded crustal section vertically while thinning individual fold limbs (Fig. 11). In this case, it would be misleading to use the state of strain at individual points to infer the overall flow field of the Main Central thrust hanging wall (cf. Law et al., 2004).

In the Main Central thrust footwall, phyllite and slate constitute a major fraction of the Lesser Himalayan Sequence throughout the Himalaya (e.g., Upreti, 1996; DeCelles et al., 2001; Yin, 2006). They are exclusively deformed by intraformational folding associated with slaty cleavage (e.g., Valdiya, 1980; LeFort, 1996). In our study area, the phyllite units in the Rupa Group experienced isoclinal folding that transposed the original bedding into slaty cleavage. Because phyllite takes up more than one-third of the total thickness of the exposed Lesser Himalayan Sequence in Arunachal, it is essential to quantify the effect of folding on crustal shortening in this type of rocks. To illustrate this, we conducted both area and line balancing of actual folds shown in Figure 5B. We first used bedding-parallel simple shear to restore folds and then laid the beds horizontally to calculate the original bed length. Using the current width of the folds in the outcrop, we obtain a shortening strain of 60%–65% (Figs. 12A and 12B). Because bed thickness does not stay constant during similar folding, we used an area balancing method to calculate the shortening strain. We selected the thickest part of the fold limb to represent a minimal thickness of the original bed. This assumption is justified because similar folding thins the fold limbs, and thus the observed limb thickness is always a minimum of its original thickness. The area-balancing approach yields a total shortening strain of ~40% (Fig. 12C), which is 20%–25% less than the estimated shortening strain based on a line-balancing technique. This example suggests that even under a perfect situation, when the geometry of a cross section is known completely, different section-balancing techniques can lead to significantly (>20%) different results on shortening estimates.

Nonuniqueness of Balanced Cross Sections

Accurate estimates of crustal shortening also depend on construction of balanced cross sections using surface information and known deformation mechanisms. However, surface geology alone can rarely provide sufficient constraints for making a unique cross section, due to the lack of information on (1) the number and depths of detachments below (e.g., Yin et al., 2008a, 2008b), (2) spatial variation of structural style and temporal variation of deformation mechanisms, (3) thickness variation of individual units (Yin, 2006), and (4) structural framework of the region induced by early deformational events. We use the geology of the Bhalukpong-Zimithang traverse to illustrate the issue of nonuniqueness. We begin by making a cross section shown in Figure 4B using the standard dip domain method and assume a *single* décollement dipping parallel to the inclined Moho obtained from extrapolating the two-point results of Mitra et al. (2005) below our study area. However, by allowing multiple levels of décollements, we can also construct an alternative section with two levels of duplex systems, as shown in Figure 4C. The two different cross sections imply very different

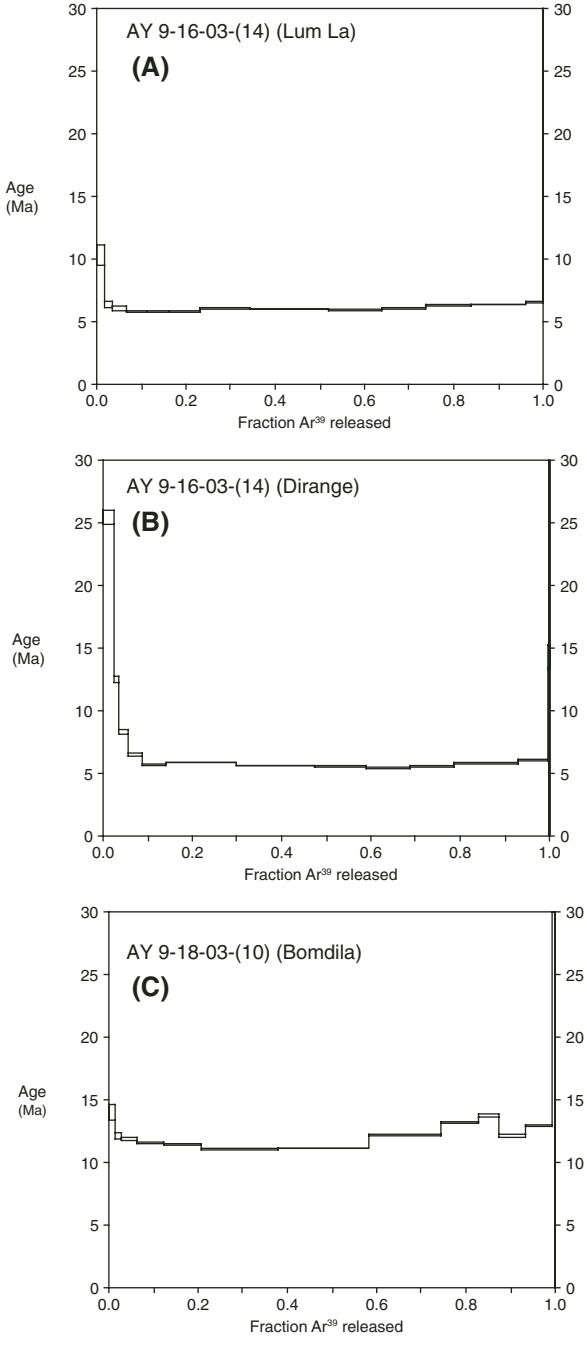

Figure 10. Argon release spectra and corresponding ages for neoblast micas in quartz arenite samples collected in the footwall of the Main Central thrust along the Bhalukpong-Zimithang traverse. See Figure 4A for sample locations. (A) Argon release spectrum for sample AY 9-16-03-(14) from the Lum La area. (B) Argon release spectrum for sample AY 9-17-03-(15) from the Dirang area. (C) Argon release spectrum for sample AY 9-18-03-(10) from the Bomdila area.

kinematics. For the cross section in Figure 4B, motion on the Main Central thrust produces a duplex system in its footwall and the deformation front propagates southward. In contrast, the cross section in Figure 4C consists of an upper-level duplex system associated with motion on the Main Central thrust and a lower-level duplex system associated with motion on the Main Boundary thrust and Main Frontal thrust zone. Importantly, structural geometry in Figure 4C requires the Himalayan interior to experience active crustal shortening and thus upward warping. This may explain widespread seismicity in the eastern Himalayan interior (Drukpa et al., 2006; Velasco et al., 2007).

We may also consider two competing situations: one assumes a significant basement topography induced by early Paleozoic contraction as seen in the Shillong Plateau (Yin, 2009) (Fig. 4D), and another assumes all strata were flat-lying with a thin-skinned style of deformation as commonly assumed in Himalayan research (e.g., Murphy and Yin, 2003) (Fig. 4F). Given the lack of subsurface constraints on the geometry of the major thrusts and the poor knowledge of the pre-Cenozoic stratigraphic framework of the eastern Himalaya, we are currently unable to differentiate among the possibilities.

Shortening Estimates

Around the Siang window (Figs. 1 and 13) (Kumar, 1997), the Main Boundary thrust places the Lesser Himalayan Sequence over Cretaceous and Paleogene strata, and the Bome thrust juxtaposes the Lesser Himalayan Sequence units over Permian strata. These relationships require the Bome fault to have a minimum slip of ~95 km and the Main Boundary thrust to have a minimum slip of ~80 km (Fig. 13A). Finally, we use the northernmost exposure of the Lum La window of Yin et al. (2006; also see Fig. 4A) and the southernmost exposure of the Main Central thrust mapped across the Kimin-Geevan traverse to determine a minimum slip of 140 km on the Main Central thrust. Assuming that slip on major faults does not vary along strike in the western Arunachal Himalaya, we obtain a minimum shortening of ~315 km accommodated solely by the Main Central thrust, Main Boundary thrust, and Bome fault across the region. As the Main Central thrust and Main Boundary thrust are Cenozoic in age and the Bome fault is likely a Cenozoic contractional structure because it cuts Permian strata and there was no post-Permian contraction except the Cenozoic Himalayan event, the above estimated shortening was all induced during the Indian-Asia collision. If we project the map relationship around the Siang window (Fig. 13B) and the early Paleozoic Central Shillong thrust system below the Bhalukpong traverse with ~15 km of basement relief as seen in the Shillong region (Fig. 3b *in* Yin et al. 2009), we obtain an estimated total shortening of ~775 km (i.e., ~76% shortening strain) using the line-balancing method (Figs. 4D and 4E). If the Himalayan basement was not deformed and all pre-Cenozoic strata were flat-lying prior to India-Asia collision, as commonly assumed in balanced cross sections across the central Himalaya (e.g., Murphy and Yin, 2003) (Fig. 4F), we obtain an estimated shortening of ~515 km (i.e., ~70% shortening strain) (Fig. 4G) across the eastern Himalaya. The difference in shortening estimates from the two cross sections highlights the importance of pre-Cenozoic stratigraphic and structural frameworks below the Himalaya in estimating crustal shortening strain. Considering the possible effect of similar folding in the Lesser Himalayan Sequence and ductile behavior of the Main Central thrust hanging wall, the uncertainty of our shortening estimates must be greater than 20%–30%.

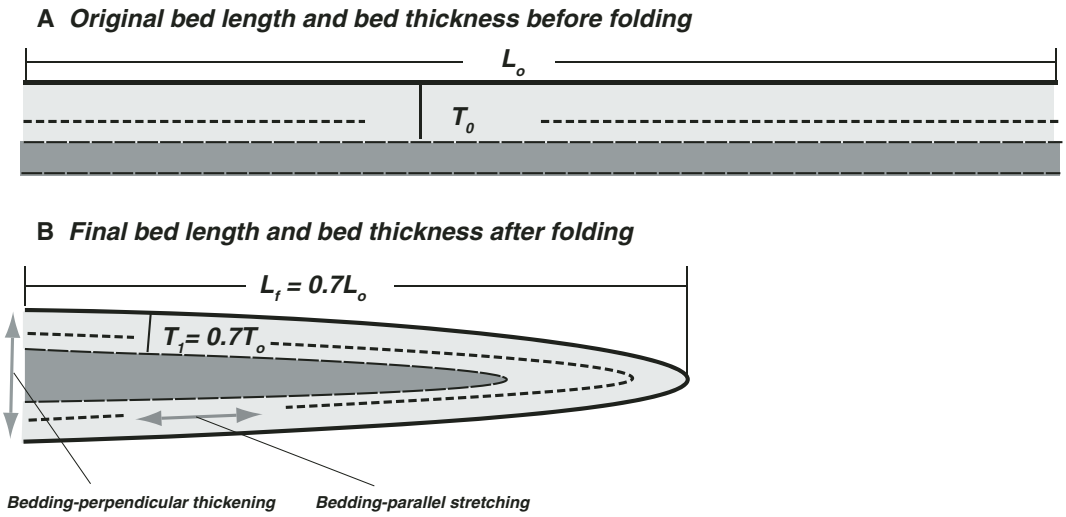

Figure 11. Schematic diagram showing the relationship between bedding-perpendicular thickening and bedding-parallel thinning during folding: (A) Bed before folding. (B) Bed after folding. Note that the overall section is thickened by 140%, while the marker bed in the fold limbs is thinned by 70%.

Greater Himalayan Crystalline Complex Provenance and Style of Himalayan Thrusting

Our geochronologic results indicate that the Greater Himalayan Crystalline Complex is composed of plutonic rocks with ages at 500 Ma, 880 Ma, and 1745 Ma (Fig. 14). The presence of 1745 Ma gneiss in the Main Central thrust hanging wall suggests that the Greater Himalayan Crystalline Complex in the eastern Himalayan orogen may have originated from the Indian craton. In northeastern India, magmatic events at 1772–1620 Ma (U-Pb zircon ages) (Ameen et al., 2007; Yin et al., 2009), 1100 Ma (U-Pb zircon ages) (Yin et al., 2009), 770–880 Ma (Rb-Sr ages; Ghosh et al., 2005), and 530–480 Ma (Ghosh et al., 2005; Yin et al., 2009) have been recorded. There, the sedimentary cover sequence is represented by the Proterozoic Shillong Group, which has an initial depositional age younger than 1100 Ma (youngest zircon age in the lower section of the exposed part of the sequence; the contact with the basement is not exposed in the Shillong Plateau) to a terminal depositional age younger than 560 Ma (oldest pluton that intrudes the upper part of the exposed sequence) (Yin et al., 2009). In the eastern Himalaya, igneous crystalline rocks are represented by the 1750 Ma (U-Pb zircon ages) (Daniel et al., 2003; Richards et al., 2006; this study), 1100 Ma (Rb-Sr ages) (Bhargava, 1995), 830–880 Ma (Richards et al., 2006; this study) augen gneisses, and 500 Ma orthogneiss (this study). The age of the middle Rupa Group in the eastern Himalaya is younger than the 1750 Ma augen gneiss, and its terminal deposition may have occurred in the early Cambrian (Tewari, 2001; McQuarrie et al., 2008). These age constraints suggest that the Precambrian basement and Proterozoic cover sequences of the northeastern Indian craton and eastern Himalaya are generally correlative.

Correlation of the Precambrian Himalayan and Indian cratonal units has three important implications. First, the Himalayan orogen must have been constructed in situ by rocks of the Precambrian Indian craton rather than from Tibetan middle crust (e.g., Nelson et al., 1996). This is because our study indicates a lack of Cretaceous-Tertiary Gangdese Batholith components in the Main Central thrust hanging wall (e.g., Quidelleur et al., 1997; Yin and Harrison, 2000; Harrison et al., 2000; Yin, 2006). Second, the style of thrusting in the Himalaya is not thin-skinned, as is commonly assumed throughout the Himalaya (e.g., Steck et al., 1993, 1998; Steck, 2003; DeCelles et al., 2001, 2002; Murphy and Yin, 2003; Robinson et al., 2006), but it is thick-skinned, involving vertical stacking of Indian basement and sedimentary cover sequences as envisioned by Heim and Gansser (1939) followed by LeFort (1975). Current crustal thickening in the Shillong Plateau region may represent the incipient stage of this shortening mechanism (e.g., Yin et al., 2009). Third, if the Greater Himalayan Crystalline Complex was an exotic terrane accreted in the Cambrian-Ordovician onto Indian continent (DeCelles et al., 2000; cf. Cawood et al., 2007), the inferred terrane must have had a close geologic tie with India from 1750 Ma to ca. 500 Ma. That is, the Greater Himalayan Crystalline Complex could have been a first continental strip rifted away from the Indian continent after ca. 880–830 Ma and was later accreted back to India at 500–480 Ma, as originally suggested by DeCelles et al. (2000).

Along-Strike Variation of Himalayan Geology

In Bhutan, the Main Central thrust cuts 16 Ma leucogranite, whereas the Kakthang thrust cuts a leucogranite with an age of 14–15 Ma (Grujic et al., 2002). Grujic et al. (2002) used these observations to suggest that the Kakthang thrust is an out-of-sequence structure with respect to the Main Central thrust. However, this crosscutting relationship does not constrain the initiation and termination ages of the two structures and thus cannot uniquely establish the true sequence of thrusting across the Bhutan Himalaya. U-Pb dating of monazite and xenotime suggests that the Main Central thrust in Bhutan was already active at ca. 22 Ma and continued after 14 Ma (Daniel et al., 2003). The early initiation of the Main Central thrust in Bhutan is also recorded in the metamorphic history of the fault zone, which experienced a peak *P-T* condition of ~750–800 °C and 10–14 kbar at ca. 18 Ma, followed by a retrograde metamorphic event under conditions of 500–600 °C and 5 kbar at 14–11 Ma (Stüwe and Foster, 2001; Daniel et al., 2003). While the retrograde event correlates with the cooling history of the Arunachal Himalaya obtained by this study, the prograde metamorphic event and early initiation of the Main Central thrust in Bhutan are not in evidence in our study areas. For example, our thermochronological data and the U-Th monazite-inclusion ages (Yin et al., 2006) suggest that the Main Central thrust was active at 10 Ma. If this age represents the onset time of the Main Central thrust, it implies the thrust in Arunachal is ~10–12 Ma younger than its equivalent structure in the Nepal and Bhutan Himalaya (Hubbard and Harrison, 1989; Daniel

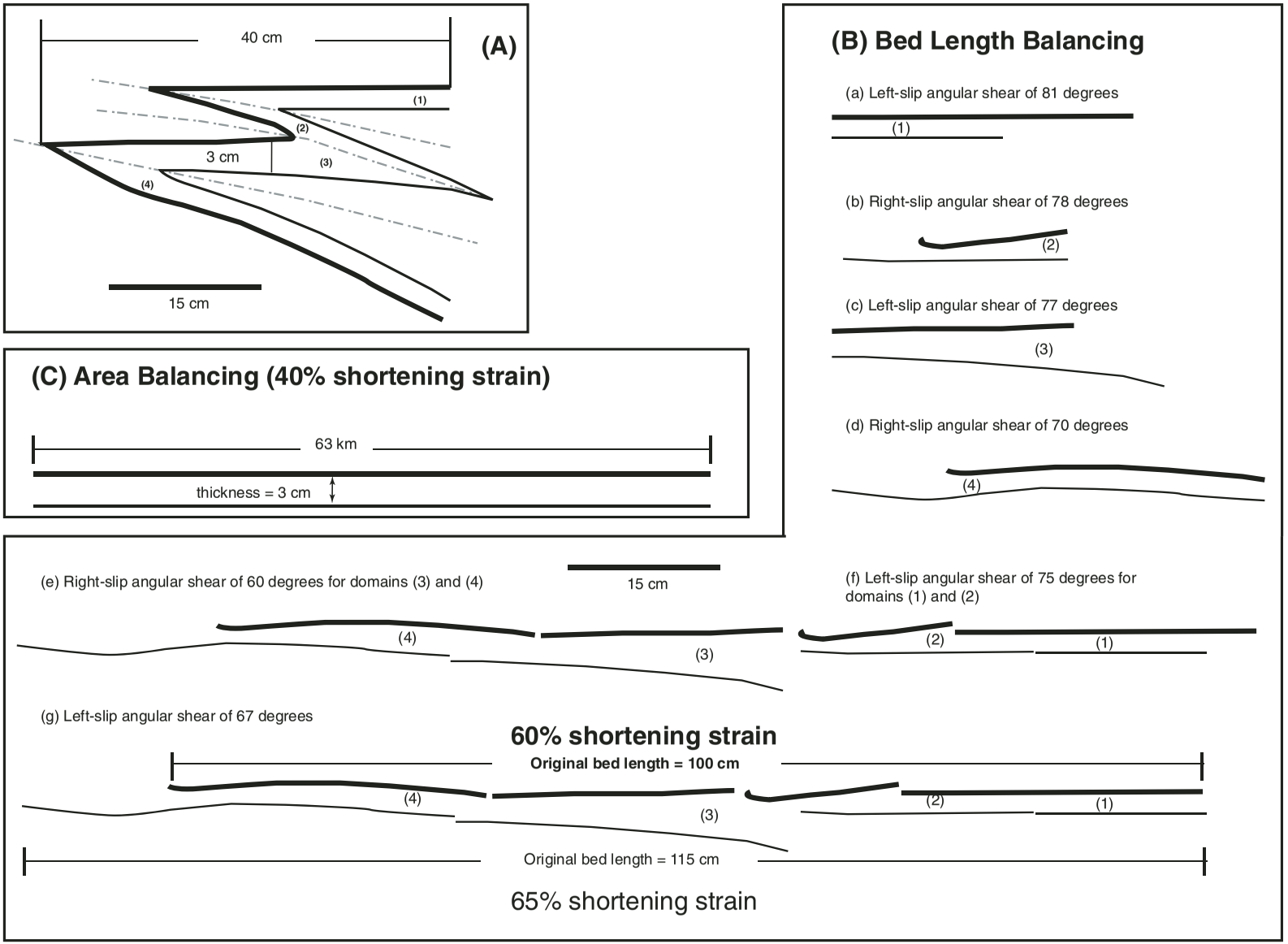

Figure 12. (A) Line drawing of similar folds based on Figure 5B. Numbers in parentheses represent individual dip domains divided by axial surfaces of the folds. (B) Bend-length balancing of the folds. Steps a to d show restoration of individual fold limbs by applying bedding-parallel simple shear. Steps e and f show bedding-parallel simple shear used to restore the combined domains of 1 and 2 and domains 3 and 4. This procedure implies that the folds were produced in two stages, with domains 1 and 2 forming one long limb and domains 3 and 4 forming another long limb before each limb was itself folded. Step g arbitrarily uses the right end of the section as a pin-line to calculate the original bed length. (C) Shortening estimate based on area-balancing technique. We assume the thickest part of the fold limb to be a minimum value for the original bed thickness and use the area bounded by the two fold limbs to calculate the original bed length. See text for detailed discussion on comparison of the two methods.

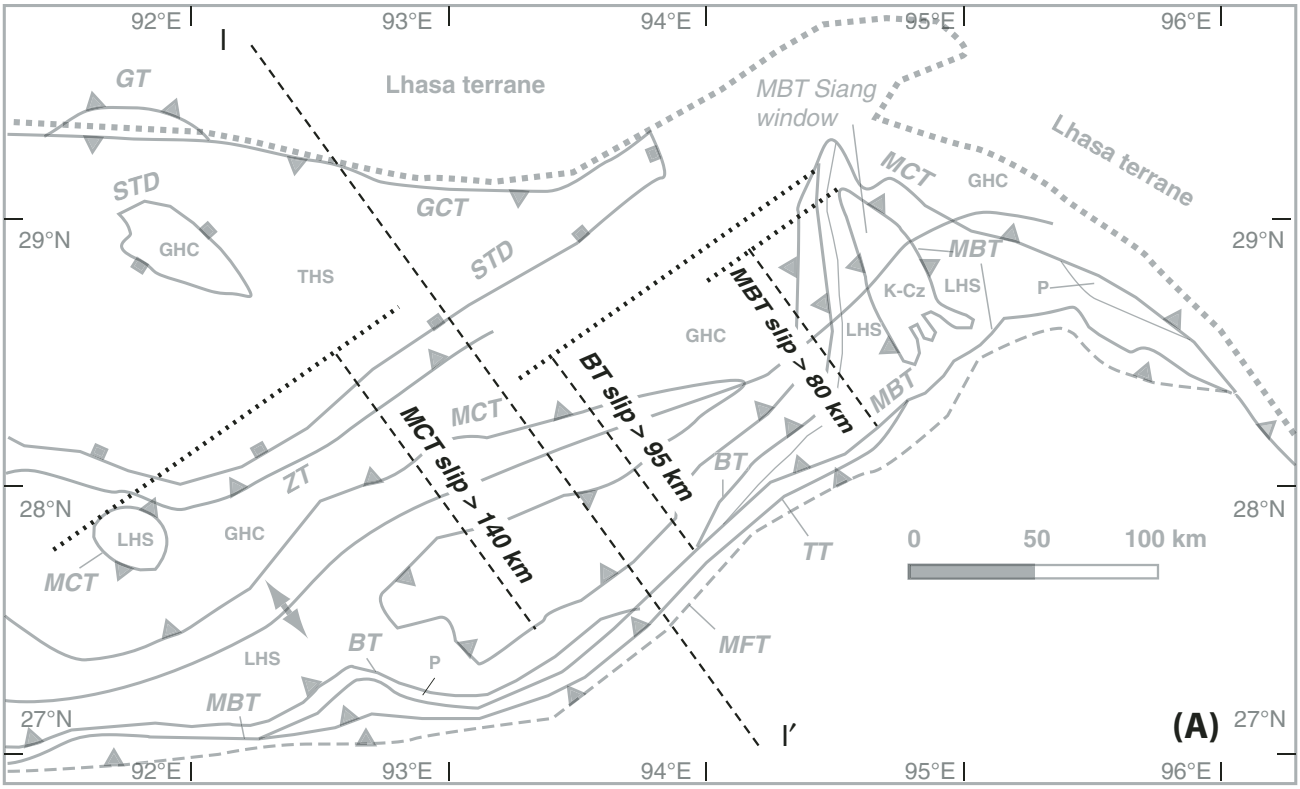

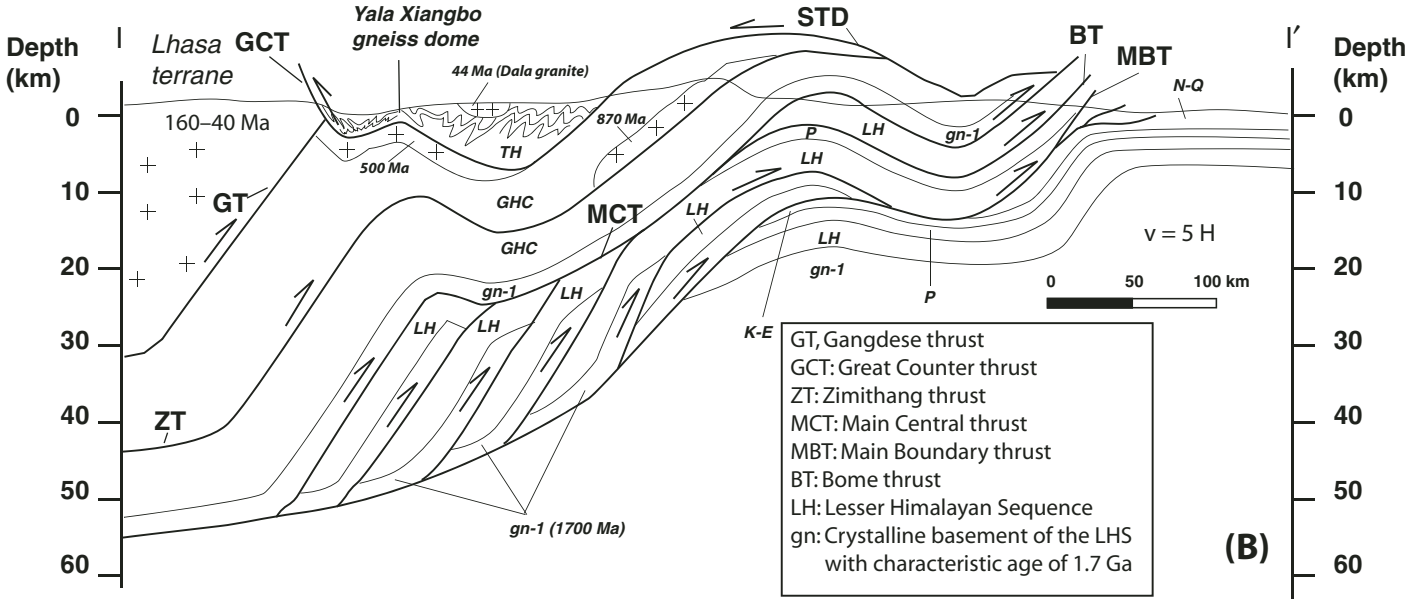

Figure 13. (A) Simplified geologic map of the eastern Himalaya. See Figure 1 for location. The relationship between thrust windows and the frontal thrust trace provides an estimate of minimum slip on the Main Central thrust (MCT), Bome thrust (BT), and Main Boundary thrust (MBT). (B) Schematic cross section of the eastern Himalaya along line II′. The ages of orthogneiss and granites in the eastern Himalaya are also shown. STD—South Tibetan detachment.

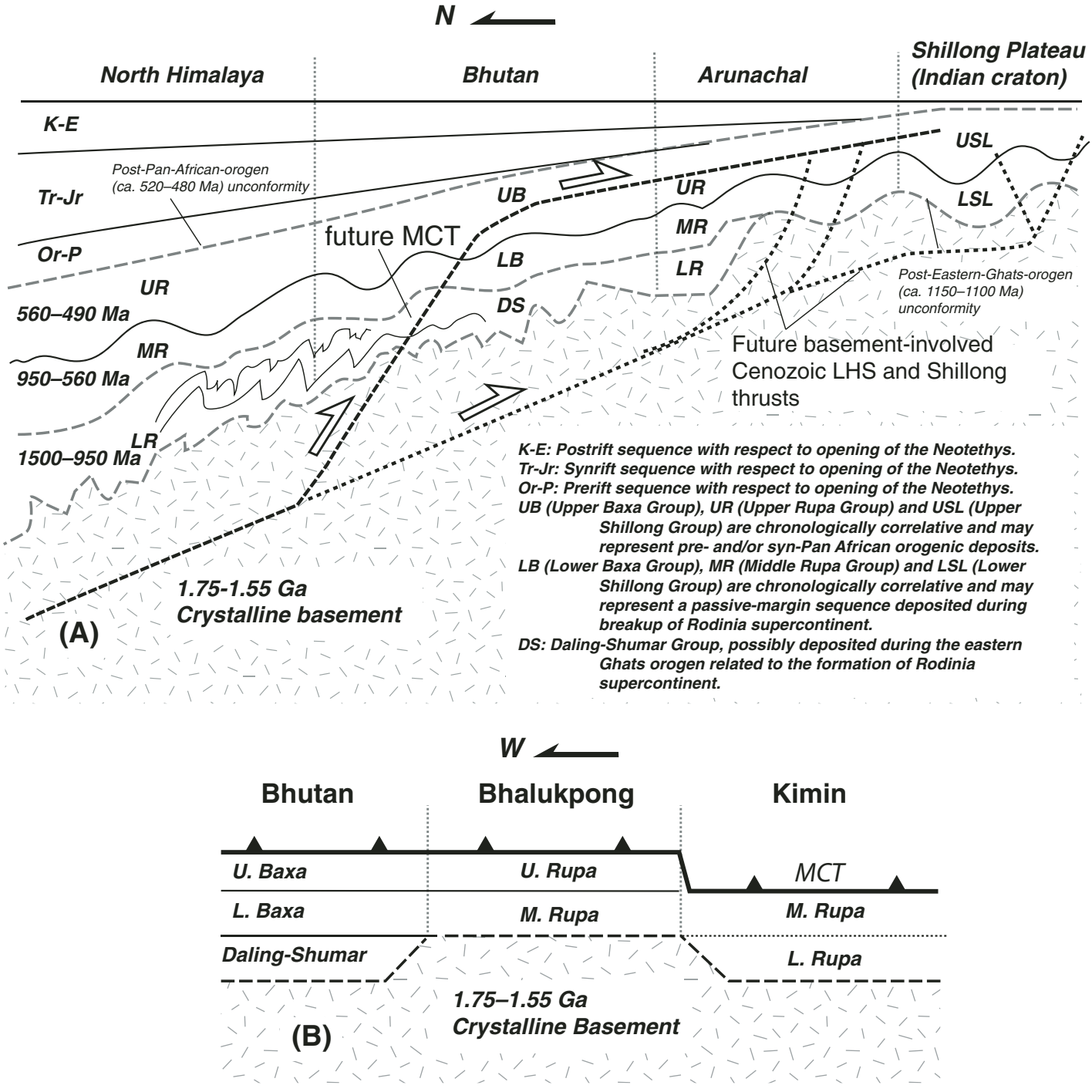

Figure 14. (A) Schematic cross section showing possible lithologic correlations between Indian craton and the eastern Himalaya. MCT—Main Central thrust. (B) Possible along-strike variation of stratigraphic relationships across Bhutan and Arunachal. The lower Rupa Group appears to be missing along the Bhalukpong-Tawang traverse but is present in Bhutan and across the Kimin traverse, suggesting possible existence of paleotopography in the region.

et al., 2003). The differences in the timing of the Main Central thrust motion could be explained by either progressive eastward initiation of the Main Central thrust zone or, more likely, the variation of exposure levels of the Main Central thrust zone that record different slip history of the complex Main Central thrust zone.

The chronostratigraphy of the Lesser Himalayan Sequence appears to vary along strike over relatively short distances in the eastern Himalaya. In Bhutan, the Daling-Shumar Group, correlative to the lower Rupa Group (Figs. 3 and 14B), is present. In contrast, the lower Rupa Group appears to be missing along the Bhalukpong-Zimithang traverse. Finally, the Kimin-Geevan traverse appears to preserve the lower and middle Rupa Group below the Main Central thrust but is missing the upper Rupa Group (Fig. 14B). The lack of lower Rupa Group along the Bhalukpong-Zimithang traverse may explain the dominance of augen gneiss involved in the Cenozoic thrust belt, since the latter represents the Precambrian basement of the Lesser Himalayan Sequence and Indian craton. The lack of the upper member of the Rupa Group along the Kimin-Geevan traverse indicates either the unit was eroded away after its deposition or the Main Central thrust cuts down section laterally to the east from the Bhalukpong-Zimithang traverse to the Kimin-Geevan traverse (Fig. 14B).

Our $^{40}Ar/^{39}Ar$ mica ages between 7 Ma and 12 Ma in the Main Central thrust hanging wall are significantly younger than those obtained mostly in the western Himalaya between 15 Ma and 25 Ma (Searle et al., 1999; Dézes et al., 1999; Stephenson et al., 2001), but they are similar in age range to those from the Nepal and Bhutan Himalaya between 0.4 Ma and 14 Ma (e.g., Catlos et al., 2001; Stüwe and Foster, 2001).

Cenozoic Evolution of the Eastern Himalaya

The work of Aikman et al. (2008) suggests that the Triassic to Cretaceous Tethyan Himalayan Sequence in southeastern Tibet north of our study area experienced intense folding and thrusting in the early Tertiary prior to ca. 44 Ma. Folding and the related cleavage development in the fine-grained Tethyan Himalayan Sequence units in the area have completely transposed the original bedding during this early contractional event (Yin et al., 1999). Because the Neogene Main Central thrust and South Tibetan detachment were rooted into an already complexly deformed orogen, they must have cut across the folded Precambrian and Phanerozoic strata in the middle and lower crust. As the normal stratigraphic sequence was severely modified by the Paleogene shortening, the South Tibetan detachment and Main Central thrust may have variable older-over-younger and younger-over-older relationships across the faults. In southern Tibet directly north of Bhutan, the South Tibetan detachment places Cretaceous strata over Greater Himalayan Crystalline Complex units (Pan et al., 2004; Dai et al., 2008), whereas in Bhutan to the south, the South Tibetan detachment places Neoproterozoic and Cambrian strata over the Greater Himalayan Crystalline Complex. This relationship suggests that the South Tibetan detachment cuts up section of its hanging-wall strata in its northward transport direction, and this relationship is inconsistent with normal-fault but consistent with thrust-fault geometry. From the observations made along the Bhalukpong-Zimithang traverse, where foliation development has completely transposed the original bedding of phyllite and slate in the Main Central thrust footwall, one may conclude that the foliation may not be used as a marker surface for cross-section restoration because it was developed during rather than before Cenozoic deformation (cf. Robinson et al., 2006).

Based on these age constraints, we propose the following evolutionary history for the development of the eastern Himalaya (Fig. 15). To simplify our illustration, we assume flat-lying beds in the northern Indian margin prior to the India-Asia collision by neglecting that Cambrian-Ordovician contraction (Fig. 15A). Following Aikman et al. (2008), the northern Indian margin sequence experienced intense isoclinal folding in the early Cenozoic (Fig. 15B), which caused crustal thickening and strong modification of the original pre-Cenozoic stratigraphic architecture. Because the South Tibetan detachment and Main Central thrust are rooted northward into the middle or lower crust of the northern Himalaya, these structures must have cut the isoclinally folded basement and cover rocks, producing complex juxtaposition relationships across the fault. At ca. 20–15 Ma in Bhutan, and perhaps later in the Arunachal Himalaya, motion on the Main Central thrust may have caused southward propagation of crustal thickening via ductile folding in its footwall. The presence of a major thrust ramp along the Main Central thrust allows transport of its hanging-wall rocks from the lower to upper crust (Fig. 15C). During 15–10 Ma, the Tenga thrust was initiated in the footwall of the Main Central thrust below the frontal part of the Main Central thrust flat (Fig. 15D). This was followed by the nearly coeval initiation of the Bomdila thrust and Lum La thrust duplex in the Main Central thrust footwall and the Zimithang thrust in the Main Central thrust hanging wall in an out-of-sequence fashion (Fig. 15E). Together, the Lum La and Bomdila duplex systems produced two antiforms bounding the Se La synclinorium in the middle. In our reconstructions, the Greater Himalayan Crystalline Complex, Lesser Himalayan Sequence, and Tethyan Himalayan Sequence were all originated from the northern Indian margin section, including its crystalline basement and the Proterozoic to Cretaceous cover sequence (Fig. 15E).

CONCLUSIONS

The eastern Himalaya experienced a series of magmatic events at ca. 1750 Ma, 825–878 Ma, 500 Ma, and 28–20 Ma. The first three events are correlative to those in the Indian craton, while the last event was associated with the Cenozoic development of the Himalaya during the India-Asia collision. Correlation of the magmatic events suggests that the Himalayan units were derived from the Indian craton, and the formation of the eastern Himalaya was accomplished by vertical stacking of basement-involved thrust sheets of the Indian cratonal rocks. This correlation also rules out the possibility that the high-grade rocks of the Himalaya were derived from Tibetan middle crust via channel flow. The Main Central thrust in the eastern Himalaya is broadly warped due to the presence of two large thrust duplexes in its footwall. The $^{40}Ar/^{39}Ar$ thermochronology indicates that the northern duplex was initiated at or prior to ca. 13 Ma, while the southern duplex started at or prior to ca. 10 Ma. The differential cooling ages may result from out-of-sequence thrusting. The formation of the two duplexes lasted until at least 6 Ma in the late Miocene and may have continued until the Pliocene. Although the outcrop pattern indicates that the minimum Cenozoic shortening is ~315 km, it is difficult to estimate the total crustal shortening strain across the eastern Himalaya due to great uncertainties in the number, geometry, and depths of detachment horizons below the mountain belt, the original thickness of individual lithologic units and their spatial variation, deformation mechanisms, their variations in time and space responsible for the development of the eastern Himalaya, and finally out-of-sequence thrusting. Detailed analysis of mesoscopic fold geometry in the study area indicates that the traditional line-balancing methods can overestimate as much as 20% of the total Himalayan shortening. Also, because the Himalaya and northern Indian craton had experienced a significant crustal shortening event in the early Paleozoic (520–470 Ma), shortening estimated from balancing Precambrian strata represents a combined effect of early Paleozoic and Cenozoic deformation.

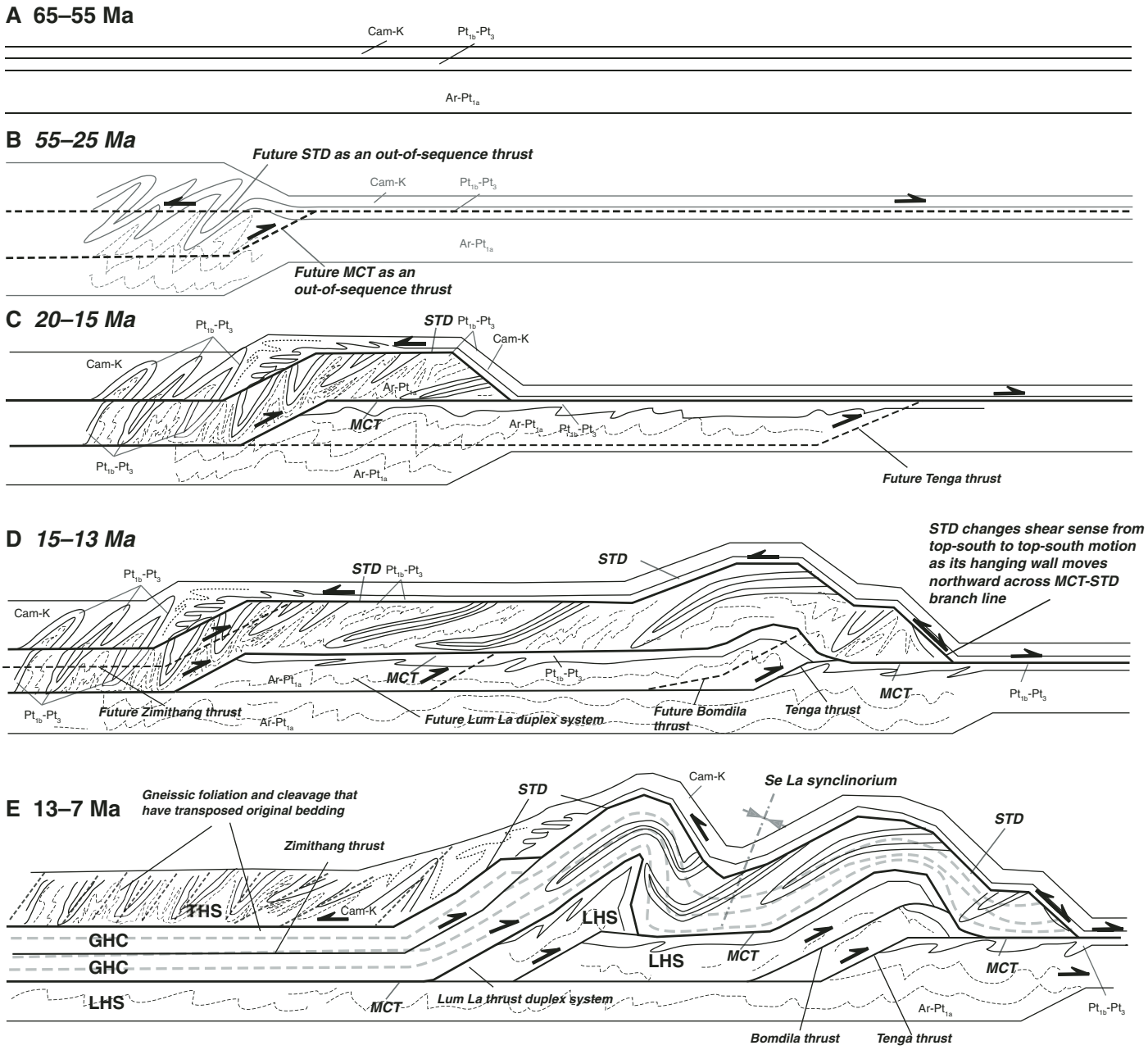

Figure 15. Cenozoic evolution of the eastern Himalaya. Lithologic units: Ar-Pt$_{1a}$ (older than 1750 Ma), Archean and Lower Paleoproterozoic metasedimentary and orthogneiss representing the basement of the Indian craton; Pt1b-Pt3 (1750–540 Ma), Upper Paleoproterozoic to Upper Proterozoic strata; Cam-K, Cambrian to Cretaceous strata. (A) Stage 1 (65–55 Ma): a highly simplified stratigraphic framework of the northern Indian continental margin prior to the India-Asia collision that does not consider the effect of Cambrian-Ordovician contraction and Mesozoic extension on northern Indian margin stratigraphy. (B) Stage 2 (55–20 Ma): Intense Cenozoic contraction possibly involving the crystalline basement of northern Indian craton causing crustal thickening and modification of the pre-Cenozoic crustal architecture. Future South Tibetan detachment (STD) and Main Central thrust (MCT) are rooted in this highly deformed middle crust, cutting isoclinally folded basement and cover rocks. (C) Stage 3 (20–15 Ma): Motion on the Main Central thrust causing southward propagation of crustal thickening in the Himalaya. Ductile folding may have accommodated its footwall deformation. The presence of a major thrust ramp along the Main Central thrust allows transport of middle- and lower-crustal rocks to the upper-crustal levels. (D) Stage 4 (15–13 Ma): Initiation and subsequent development of the Bomdila thrust in the Main Central thrust footwall and a duplex structure producing an antiform over the Bomdila thrust hanging wall. (E) Stage 5 (13–7 Ma): Development of the Lum La thrust duplex due to out-of-sequence thrusting north of the Bomdila thrust, causing the formation of an antiform above. Together, the Lum La and Bomdila duplex systems produced the Se La synclinorium. Following the traditional definition, the Greater Himalayan Crystalline Complex (GHC) lies in the Main Central thrust hanging wall, the Lesser Himalayan Sequence (LHS) lies in the Main Central thrust footwall, and the Tethyan Himalayan Sequence (THS) lies in the hanging wall of the South Tibet detachment (STD).

ACKNOWLEDGMENTS

An Yin's research was supported by a University of California (UCLA) Faculty Research Grant and partially from the Tectonics Program of the US National Science Foundation. The Department of Science and Technology of India supported C.S. Dubey's work. We thank Nadine McQuarrie, Djordje Grujic, and Associated Editor Matt Kohn for their critical, careful, and very constructive reviews that have helped improve the clarity and interpretations of the original manuscript. We are especially grateful to Nadine McQuarrie's comments on our original cross sections. Her detailed suggestions guided us to construct the cross section shown in Figure 4F as an end-member solution of our balanced cross sections.

REFERENCES CITED

Acharyya, S.K., 1994, The Cenozoic foreland basin and tectonics of the eastern sub-Himalaya: Problems and prospects: Himalayan Geology, v. 15, p. 3–21.

Acharyya, S.K., 1998, Thrust tectonics and evolution of domes and the syntaxis in eastern Himalaya, India: Journal of Nepal Geological Society, v. 18, p. 1–17.

Acharyya, S.K., Ghosh, S.C., Ghosh, R.N., and Shah, S.C., 1975, The Gondwana Group and associated marine sequences of Arunachal Pradesh (NEFA), eastern Himalaya: Himalayan Geology, v. 5, p. 60–80.

Aikman, A.B., Harrison, T.M., and Lin, D., 2008, Evidence for early (> 44 Ma) Himalayan crustal thickening, Tethyan Himalaya, southeastern Tibet: Earth and Planetary Science Letters, v. 274, p. 14–23, doi: 10.1016/j.epsl.2008.06.038.

Aitchison, J.C., Ali, J.R., and Davis, A.M., 2007, When and where did the India and Asia collide?: Journal of Geophysical Research, v. 112, p. B05423, doi: 10.1029/2006JB004706.

Ameen, S.M.M., Wilde, S.A., Kabir, Z., Akon, E., Chowdhury, K.R., and Khan, S.H., 2007, Paleoproterozoic granitoids in the basement of Bangladesh: A piece of the Indian shield or an exotic fragment of the Gondwana jigsaw?: Gondwana Research, v. 12, p. 380–387, doi: 10.1016/j.gr.2007.02.001.

Argles, T.W., Prince, C.I., Foster, G.L., and Vance, D., 1999, New garnets for old? Cautionary tales from young mountain belts: Earth and Planetary Science Letters, v. 172, p. 301–309, doi: 10.1016/S0012-821X(99)00209-5.

Armijo, R., Tapponnier, P., Mercier, J.L., and Han, T.-L., 1986, Quaternary extension in southern Tibet: Field observations and tectonic implications: Journal of Geophysical Research, v. 91, p. 13,803–13,872, doi: 10.1029/JB091iB14p13803.

Avouac, J.P., 2003, Mountain building, erosion, and the seismic cycle in the Nepal: Advances in Geophysics, v. 46, p. 1–80.

Avouac, J.P., and Tapponnier, P., 1993, Kinematic model of active deformation in central Asia: Geophysical Research Letters, v. 20, p. 895–898, doi: 10.1029/93GL00128.

Baillie, I.C., and Norbu, C., 2004, Climate and other factors in the development of river and interfluve profiles in Bhutan, eastern Himalaya: Journal of Asian Earth Sciences, v. 22, p. 539–553, doi: 10.1016/S1367-9120(03)00092-0.

Beaumont, C., Jamieson, R.A., Nguyen, M.H., and Lee, B., 2001, Himalayan tectonics explained by extrusion of a low-viscosity crustal channel coupled to focused surface denudation: Nature, v. 414, p. 738–742, doi: 10.1038/414738a.

Beaumont, C., Jamieson, R.A., Nguyen, M.H., and Medvedev, S., 2004, Crustal channel flows: 1. Numerical models with applications to the tectonics of the Himalayan-Tibetan orogen: Journal of Geophysical Research, v. 109, p. B06406, doi: 10.1029/2003JB002809.

Beaumont, C., Nguyen, M.H., Jamieson, R.A., and Ellis, S., 2006, Crustal flow models in large hot orogens, *in* Law, R.D., Searle, M.P., and Godin, L. eds., Channel Flow, Ductile Extrusion and Exhumation in Continental Collision Zones: Geological Society of London Special Publication 268, p. 91–145.

Bhargava, O.N., 1995, The Bhutan Himalaya: A Geological Account: Geological Survey of India Special Publication 39, 244 p.

Bilham, R., and England, P., 2001, Plateau 'pop-up' in the great 1897 Assam earthquake: Nature, v. 410, p. 806–809, doi: 10.1038/35071057.

Biswas, S., Isabelle, C., Grujic, D., Hager, C., Stockli, D., and Grasemann, B., 2007, Exhumation and uplift of the Shillong Plateau and its influence on the eastern Himalayas: New constraints from apatite and zircon (U-Th-[Sm])/He and apatite fission track analyses: Tectonics, v. 26, p. TC6013, doi: 10.1029/2007TC002125.

Brown, C.J., 1912, A geologic reconnaissance through the Dihang Valley, being the geological result of the Abor Expedition, 1911–12: Records of Geological Survey of India, v. 42, no. 4, p. 231–264.

Brunel, M., 1986, Ductile thrusting in the Himalayas: Shear sense criteria and stretching lineation: Tectonics, v. 5, p. 247–265, doi: 10.1029/TC005i002p00247.

Burchfiel, B.C., and Royden, L.H., 1985, North-south extension within the convergent Himalayan region: Geology, v. 13, p. 679–682, doi: 10.1130/0091-7613(1985)13<679:NEWTCH>2.0.CO;2.

Burg, J.P., Nievergelt, P., Oberli, F., Seward, D., Davy, P., Maurin, J.C., Diao, Z.Z., and Meier, M., 1998, The Namche Barwa syntaxis: Evidence for exhumation related to compressional crustal folding: Journal of Asian Earth Sciences, v. 16, p. 239–252, doi: 10.1016/S0743-9547(98)00002-6.

Carosi, R., Montomoli, C., Rubatto, D., and Visona, D., 2006, Normal-sense shear zones in the fore of the Higher Himalayan Crystallines (Bhutan Himalaya): Evidence for extrusion?, *in* Law, R.D., Searle, M.P., and Godin, L., eds., Channel Flow, Ductile Extrusion and Exhumation in Continental Collision Zones: Geological Society of London Special Publication 268, p. 425–444.

Catlos, E.J., Harrison, T.M., Kohn, M.J., Grove, M., Ryerson, F.J., Manning, C.E., and Upreti, B.N., 2001, Geochronologic and thermobarometric constraints on the evolution of the Main Central thrust, central Nepal Himalaya: Journal of Geophysical Research, v. 106, p. 16,177–16,204, doi: 10.1029/2000JB900375.

Catlos, E.J., Harrison, T.M., Manning, C.E., Grove, M., Rai, S.M., Hubbard, M.S., and Upreti, B.N., 2002, Records of the evolution of the Himalayan orogen from in situ Th–Pb ion microprobe dating of monazite: Eastern Nepal and western Garhwal: Journal of Asian Earth Sciences, v. 20, p. 459–479, doi: 10.1016/S1367-9120(01)00039-6.

Cawood, P.A., Johnson, M.R.W., and Nemchin, A.A., 2007, Early Palaeozoic orogenesis along the Indian margin of Gondwana: Tectonic response to Gondwana assembly: Earth and Planetary Science Letters, v. 255, p. 70–84, doi: 10.1016/j.epsl.2006.12.006.

Chemenda, A.I., Mattauer, M., Malavielle, J., and Bokun, A.N., 1995, A mechanism for syn-collisional rock exhumation and associated normal faulting—Results from physical modeling: Earth and Planetary Science Letters, v. 132, p. 225–232, doi: 10.1016/0012-821X(95)00042-B.

Chemenda, A.I., Burg, J.P., and Mattauer, M., 2000, Evolution model of the Himalaya-Tibet system: Geopoem based on new modeling, geological and geophysical data: Earth and Planetary Science Letters, v. 174, p. 397–409, doi: 10.1016/S0012-821X(99)00277-0.

Clark, M.K., and Bilham, R., 2008, Miocene rise of the Shillong Plateau and the beginning of the end for the eastern Himalaya: Earth and Planetary Science Letters, v. 269, p. 337–350, doi: 10.1016/j.epsl.2008.01.045.

Dai, J.G., Yin, A., Liu, W.C., and Wang, C.S., 2008, Nd isotopic compositions of the Tethyan Himalayan Sequence in southeastern Tibet: Science in China, Series D–Earth Science, v. 51, p. 1306–1316.

Daniel, C.G., Hollister, L.S., Parrish, R.R., and Grujic, D., 2003, Exhumation of the Main Central thrust from lower crustal depths, Eastern Bhutan Himalaya: Journal of Metamorphic Geology, v. 21, p. 317–334.

Das Gupta, A.B., and Biswas, A.K., 2000, Geology of Assam: Banglore, Geological Society of India, 169 p.

Davidson, C., Grujic, D.E., Hollister, L.S., and Schmid, S.M., 1997, Metamorphic reactions related to decompression and synkinematic intrusion of leucogranite, High Himalayan Crystallines, Bhutan: Journal of Metamorphic Geology, v. 15, p. 593–612, doi: 10.1111/j.1525-1314.1997.00044.x.

DeCelles, P.G., Gehrels, G.E., Quade, J., and Ojha, T.P., 1998, Eocene–early Miocene foreland basin development and the history of Himalayan thrusting, western and central Nepal: Tectonics, v. 17, p. 741–765, doi: 10.1029/98TC02598.

DeCelles, P.G., Gehrels, G.E., Quade, J., LaReau, B., and Spurlin, M., 2000, Tectonic implications of U-Pb zircon ages of the Himalayan orogenic belt in Nepal: Science, v. 288, p. 497–499, doi: 10.1126/science.288.5465.497.

DeCelles, P.G., Robinson, D.M., Quade, J., Ojha, T.P., Garzione, C.N., Copeland, P., and Upreti, B.N., 2001, Stratigraphy, structure, and tectonic evolution of the Himalayan fold-thrust belt in western Nepal: Tectonics, v. 20, p. 487–509.

DeCelles, P.G., Robinson, D.M., and Zandt, G., 2002, Implications of shortening in the Himalayan fold-thrust belt for uplift of the Tibetan Plateau: Tectonics, v. 21, no. 6, p. 1062, doi: 10.1029/2001TC001322.

Dézes, P.J., Vannay, J.C., Steck, A., Bussy, F., and Cosca, M., 1999, Synorogenic extension: Quantitative constraints on the age and displacement of the Zanskar shear zone (northwest Himalaya): Geological Society of America Bulletin, v. 111, p. 364–374, doi: 10.1130/0016-7606(1999)111<0364:SEQCOT>2.3.CO;2.

Dikshitulu, G.R., Pandey, B.K., Krishna, V., and Dhana, R., 1995, Rb/Sr systematics of granitoids of the Central Gneissic Complex, Arunachal Himalaya: Implications on tectonics, stratigraphy, and source: Journal of the Geological Society of India, v. 45, p. 51–56.

Ding, L., Zhong, D.L., Yin, A., Kapp, P., and Harrison, T.M., 2001, Cenozoic structural and metamorphic evolution of the eastern Himalayan syntaxis (Namche Barwa): Earth and Planetary Science Letters, v. 192, p. 423–438, doi: 10.1016/S0012-821X(01)00463-0.

Ding, L., Kapp, P., and Wan, X.Q., 2005, Paleocene–Eocene record of ophiolite obduction and initial India–Asia collision, south central Tibet: Tectonics, v. 24, p. TC3001, doi: 10.1029/2004TC001729.

DiPietro, J.A., and Pogue, K.R., 2004, Tectonostratigraphic subdivisions of the Himalaya: A view from the west: Tectonics, v. 23, doi: 10.1029/2003TC001554.

Drukpa, D., Velasco, A.A., and Doser, D.I., 2006, Seismicity in the Kingdom of Bhutan (1937–2003): Evidence for crustal transcurrent deformation: Journal of Geophysical Research, v. 111, p. B06301, doi: 10.1029/2004JB003087.

Dunlap, W.J., Hirth, G., and Teyssier, C., 1997, Thermomechanical evolution of a ductile duplex: Tectonics, v. 16, p. 983–1000, doi: 10.1029/97TC00614.

Edwards, M.A., Kidd, W.S.F., Li, J.X., Yu, Y.J., and Clark, M., 1996, Multi-stage development of the southern Tibet detachment system near Khula Kangri. New data from Gonto La: Tectonophysics, v. 260, p. 1–19, doi: 10.1016/0040-1951(96)00073-X.

England, P., and Houseman, G., 1986, Finite strain calculations of continental deformation: 2. Comparison with the India-Asia collision zone: Journal of Geophysical Research, v. 91, p. 3664–3676, doi: 10.1029/JB091iB03p03664.

Frank, W., Grasemann, B., Guntli, P., and Miller, C., 1995, Geological map of the Kishwar-Chamba-Kulu region (NW Himalayas, India): Jahrbuch der Geologischen Bundesanstalt, v. 138, p. 299–308.

Fuchs, G., and Linner, M., 1995, Geological traverse across the western Himalaya—A contribution to the geology of eastern Ladakh, Lahul, and Chamba: Jahrbuch der Geologischen Bundesanstalt, v. 138, p. 665–685.

Gansser, A., 1964, The Geology of the Himalayas: New York, Wiley Interscience, 289 p.

Gansser, A., 1983, Geology of the Bhutan Himalaya: Boston, Birkhäuser Verlag, 181 p.

Gehrels, G.E., DeCelles, P.G., Martin, A., Ojha, T.P., Pinhassi, G., and Upreti, B.N., 2003, Initiation of the Himalayan orogen as an early Paleozoic thin-skinned

thrust belt: GSA Today, v. 13, no. 9, p. 4–9, doi: 10.1130/1052-5173(2003)13<4:IOTHOA>2.0.CO;2.

Gehrels, G.E., DeCelles, P.G., Ojha, T.P., and Upreti, B.N., 2006a, Geologic and U-Th-Pb geochronologic evidence for early Paleozoic tectonism in the Kathmandu thrust sheet, central Nepal Himalaya: Geological Society of America Bulletin, v. 118, p. 185–198, doi: 10.1130/B25753.1.

Gehrels, G.E, DeCelles, P.G., Ojha, T.P., and Upreti, B.N., 2006b, Geologic and U-Pb geochronologic evidence for early Paleozoic tectonism in the Dadeldhura thrust sheet, far-west Nepal Himalaya: Journal of Asian Earth Sciences, v. 28, p. 385–408.

Ghosh, S., Chakraborty, S., Paul, D.K., Bhalla, J.K., Bishui, P.K., and Gupta, S.N., 1994, New Rb-Sr isotopic ages and geochemistry of granitoids from Meghalaya and their significance in middle and late Proterozoic crustal evolution: Indian Minerals, v. 48, p. 33–44.

Ghosh, S., Fallick, A.E., Paul, D.K., and Potts, P.J., 2005, Geochemistry and origin of Neoproterozoic granitoids of Meghalaya, northeast India: Implications for linkage with amalgamation of Gondwana supercontinent: Gondwana Research, v. 8, p. 421–432, doi: 10.1016/S1342-937X(05)71144-8.

Godin, L., Grujic, D., Law, R.D., and Searle, M.P., 2006, Channel flow, ductile extrusion and exhumation in continental collision: An introduction, *in* Law, R.D., Searle, M.P., and Godin, L., eds., Channel Flow, Ductile Extrusion and Exhumation in Continental Collision Zones: Geological Society of London Special Publication 268, p. 1–23.

Godwin-Austin, H.H., 1875, Notes on the geology of the Dafla Hills, Assam, lately visited by the force under Brigadier-General Stafford, C.S.: Journal of the Astronomical Society of Bangladesh, v. 44, no. 2, p. 34–41.

Grasemann, B., Fritz, H., and Vannay, J.C., 1999, Quantitative kinematic flow analysis from the Main Central thrust zone (NW-Himalaya, India): Implications for a decelerating strain path and the extrusion of orogenic wedges: Journal of Structural Geology, v. 21, p. 837–853, doi: 10.1016/S0191-8141(99)00077-2.

Grujic, D., Casey, M., Davidson, C., Hollister, L.S., Kundig, R., Pavlis, T., and Schmid, S., 1996, Ductile extrusion of the Higher Himalayan Crystalline in Bhutan: Evidence from quartz microfabrics: Tectonophysics, v. 260, p. 21–43, doi: 10.1016/0040-1951(96)00074-1.

Grujic, D., Hollister, L.S., and Parrish, R.R., 2002, Himalayan metamorphic sequence as an orogenic channel: Insight from Bhutan: Earth and Planetary Science Letters, v. 198, p. 177–191, doi: 10.1016/S0012-821X(02)00482-X.

Grujic, D., Coutand, I., Bookhagen, B., Bonnet, S., Blythe, A., and Duncan, C., 2006, Climatic forcing of erosion, landscape, and tectonics in the Bhutan Himalayas: Geology, v. 34, p. 801–804, doi: 10.1130/G22648.1.

Gururajan, N.S., and Choudhuri, B.K., 2003, Geology and tectonic history of the Lohit Valley, eastern Arunachal Pradesh, India: Journal of Asian Earth Sciences, v. 21, p. 731–741, doi: 10.1016/S1367-9120(02)00040-8.

Harrison, T.M., Yin, A., Grove, M., Lovera, O.M., Ryerson, F.J., and Zhou, X.H., 2000, The Zedong window: A record of superposed Tertiary convergence in southeastern Tibet: Journal of Geophysical Research, v. 105, p. 19,211–19,230, doi: 10.1029/2000JB900078.

Heim, A., and Gansser, A., 1939, The Central Himalaya—Geological Observations of Swiss Expedition of 1936: Memories de la Societe Helvetique des Sciences Naturalles, v. 73, 245 p.

Hodges, K.V., Hurtado, J.M., and Whipple, K.X., 2001, Southward extrusion of Tibetan crust and its effect on Himalayan tectonics: Tectonics, v. 20, p. 799–809, doi: 10.1029/2001TC001281.

Hollister, L.S., and Grujic, D., 2006, Pulse channel flow in Bhutan, *in* Law, R.D., Searle, M.P., and Godin, L., eds., Channel Flow, Ductile Extrusion and Exhumation in Continental Collision Zones: Geological Society of London Special Publication 268, p. 415–423.

Hubbard, M.S., and Harrison, T.M., 1989, $^{40}Ar/^{39}Ar$ age constraints on deformation and metamorphism in the MCT zone and Tibetan slab, eastern Nepal Himalaya: Tectonics, v. 8, p. 865–880, doi: 10.1029/TC008i004p00865.

Jade, S.M.M., Bhattacharyya, A.K., Vijayan, M.S.M., Jaganathan, S., Kumar, A., Tiwari, R.P., Kumar, A., Kalita, S., Sahu, S.C., Krishna, A.P., Gupta, S.S., Murthy, M.V.R.L., and Gaur, V.K., 2007, Estimates of interseismic deformation in northeast India from GPS measurements: Earth and Planetary Science Letters, v. 263, p. 221–234, doi: 10.1016/j.epsl.2007.08.031.

Jain, A.K., Thakur, V.C., and Tandon, S.K., 1974, Stratigraphy and structure of the Siang district, Arunachal (NEFA) Himalaya: Himalayan Geology, v. 4, p. 28–60.

Jangpangi, B.S., 1974, Stratigraphy and tectonics of parts of eastern Bhutan: Himalayan Geology, v. 4, p. 117–136.

Klemperer, S., 2006, Crustal flow in Tibet: Geophysical evidence for the physical state of Tibetan lithosphere, and inferred patterns of active flow, *in* Law, R.D., Searle, M.P., and Godin, L., eds., Channel Flow, Ductile Extrusion and Exhumation in Continental Collision Zones: Geological Society of London Special Publication 268, p. 39–70.

Kohn, M.J., 2008, *P-T-t* data from central Nepal support critical taper and repudiate large-scale channel flow of the Greater Himalayan Sequence: Geological Society of America Bulletin, v. 120, p. 259–273, doi: 10.1130/B26252.1.

Kohn, M.J., Wieland, M.S., Parkinson, C.D., and Upreti, B.N., 2004, Miocene faulting at plate tectonic velocity in the Himalayan of central Nepal: Earth and Planetary Science Letters, v. 228, p. 299–310, doi: 10.1016/j.epsl.2004.10.007.

Kohn, M.J., Wieland, M.S., Parkinson, C.D., and Upreti, B.N., 2005, Five generation of monazite in Langtang gneisses: Implications for chronology of the Himalayan metamorphic core: Journal of Metamorphic Geology, v. 23, p. 399–406, doi: 10.1111/j.1525-1314.2005.00584.x.

Kumar, G., 1997, Geology of Arunachal Pradesh: Bangalore, Geological Society of India, 217 p.

La Touche, T.D., 1885, Notes on the geology of the Aka Hills, Assam: Records of the Geological Survey of India, v. 18, p. 121–124.

Law, R.D., Searle, M.P., and Simpson, R.L., 2004, Strain, deformation temperatures and vorticity of flow at the top of the Greater Himalayan slab, Everest Massif, Tibet: Journal of the Geological Society of London, v. 161, p. 305–320, doi: 10.1144/0016-764903-047.

LeFort, P., 1975, Himalayas—collided range—present knowledge of continental arc: American Journal of Science, v. A275, p. 1–44.

LeFort, P., 1996, Evolution of the Himalaya, *in* Yin, A., and Harrison, T.M., eds., The Tectonics of Asia: New York, Cambridge University Press, p. 95–106.

Lyon-Caen, H., and Molnar, P., 1985, Gravity anomalies, flexure of the Indian plate, and the structure, support and evolution of the Himalaya and the Ganga Basin: Tectonics, v. 4, p. 513–538, doi: 10.1029/TC004i006p00513.

MacLaren, J.M., 1904, Geology of Upper Assam: Records of the Geological Survey of India, v. 31, p. 179–204.

Martin, A.J., Gehrels, G.E., and DeCelles, P.G., 2007, The tectonic significance of (U,Th)/Pb ages of monazite inclusions in garnet from the Himalaya of central Nepal: Chemical Geology, v. 244, p. 1–24, doi: 10.1016/j.chemgeo.2007.05.003.

McDougall, I., and Harrison, T.M., 1999, Geochronology and Thermochronology by the $^{40}Ar/^{39}Ar$ Method: New York, Oxford University Press, 267 p.

McQuarrie, N., Robinson, D., Long, S., Tobgay, T., Grujic, D., Gehrels, G., and Ducea, M., 2008, Preliminary stratigraphic and structural architecture of Bhutan: Implications for the along strike architecture of the Himalayan system: Earth and Planetary Science Letters, v. 272, p. 105–117, doi: 10.1016/j.epsl.2008.04.030.

Meyer, M.C., Wiesmayr, G., Brauner, M., Hausler, H., and Wangda, D., 2006, Active tectonics in eastern Lunana (NW Bhutan): Implications for the seismic and glacial hazard potential of the Bhutan Himalaya: Tectonics, v. 25, p. TC3001, doi: 10.1029/2005TC001858.

Mitra, S., Priestley, K., Bhattqacharyya, A.K., and Gaur, V.K., 2005, Crustal structure and earthquake focal depths beneath northeastern India and southern Tibet: Geophysical Journal International, v. 160, p. 227–248.

Mojzsis, S.J., and Harrison, T.M., 2002, Establishment of a 3.83-Ga magmatic age for the Akilia tonalite (southern West Greenland): Earth and Planetary Science Letters, v. 202, p. 563–576, doi: 10.1016/S0012-821X(02)00825-7.

Murphy, M.A., and Yin, A., 2003, Structural evolution and sequence of thrusting in the Tethyan fold-thrust belt and Indus-Yalu suture zone, southwest Tibet: Geological Society of America Bulletin, v. 115, p. 21–34, doi: 10.1130/0016-7606(2003)115<0021:SEASOT>2.0.CO;2.

Nelson, K.D., et al., 1996, Partially molten middle crust beneath Southern Tibet: Synthesis of Project INDEPTH results: Science, v. 274, p. 1684–1696, doi: 10.1126/science.274.5293.1684.

Paces, J.B., and Miller, J.D., 1993, Precise U-Pb age of the Duluth Complex and related mafic intrusions, northeastern Minnesota: Geochronological insights in physical, petrogenetic, paleomagnetic, and tectonomagmatic processes associated with the 1.1 Ga midcontinent rift system: Journal of Geophysical Research, v. 98, p. 13,997–14,013, doi: 10.1029/93JB01159.

Pan, G.T., Ding, J., Yao, D., and Wang, L., 2004, Geological Map of Qinghai-Xiang (Tibet) Plateau and Adjacent Areas: Chengdu, China, Chengdu Institute of Geology and Mineral Resources, China Geological Survey, Chengdu Cartographic Publishing House, scale 1:1,500,000.

Pogue, K.R., Hylland, M.D., Yeats, R.S., Khattak, W.U., and Hussain, A., 1999, Stratigraphic and structural framework of Himalayan foothills, northern Pakistan, in Himalaya and Tibet, *in* Macfarlane, A., Sorkhabi, R.B., and Quade, J., eds., Mountain Roots to Mountain Tops: Geological Society of America Special Paper 328, p. 257–274.

Quidelleur, X., Grove, M., Lovera, O.M., Harrison, T.M., Yin, A., and Ryerson, F.J., 1997, The thermal evolution and slip history of the Renbu Zedong thrust, southeastern Tibet: Journal of Geophysical Research, v. 102, p. 2659–2679.

Ray, S.K., 1995, Lateral variation in geometry of thrust planes and its significance, from studies in the Shumar allochthon, Lesser Himalayas, eastern Bhutan: Tectonophysics, v. 249, p. 125–139.

Ray, S.K., Bandyopadhyay, B.K., and Razdan, R.K., 1989, Tectonics of a part of the Shumar allochthon in eastern Bhutan: Tectonophysics, v. 169, p. 51–58, doi: 10.1016/0040-1951(89)90182-0.

Richards, A., Parrish, R., Harris, N., Argles, T., and Zhang, L., 2006, Correlation of lithotectonic units across the eastern Himalaya, Bhutan: Geology, v. 34, p. 341–344, doi: 10.1130/G22169.1.

Robinson, D.M., and Pearson, O.N., 2006, Exhumation of Greater Himalayan rock along the Main Central thrust in Nepal: Implications for channel flow, *in* Law, R.D., Searle, M.P., and Godin, L., eds., Channel Flow, Ductile Extrusion and Exhumation in Continental Collision Zones: Geological Society of London Special Publication 268, p. 255–267.

Robinson, D.M., DeCelles, P.G., Garzione, C.N., Pearson, O.N., Harrison, T.M., and Catlos, E.J., 2003, Kinematic model for the Main Central thrust in Nepal: Geology, v. 31, p. 359–362, doi: 10.1130/0091-7613(2003)031<0359:KMFTMC>2.0.CO;2.

Robinson, D.M., DeCelles, P.G., and Copeland, P., 2006, Tectonic evolution of the Himalayan thrust belt in western Nepal: Implications for channel flow models: Geological Society of America Bulletin, v. 118, p. 865–885, doi: 10.1130/B25911.1.

Schelling, D., and Arita, K., 1991, Thrust tectonics, crustal shortening, and the structure of the far-eastern Nepal, Himalaya: Tectonics, v. 10, p. 851–862, doi: 10.1029/91TC01011.

Searle, M.P., Waters, D.J., Dransfield, M.W., Stenphenson, B.J., Walker, C.B., Walker, J.D., and Rex, D.C., 1999, Thermal and mechanical models for the structural and metamorphic evolution of the Zanskar High Himalaya, *in* MacNiocaill, C., and Ryan, P.D., eds., Continental Tectonics: Geological Society of London Special Publication 164, p. 139–156.

Searle, M.P., Simpson, R.L., Law, R.D., Parrish, R.R., and Waters, D.J., 2003, The structural geometry, metamorphic and magmatic evolution of the Everest massif,

High Himalaya of Nepal–South Tibet: Journal of the Geological Society of London, v. 160, p. 345–366, doi: 10.1144/0016-764902-126.

Searle, M.P., Law, R.D., Godin, L., Larson, K.P., Streule, M.J., Cottle, J.M., and Jessup, M.J., 2008, Defining the Himalayan Main Central thrust in Nepal: Journal of the Geological Society of London, v. 165, p. 523–534, doi: 10.1144/0016-76492007-081.

Singh, S., 1993, Geology and tectonics of the eastern syntaxis bend, Arunachal Himalaya: Journal of Himalayan Geology, v. 4, p. 149–163.

Singh, S., and Chowdhary, P.K., 1990, An outline of the geological framework of the Arunachal Himalaya: Journal of Himalayan Geology, v. 1, p. 189–197.

Srivastava, P., and Mitra, G., 1994, Thrust geometries and deep structure of the outer and lesser Himalaya, Jumoan and Garhwal (India): Implications for evolution of the Himalayan fold and thrust belt: Tectonics, v. 13, p. 89–109, doi: 10.1029/93TC01130.

Stacey, J.S., and Kramers, J.D., 1975, Approximation of terrestrial lead isotope evolution by a two-stage model: Earth and Planetary Science Letters, v. 26, p. 207–221, doi: 10.1016/0012-821X(75)90088-6.

Steck, A., 2003, Geology of the NW Indian Himalaya: Eclogae Geologicae Helvetiae, v. 96, p. 147–193.

Steck, A., Spring, L., Vannay, J.-C., Masson, H., Bucher, H., Stutz, E., Marchant, R., and Tieche, J.-C., 1993, The tectonic evolution of the northwestern Himalaya in eastern Ladakh and Lahul, India, *in* Treloar, P.J., and Searle, M.P., eds., Himalayan Tectonics: Geological Society of London Special Publication 74, p. 265–276.

Steck, A., Epard, J.L., Vannay, J.C., Hunziker, J., Girard, M., Morard, A., and Robyr, M., 1998, Geological transect across the Tso Morari and Spiti areas: The nappe structures of the Tethys Himalaya: Eclogae Geologicae Helvetiae, v. 91, p. 103–122.

Stephenson, B.J., Searle, M.P., Waters, D.J., and Rex, D.C., 2001, Structure of the Main Central thrust zone and extrusion of the High Himalayan deep crustal wedge, Kishtwar-Zanskar Himalaya: Journal of the Geological Society of London, v. 158, p. 637–652.

Stüwe, K., and Foster, D., 2001, Ar-40/Ar-39, pressure, temperature and fission-track constraints on the age and nature of metamorphism around the Main Central thrust in the eastern Bhutan Himalaya: Journal of Asian Earth Sciences, v. 19, p. 85–95, doi: 10.1016/S1367-9120(00)00018-3.

Swapp, S.M., and Hollister, L.S., 1991, Inverted metamorphism within the Tibetan slab of Bhutan—Evidence for a tectonically transported heat source: Canadian Mineralogist, v. 29, p. 1019–1041.

Tangri, S.K., Bhargava, O.N., and Pande, A.C., 2003, Late Precambrian–Early Cambrian trace fossils from Tethyan Himalaya, Bhutan, and their bearing on the Precambrian-Cambrian boundary: Journal of the Geological Society of India, v. 62, p. 708–716.

Taylor, M., Yin, A., Ryerson, F., Kapp, P., and Ding, L., 2003, Conjugate strike-slip fault accommodates coeval north-south shortening and east-west extension along the Bangong-Nujiang suture zone in central Tibet: Tectonics, v. 22, doi: 10.1029/2002TC001361.

Tewari, V.C., 2001, Discovery and sedimentology of microstromatolites from Menga Limestone (Neoproterozoic/Vendian), Upper Subansiri District, Arunachal Pradesh, NE Himalaya, India: Indian Current Science Association, v. 80, p. 1440–1444.

Thakur, V.C., 1986, Tectonic zonation and regional framework of eastern Himalaya: Science de la Terre Memoir, v. 47, p. 347–360.

Thakur, V.C., 1992, Geology of Western Himalaya: New York, Pergamon Press, 363 p.

Thakur, V.C., 1998, Structure of the Chamba nappe and position of the Main Central thrust in Kashmir Himalaya: Journal of Asian Earth Sciences, v. 16, p. 269–282, doi: 10.1016/S0743-9547(98)00011-7.

Thakur, V.C., and Jain, A.K., 1974, Tectonics of eastern region: Indian Current Science Association, v. 43, p. 783–785.

Tripathi, C., Dungrakoti, B.D., Jain, L.S., Kauro, S.C., Babu Roy, S., and Laxmipathi, N.S., 1982, Geology of Dirang-Doimara area, Kameng District, Arunachal Pradesh, with special reference to structure and tectonics: Himalayan Geology, v. 10, p. 353–365.

Upreti, B.N., 1999, An overview of the stratigraphy and tectonics of the Nepal Himalaya: Journal of Asian Earth Sciences, v. 17, p. 577–606.

Valdiya, K.S., 1980, Geology of the Kumaon Lesser Himalaya: Dehra Dun, India, Wadia Institute of Himalaya, 291 p.

Velasco, A.A., Gee, V.L., Rowe, C., Grujic, D., Hollister, L.S., Hernandez, D., Miller, K.C., Tobgay, T., Fort, M., and Harder, S., 2007, Using small, temporary seismic networks for investigating tectonic deformation: Brittle deformation and evidence for strike-slip faulting in Bhutan: Seismological Research Letters, v. 78, p. 446–453, doi: 10.1785/gssrl.78.4.446.

Verma, P.K., ed., 2002, Geological Studies in the Eastern Himalayas: Delhi, Pilgrams Book (Pvt.) Ltd., 256 p.

Verma, P.K., and Tandon, S.K., 1976, Geological observations in parts of Kameng District, Arunachal Pradesh (NEFA): Himalayan Geology, v. 6, p. 259–286.

Webb, A.A.G., 2008, Structural evidence for the leading edge of the Greater Himalayan Crystalline Complex in the Kathmandu region, central Nepal Himalaya: San Francisco, Eos (American Geophysical Union), 2008 Annual Meeting, abs. T33B–2045.

Webb, A.A.G., Yin, A., Harrison, T.M., Celerier, J., and Burgess, P., 2007, The leading edge of the Greater Himalayan Crystalline complex revealed in the NW Indian Himalaya: Implications for the evolution of the Himalayan orogen: Geology, v. 35, p. 955–958, doi: 10.1130/G23931A.1.

Wiedenbeck, M., Hanchar, J.M., Peck, W.H., Sylvester, P., Valley, J., Whitehouse, M., Kronz, A., Morishita, Y., Nasdala, L., Fiebig, J., Franchi, I., Girard, J.P., Greenwood, R.C., Hinton, R., Kita, N., Mason, P.R.D., Norman, M., Ogasawara, M., Piccoli, P.M., Rhede, D., Satoh, H., Schulz-Dobrick, B., Skar, O., Spicuzza, M.J., Terada, K., Tindle, A., Togashi, S., Vennemann, T., Xie, Q., and Zheng, Y.F., 2004, Further characterisation of the 91500 zircon crystal: Geostandard and Geoanalysis Research, v. 28, p. 9–39, doi: 10.1111/j.1751-908X.2004.tb01041.x.

Wiesmayr, G., Edwards, M.A., Meyer, M., Kidd, W.S.F., Leber, D., Hausler, H., and Wangda, D., 2002, Evidence for steady fault-accommodated strain in the High Himalaya: Progressive fault rotation of the Southern Tibet detachment system in NW Bhutan, *in* De Meer, S., Drury, M.R., De Bresser, J.H.P., and Pennock, G.M., eds., Deformation Mechanisms, Rheology and Tectonics: Current Status and Future Perspectives: Geological Society of London Special Publication 200, p. 1–27, doi: 10.1144/GSL.SP.2001.200.01.01.

Yeats, R.S., and Lawrence, R.D., 1984. Tectonics of the Himalayan thrust belt in northern Pakistan, *in* Haq, B.U., and Milliman, J.D., eds., Marine Geology and Oceanography of Arabian Sea and Coastal Pakistan: New York, Van Nostrand Reinhold, p. 177–198.

Yin, A., 2000, Mode of Cenozoic east-west extension in Tibet suggesting a common origin of rifts in Asia during the Indo-Asian collision: Journal of Geophysical Research, v. 105, p. 21,745–21,759, doi: 10.1029/2000JB900168.

Yin, A., 2006, Cenozoic tectonic evolution of the Himalayan orogen as constrained by along-strike variation of structural geometry, exhumation history, and foreland sedimentation: Earth-Science Reviews, v. 76, p. 1–131, doi: 10.1016/j.earscirev.2005.05.004.

Yin, A., and Harrison, T.M., 2000, Geologic evolution of the Himalayan-Tibetan orogen: Annual Review of Earth and Planetary Sciences, v. 28, p. 211–280.

Yin, A., Harrison, T.M., Ryerson, F.J., Chen, W., Kidd, W.S.F., and Copeland, P., 1994, Tertiary structural evolution of the Gangdese thrust system, southeastern Tibet: Journal of Geophysical Research, v. 99, p. 18,175–18,201, doi: 10.1029/94JB00504.

Yin, A., Harrison, T.M., Murphy, M.A., Grove, M., Nie, S., Ryerson, F.J., Feng, W.X., and Le, C.Z., 1999, Tertiary deformation history of southeastern and southwestern Tibet during the Indo-Asian collision: Geological Society of America Bulletin, v. 111, p. 1644–1664.

Yin, A., Dubey, C.S., Kelty, T.K., Gehrels, G.E., Chou, C.Y., Grove, M., and Lovera, O., 2006, Structural evolution of the Arunachal Himalaya and implications for asymmetric development of the Himalayan orogen: Indian Current Science Association, v. 90, p. 195–206.

Yin, A., Dang, Y.-Q., Wang, L.C., Jiang, W.-M., Zhou, S.-P., Chen, X.-H., Gehrels, G. E., and McRivette, M. W., 2008a, Cenozoic tectonic evolution of Qaidam basin and its surrounding regions: Part 1. The southern Qilian Shan–Nan Shan thrust belt and northern Qaidam basin: Geological Society of America Bulletin, v. 120, p. 813–846, doi: 10.1130/B26180.1.

Yin, A., Dang, Y.-Q., Zhang, M., Chen, X.-H., and McRivette, M.W., 2008b, Cenozoic tectonic evolution of the Qaidam basin and its surrounding regions: Part 3. Structural geology, sedimentation, and regional tectonic reconstruction: Geological Society of America Bulletin, v. 120, p. 847–876, doi: 10.1130/B26232.1.

Yin, A., Dubey, C.S., Webb, A.A.G., Kelty, T.K., Grove, M., Gehrels, G.E., and Burgess, W.P., 2009, Geologic correlation of the Himalayan orogen and Indian craton: Part 1. Structural geology, U-Pb zircon geochronology, and tectonic evolution of the Shillong Plateau and its neighboring regions in NE India: Geological Society of America Bulletin (in press).

Zeitler, P.K., Koons, P.O., Bishop, M.P., Chamberlain, C.P., Craw, D., Edwards, M.A., Hamidullah, S., Jan, M.Q., Khan, M.A., Khattak, M.U.K., Kidd, W.S.F., Mackie, R.L., Meltzer, A.S., Park, S.K., Pecher, A., Poage, M.A., Sarker, G., Schneider, D.A., Seeber, L., and Shroder, J.F., 2001, Crustal reworking at Nanga Parbat, Pakistan: Metamorphic consequences of thermal-mechanical coupling facilitated by erosion: Tectonics, v. 20, p. 712–728, doi: 10.1029/2000TC001243.

Zhu, B., Kidd, W.S.F., Rowley, D.B., Currie, B.S., and Shafique, N., 2005, Age of initiation of the India-Asia collision in the east-central Himalaya: The Journal of Geology, v. 113, p. 265–285, doi: 10.1086/428805.

Manuscript Received 11 May 2008
Revised Manuscript Received 13 February 2009
Manuscript Accepted 2 June 2009

Printed in the USA